RMZ

MATERIALS and GEOENVIRONMENT

MATERIALI in GEOOKOLJE

RMZ – M&G, **Vol. 62**, No. 1
pp. 1–70 (2015)

Ljubljana, April 2015

RMZ – Materials and Geoenvironment
RMZ – Materiali in geookolje
ISSN 1408-7073

Old title/Star naslov
Mining and Metallurgy Quarterly/Rudarsko-metalurški zbornik
ISSN 0035-9645, 1952–1997

Published by/Izdajatelj
Faculty of Natural Sciences and Engineering, University of Ljubljana/
Naravoslovnotehniška fakulteta, Univerza v Ljubljani

Associated Publisher/Soizdajatelj
Institute for Mining, Geotechnology and Environment, Ljubljana/
Inštitut za rudarstvo, geotehnologijo in okolje
Velenje Coal Mine/Premogovnik Velenje

Editorial Office/Uredništvo
Secretary/Tajnica Ines Langerholc
Technical Editor/Tehnična urednica Helena Buh
Editor of website/Urednik spletne strani Timotej Verbovšek

Editorial Address/Naslov uredništva
RMZ – Materials and Geoenvironment
Aškerčeva cesta 12, p. p. 312
1001 Ljubljana, Slovenija
Tel.: +386 (0)1 470 45 00
Fax.: +386 (0)1 470 45 60
E-mail: rmz-mg@ntf.uni-lj.si

Linguistic Advisor/Lektor
Jože Gasperič

Design and DTP/Oblikovanje, prelom in priprava za tisk
IDEJA.si

Print/Tisk
Birografika BORI, d. o. o.
Printed in 200 copies./Naklada 200 izvodov.

Published/Izhajanje
4 issues per year/4 številke letno

Partly funded by Ministry of Education, Science and Sport of Republic of Slovenia./Pri financiranju revije sodeluje Ministrstvo za izobraževanje, znanost in šport Republike Slovenije.

Articles published in Journal "RMZ M&G" are indexed in international secondary periodicals and databases:/Članki, objavljeni v periodični publikaciji „RMZ M&G", so indeksirani v mednarodnih sekundarnih virih:
CA SEARCH® – Chemical Abstracts®, METADEX®, GeoRef.

The authors themselves are liable for the contents of the papers./
Za mnenja in podatke v posameznih sestavkih so odgovorni avtorji.

Annual subscription for individuals in Slovenia: 16.69 EUR, for institutions: 22.38 EUR. Annual subscription for the rest of the world: 20 EUR, for institutions: 40 EUR/Letna naročnina za posameznike v Sloveniji: 16,69 EUR, za inštitucije: 33,38 EUR. Letna naročnina za tujino: 20 EUR, inštitucije: 40 EUR.

Current account/Tekoči račun
Nova Ljubljanska banka, d. d., Ljubljana: UJP 01100-6030708186

VAT identification number/Davčna številka
24405388

Online Journal/Elektronska revija
www.rmz-mg.com

Table of Contents

Kazalo

Original scientific papers
Izvirni znanstveni članki

Co–Sn–Zn liquid phase thermodynamic properties investigation performed by different geometric models and by CALPHAD method **3**
Raziskava termodinamičnih lastnosti tekoče faze Co-Sn-Zn z različnimi geometričnimi modeli in CALPAD-metodo
Vanya Gandova

Fragility curves of RC columns estimated by the CAE method **9**
Ocena krivulj ranljivosti AB-stebrov s CAE-metodo
Klemen Sinkovic, Iztok Perus

Geochemical and isotopic characterization of coalbed gases in active excavation fields at Preloge and Pesje (Velenje Basin) mining areas **21**
Geokemijska in izotopska karakterizacija premogovnih plinov iz aktivnih odkopov rudarskih območij Preloge in Pesje (Velenjski bazen)
Tjaša Kanduč, Fausto Grassa, Jerneja Lazar, Simon Zavšek

Indicator Kriging porosity maps of Upper Miocene sandstones, Sava Depression, Northern Croatia **37**
Indikatorsko krigiranje poroznosti zgornjemiocenskih peščenjakov v Posavski kadunji v severni Hrvaški
Tomislav Malvić, Karolina Novak, Kristina Novak Zelenika

Professional papers
Strokovni članki

Design of product properties by suitable planning of a cold forging process **47**
Oblikovanje lastnosti izdelka z ustreznim načrtovanjem procesa hladnega kovanja
Vid Krušič, Martin Fabjan

Petrophysical evaluation of reservoirs in 'y' prospect Niger delta **55**
Petrofizikalna ocena rezervoarjev na raziskovalnem območju 'y' v delti Nigra
Yemisi. C. Ajisafe

Historical Review

More than 90 years have passed since the University Ljubljana in Slovenia was founded in 1919. Technical fields were united in the School of Engineering that included the Geologic and Mining Division, while the Metallurgy Division was established only in 1939. Today, the Departments of Geology, Mining and Geotechnology, Materials and Metallurgy are all part of the Faculty of Natural Sciences and Engineering, University of Ljubljana.

Before World War II, the members of the Mining Section together with the Association of Yugoslav Mining and Metallurgy Engineers began to publish the summaries of their research and studies in their technical periodical Rudarski zbornik (Mining Proceedings). Three volumes of Rudarski zbornik (1937, 1938 and 1939) were published. The War interrupted the publication and it was not until 1952 that the first issue of the new journal Rudarsko-metalurški zbornik – RMZ (Mining and Metallurgy Quarterly) was published by the Division of Mining and Metallurgy, University of Ljubljana. Today, the journal is regularly published quarterly. RMZ – M&G is co-issued and co-financed by the Faculty of Natural Sciences and Engineering Ljubljana, the Institute for Mining, Geotechnology and Environment Ljubljana, and the Velenje Coal Mine. In addition, it is partly funded by the Ministry of Education, Science and Sport of Slovenia.

During the meeting of the Advisory and the Editorial Board on May 22, 1998, Rudarsko-metalurški zbornik was renamed into "RMZ – Materials and Geoenvironment (RMZ – Materiali in Geookolje)" or shortly RMZ – M&G. RMZ – M&G is managed by an advisory and international editorial board and is exchanged with other world-known periodicals. All the papers submitted to the RMZ – M&G undergoes the course of the peer-review process.

RMZ – M&G is the only scientific and professional periodical in Slovenia which has been published in the same form for 60 years. It incorporates the scientific and professional topics on geology, mining, geotechnology, materials and metallurgy. In the year 2013, the Editorial Board decided to modernize the journal's format.

A wide range of topics on geosciences are welcome to be published in the RMZ – Materials and Geoenvironment. Research results in geology, hydrogeology, mining, geotechnology, materials, metallurgy, natural and anthropogenic pollution of environment, biogeochemistry are the proposed fields of work which the journal will handle.

Editor-in-Chief

Zgodovinski pregled

Že več kot 90 let je minilo od ustanovitve Univerze v Ljubljani leta 1919. Tehnične stroke so se združile v tehniški visoki šoli, ki sta jo sestavljala oddelka za geologijo in rudarstvo, medtem ko je bil oddelek za metalurgijo ustanovljen leta 1939. Danes oddelki za geologijo, rudarstvo in geotehnologijo ter materiale in metalurgijo delujejo v sklopu Naravoslovnotehniške fakultete Univerze v Ljubljani.

Pred 2. svetovno vojno so člani rudarske sekcije skupaj z Združenjem jugoslovanskih inženirjev rudarstva in metalurgije začeli izdajanje povzetkov njihovega raziskovalnega dela v Rudarskem zborniku. Izšli so trije letniki zbornika (1937, 1938 in 1939). Vojna je prekinila izdajanje zbornika vse do leta 1952, ko je izšel prvi letnik nove revije Rudarsko-metalurški zbornik – RMZ v izdaji odsekov za rudarstvo in metalurgijo Univerze v Ljubljani. Danes revija izhaja štirikrat letno. RMZ – M&G izdajajo in financirajo Naravoslovnotehniška fakulteta v Ljubljani, Inštitut za rudarstvo, geotehnologijo in okolje ter Premogovnik Velenje. Prav tako izdajo revije financira Ministrstvo za izobraževanje, znanost in šport.

Na seji izdajateljskega sveta in uredniškega odbora je bilo 22. maja 1998 sklenjeno, da se Rudarsko-metalurški zbornik preimenuje v RMZ – Materiali in geookolje (RMZ – Materials and Geoenvironment) ali skrajšano RMZ – M&G. Revijo RMZ – M&G upravljata izdajateljski svet in mednarodni uredniški odbor. Revija je vključena v mednarodno izmenjavo svetovno znanih publikacij. Vsi članki so podvrženi recenzijskemu postopku.

RMZ – M&G je edina strokovno-znanstvena revija v Sloveniji, ki izhaja v nespremenjeni obliki že 60 let. Združuje področja geologije, rudarstva, geotehnologije, materialov in metalurgije. Uredniški odbor je leta 2013 sklenil, da posodobi obliko revije.

Za objavo v reviji RMZ – Materiali in geookolje so dobrodošli tudi prispevki s širokega področja geoznanosti, kot so: geologija, hidrologija, rudarstvo, geotehnologija, materiali, metalurgija, onesnaževanje okolja in biokemija.

Glavni urednik

Original scientific paper

Received: November 25, 2014
Accepted: January 29, 2015

Co–Sn–Zn liquid phase thermodynamic properties investigation performed by different geometric models and by CALPHAD method

Raziskava termodinamičnih lastnosti tekoče faze Co-Sn-Zn z različnimi geometričnimi modeli in CALPAD-metodo

Vanya Gandova
University of Food Technologies, Inorganic and Physical Chemistry Department, 26 Mariza avenue, 4000 Plovdiv, Bulgaria
Corresponding author. E-mail: gandova_71@abv.bg

Abstract

Predictions for the liquid Co–Sn–Zn alloys thermodynamic properties (molar excess Gibbs energy) were presented in this paper. The calculations were performed in the temperature range 1 000–2 000 K. Geometric models were used and the respective calculated molar excess Gibbs energies were compared to Calphad method assessments. The concentration dependences of the liquid phase thermodynamic properties along vertical sections with Sn/Zn ratios of 1 : 5, 1 : 1 and 5 : 1 were estimated. Ternary interaction parameters (L^0, L^1 and L^2) of the liquid phase were determined using General solution (geometric) models from thermodynamic data of the binary end–systems (Co–Sn, Co–Zn, Sn–Zn).

Key words: sgeneral solution model, ternary interaction parameters, ternary systems, Calphad method

Izvleček

V članku je predstavljena napoved termodinamčnih lastnosti (molske prebitne proste Gibbsove energije) tekočih zlitin Co-Sn-Zn. Izračuni so bili izvedeni v temperaturnem območju 1 000–2 000 K. Uporabljeni so bili geometrijski modeli. Odgovarjajoče izračunane molske prebitne proste Gibbsove energije so bile primerjane z oceno po Calpad-metodi. Termodinamične lastnosti tekoče faze v odvisnosti od koncentracije so bile določene za vertikalne prereze in razmerja Sn/Zn 1 : 5, 1 : 1 ter 5 : 1. Ternarni interakcijski koeficienti (L^0, L^1 and L^2) so bili določeni z uporabo modela posplošene rešitve iz končnih birnarnih sistemov (Co–Sn, Co–Zn, Sn–Zn).

Ključne besede: model posplošene rešitve, ternarni interakcijski parametri, ternarni sistem, Calpad-metoda

Introduction

The Co–Sn–Zn system is interesting as potential materials using in industrial application like alloys applicable as lead free materials[1]. These materials are expected to be designed on the basis of systems containing low-melting elements like Sn and Zn. It is well known that the classical lead-tin based alloys represent a serious health and environmental risk. Pb-containing alloys use recently[2] but the replacement of the whole variety of Sn–Pb based materials turned out to be a very difficult task[3].
The binary end-systems Co–Sn[4] and Co–Zn[5] have been intensively studied. They exhibit a large numbers of intermetallic phases. The binary system Sn–Zn represents a simple eutectic phase diagram[6].
This ternary system is included in the thermodynamic database developed by the European concerted action Solders[6] and reliable thermodynamic optimization is available. The task of the present study is to apply different ways to assess the thermochemical properties of the ternary melt Co–Sn–Zn.

Theoretical fundamentals of the assessments

The so-called "geometric models" give the possibility to predict the thermodynamic properties of a ternary phase (in this case – liquid) using the data for the respective binary end systems. In this work, assessments were done using the most common classic geometric models of Kohler[7], Toop[8], and Hilert[9] as well as the general solution model (GSM) developed by Chou[10, 11].
Hillert[9] classified the geometric models as symmetrical (e.g.[7]) and asymmetrical (e.g.[8, 9]). Such a universal approach was developed recently by Chou[10, 11] and was successfully applied to a variety of cases[12, 13, 14]. Nevertheless, a brief description of the techniques used is described below.
The molar excess Gibbs energy (ΔG^{E}, J mol^{-1}) of the ternary liquid phase was chosen as parameter which values have to be calculated by various models and compared. This function describes the contribution of the non-ideal mixing to the thermodynamic properties of a solution phase. The molar excess Gibbs energies values of every binary end-system are necessary as starting points and calculated by means of Thermo-Calc software package[15]. The composition dependence of the binary Gibbs molar excess energies (ΔG^{E}_{ij}) was given by Redlich-Kister formalism[16].
The Gibbs molar excess energy of a ternary phase (ΔG^{E}_{123}), consisting of the elements 1, 2 and 3, was given by the expression:

$$\Delta G^{E}_{123} = x_1 x_2 \Delta G^{E}_{12} + x_2 x_3 \Delta G^{E}_{23} + x_3 x_1 \Delta G^{E}_{31} + \Delta G^{E}_{123} \quad (1)$$

where ΔG^{E}_{123} is the contribution of the ternary non-ideal mixing. In the simplest case of a regular ternary solution it may be assessed as:

$$\Delta G^{E}_{123} = x_1 x_2 x_3 L_{123} \quad (2)$$

where L_{123} is a ternary interaction parameter that might be temperature and concentration dependent.
The most essential equations, associated to the geometrical models[7, 8, 9] were used for calculations.
Equation (3) can be used as an introduction of the General solution model (GSM) of Chou[10, 11]:

$$\Delta G^{E}_{123} = x_1 x_2 x_3 f_{123} \quad (3)$$

Here f_{123} is the ternary interaction coefficient, related to the Redlich-Kister ternary interaction parameters L_{ijk} ($f_{123} = x_1 \times L^{0}_{123} + x_2 \times L^{1}_{123} + x_3 \times L^{2}_{123}$).
ξ_{ij} are "similarity coefficients", that were defined by the term η_i called "deviation sum of squares. Equation (4) presented model of Chou.

$$f_{123} = (2\xi_{12} - 1)\{L^{2}_{12}((2\xi_{12} - 1)x_3 + 2(x_1 - x_2)) + L^{1}_{12}\} + (2\xi_{23} - 1)\{L^{2}_{23}((2\xi_{23} - 1)x_1 + 2(x_2 - x_3)) + L^{1}_{23}\} + (2\xi_{31} - 1)\{L^{2}_{31}((2\xi_{12} - 1)x_2 + 2(x_3 - x_1)) + L^{1}_{31}\} \quad (4)$$

Basic thermodynamic information on the binary subsystems, needed for the assessment, was taken from[6]. The optimized Redlich-Kister parameters of each system are presented in

Table 1. They were used for the calculation of the molar excess Gibbs energies of the binary end-systems liquid phases. In this work: Co is represented as component 1, Sn - component 2 and Zn - component 3.

Results and discussion

Calculations of the coefficients f_{123} were done along three sections of the Co–Sn–Zn system with molar Sn : Zn ratios 1 : 5, 1 : 1 and 5 : 1 in the interval 1 000–2 000 K at amount fractions of cobalt equal to 0, 0.1, 0.2, 0.3, 0.4, 0.5, 0.6, 0.7, 0.8, 0.9 and 1. In such a way a large amount of data was obtained and used thereafter to derive the parameters L_{ijk}. The results for the ternary parameters are shown in Table 2.

Comparative reviews of the molar Gibbs excess energies *(ΔG^E,* J mol^{-1}*)* assessed at 1 973 K by using different geometric models (GSM[10, 11], Toop[8], Hilert[9] and Kohler[7]) and by the Calphad method (binary parameters only)[6]) are shown in Figures 1–3. Figure 1 shows calculations for the molar ratio Sn : Zn = 1 : 5. In this figure all curves exhibit positive values for the Gibbs excess energies. These positive deviations can be related to a possible miscibility gap in liquid phase at Co-Zn side in the ternary diagram. In this case, the values assessed by symmetrical models[7] were quite similar and were accompanied by the Calphad-type calculated quantities. The same conclusion is valid for the values calculated by both asymmetrical methods[8, 9]. The GSM-assessed molar Gibbs excess energies deviate from all others.

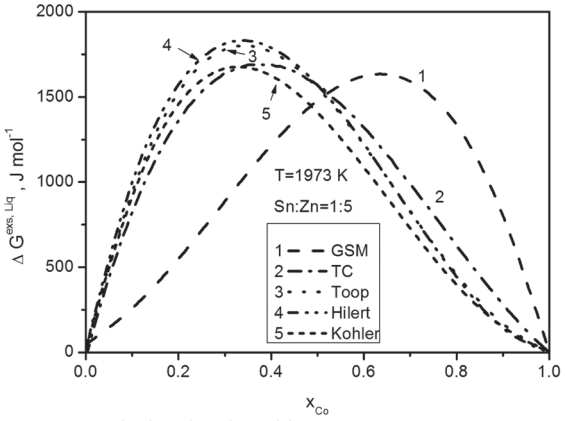

Figure 1: *Calculated molar Gibbs excess energies (ΔG^E/(J mol^{-1})) of the liquid phase, along a section with constant molar Sn/Zn ratio equal to* 1 : 5 *at* 1 973 K.

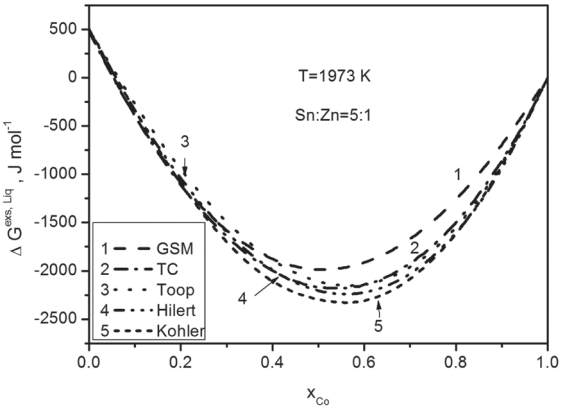

Figure 2: *Calculated molar Gibbs excess energies (ΔG^E,* J mol^{-1}*) of the liquid phase, along a section with constant molar Sn : Zn ratio equal to* 5 : 1 *at* 1 973 K.

Most of the assessments predict (in general) negative ΔG^E with a minimum in the composition interval of 0.5–0.55 amount fraction cobalt is shown in Figure 2. The calculations based on the GSM[10, 11] deviate from all others predicting a minimum at around 0.4–0.5 amount fractions cobalt.

In Figure 3 the molar Gibbs excess energies along the section with Sn:Zn molar ratio equal to 1 : 1 all curves are with sign-changing values. Small negative values, up to around –700 J mol^{-1}

Table 1: *Optimized parameters (L^0_{if}, L^1_{ij}, L^2_{ij}) for the liquid binary phases of the Co–Sn[4], Co–Zn[5] and Sn–Zn[6] systems used in the present work; T – temperature,* K

System, *i–j*	$L^o_{ij}(T)$/(J mol^{-1})	$L^1_{ij}(T)$/(J mol^{-1})	$L^2_{ij}(T)$/(J mol^{-1})
Co–Sn	–113 890 + 568.4038 * *T* –68.169 * *T* * *LN(T)*	–56 193.26 + 283.7657 * *T* –33.6875 * *T* * *LN(T)*	0
Co–Zn	–15 017 + 12.735 * *T*	+51 758 – 29.752 * *T*	0
Sn–Zn	+19 314.64 – 75.89949 * *T* + 8.751396 * *T* * *LN(T)*	–5 696.28 + 4.20198 * *T*	+1 037.22 + 0.98362 * *T*

in curves 2–5 are calculated. Sign-changing positive values are reached to 300 J mol^{-1}. Along this section a maximum in the composition interval of 0.6–0.75 amount fractions cobalt are predicted, except by the assessment done using the GSM model (Figure 3, curve 1). The latter is sign-changing as well but deviates symmetrically from each other calculation. The reason for this discrepancy could not be found. These deviations in GSM model is observed in another ternary system - Ni-Bi-Zn[17].

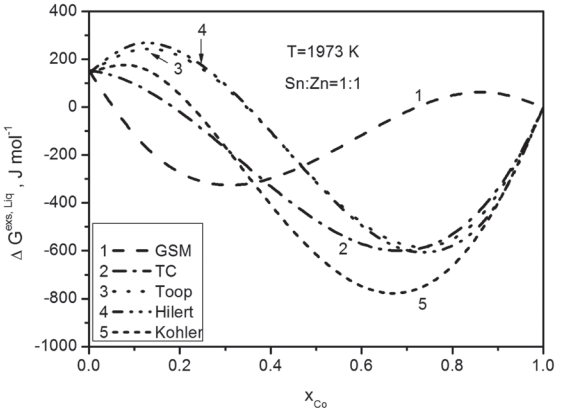

Figure 3: *Calculated molar Gibbs excess energies (ΔG^E, J mol^{-1}) of the liquid phase, along a section with constant molar Sn : Zn ratio equal to* 1 : 1 *at* 1 973 *K.*

Figure 4 presented molar Gibbs excess energies of the liquid phase in broad temperature range 1 000–2 000 K used GSM model of Chou[10, 11]. The calculations exhibit negative Gibbs energies at low temperature. But at temperatures of 1 400 K to 2 000 K Gibbs energies are shown mix of negative and positive values.

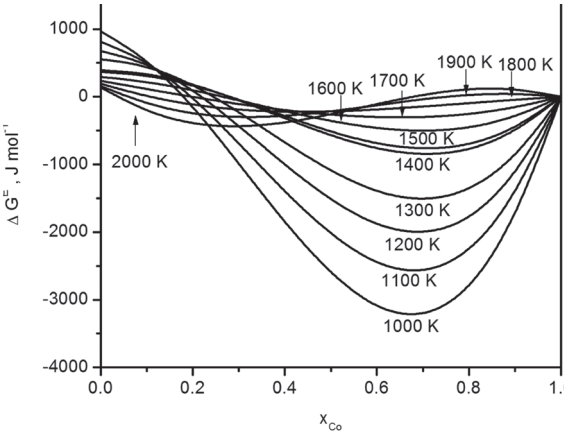

Figure 4: *Calculated molar Gibbs excess energies (ΔG^E, J mol^{-1}) of the liquid phase in all temperature range according to GSM models.*

The values of the ternary molar Gibbs excess energies (ΔG^E) in the temperature range 1 000–2 000 K and along sections with Sn : Zn molar ratios equal to 1 : 5, 1 : 1 and 5 : 1, obtained from GSM are shown in Figures 5–7, respectively.

These figures give a graphical view of the surfaces calculated at different temperature region (from 1 000 to 2 000 K) constituted by the values of the liquid phase molar Gibbs excess energies and amount fractions Co. Typically, there are maximums (positive ΔG^E values) in the Co–rich regions and especially in Co–Zn rich solutions. From another side relatively small negative ΔG^E values are predicted for the Co–Sn rich compositions.

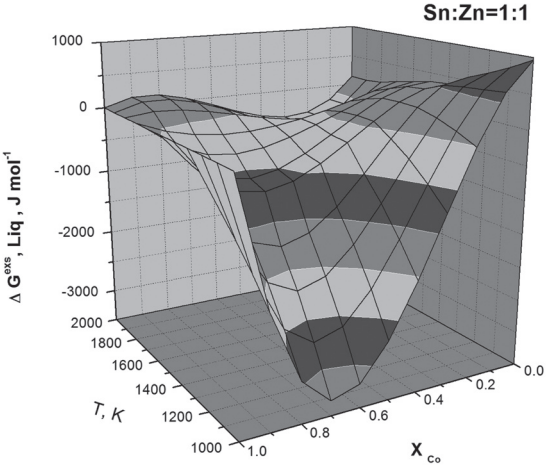

Figure 5: *Ternary molar Gibbs excess energies calculated along the selected sections and at the retained temperatures.*

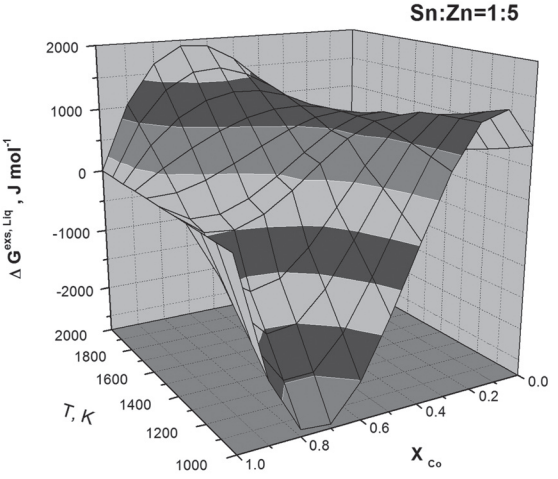

Figure 6: *Ternary molar Gibbs excess energies calculated along the selected sections and at the retained temperatures.*

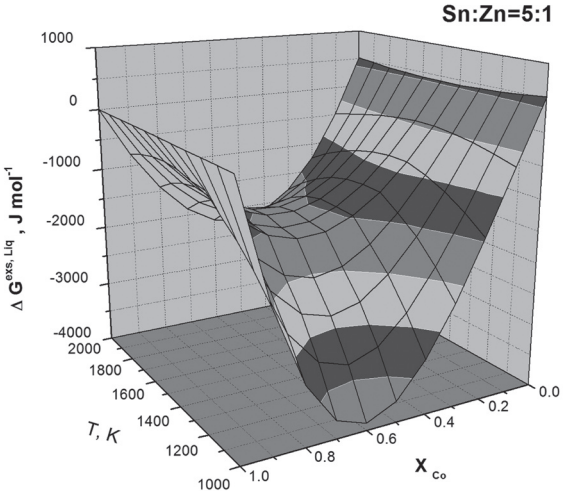

Figure 7: *Ternary molar Gibbs excess energies calculated along the selected sections and at the retained temperatures.*

Figures 8–10 presented comparative revue between molar Gibbs excess energies of the liquid phase calculated at 1 973 K with binary coefficients of liquid phase[4–6] and with ternary coefficients obtained in this work. At calculations with molar ratios Sn : Zn equal to 1 : 1 and 5 : 1 observed that Gibbs energy calculated with ternary coefficients is more negative then calculated with binary parameters only. At Sn : Zn ratio equal to 1 : 5 appeared positive values of molar Gibbs excess energy with binary and ternary parameters. This is probably connected with miscibility gap in Co-Zn corner in the ternary phase diagram.

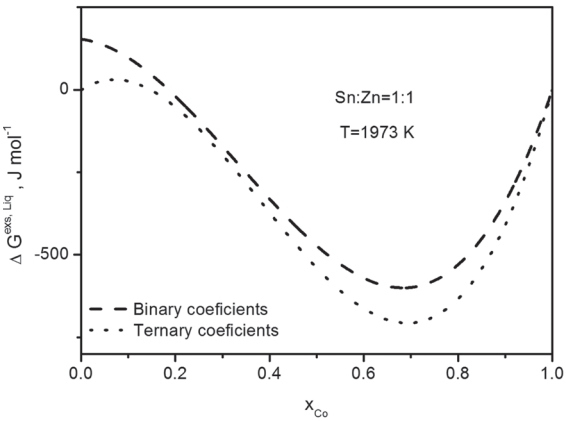

Figure 8: *Comparative analysis between Gibbs free energy of the liquid phase, along a section with constant molar Sn : Zn ratio equal to* 1 : 1.

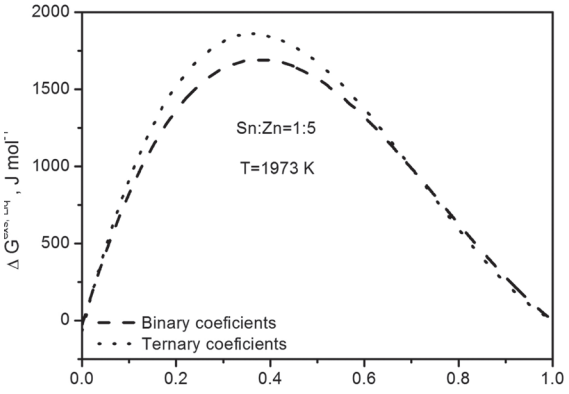

Figure 9: *Comparative analysis between Gibbs free energy of the liquid phase, along a section with constant molar Sn : Zn ratio equal to* 1 : 5.

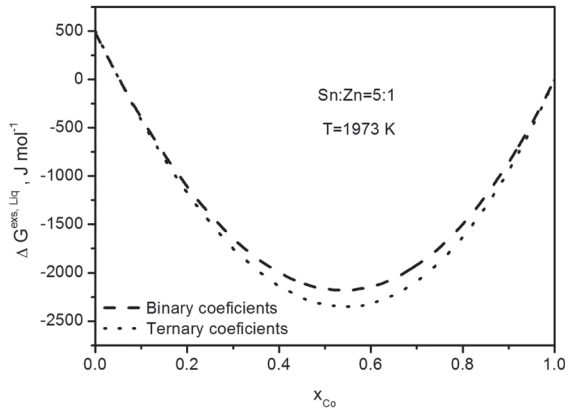

Figure 10: *Comparative analysis between Gibbs free energy of the liquid phase, along a section with constant molar Sn : Zn ratio equal to* 5 : 1.

Conclusion

Some thermodynamic properties of the Co–Sn–Zn liquid phase were predicted using the general solution model developed by Chou and have been compared with different geometrical models. The general solution model have middle place between symmetrical and asymmetrical models and give possibilities for estimating thermodynamic properties and calculating phase diagrams for ternary systems.

Ternary interaction parameters (L^0, L^1 and L^2) of the liquid phase have been determined using General solution model from thermodynamic data of the binary end–systems (Co–Sn, Co–Zn, Sn–Zn). The values of ternary parameters are: L^0 = +2 384.018 – 0.7073 * T; L^1 = +1 879.167–0.0547 * T; L^2 = +1 622.753–0.065 * T. The comparative analyses were performed between

Gibbs free energy of the liquid phase with ternary parameters obtained in this work and with binary parameters of each binary system. Good agreement was found indicating that such an approach was possible in systems where no experimental data were available.

References

[1] Chen, S. W., Wang, C. H., Lin, S. K. (2007): Phase diagrams of Pb-free solders and their related materials systems. *J. Mater. Electron.,* 18, pp. 19–37.

[2] Directive 2002/95/EC of the European Parliament and of the Council of 27 January 2003 on the restriction of the use of certain hazardous substances in electrical and electronic equipment (2003), *Official Journal of the European Union*, L37, pp. 19–24. Available on: <http://europa.eu. int/eurlex/>.

[3] Ipser, H., Mikula, A. (2001): Memorandum of Understanding for the Implementation of a European Concerted Research Action Designated as COST 531 "Lead-free solder materials", University of Vienna. Available on: <http://www.univie.ac.at/cost531>.

[4] Vassilev, G. P., Lilova, K. I. (2006): Contribution to the thermodynamics of the Co-Sn system. *Archives of metallurgy and materials*, 51, pp. 365–375.

[5] Vassilev, G. P., Jiang, M. (2004): Thermodynamic Optimization of the Co-Zn System. *Journal of Phase Equilibria and Diffusion,* 25, pp. 259–268.

[6] Dinsdale, A., Watson, A., Kroupa, A., Vrestal, J., Zemanova, A., Vizdal, J. (2008): Atlas of Phase Diagrams for the Lead-Free Soldering, COST 531 (Lead-free Solders), Printed in the Czech Republic, Vol. 1.

[7] Kohler, F. (1960): Zur Berechnung der thermodynamischen Daten eines ternären Systems aus den zugehörigen binären Systemen. Monatshefte fur Chemie, 91, pp. 738–740.

[8] Toop, G. W. (1965): Predicting ternary activities using binary data. *Trans. Metal Societe.*, 233, pp. 850–854.

[9] Hilert, M. (1980): Empirical Methods of predicting and representing thermodynamics properties of ternary solution phases. *Calphad*, 4, pp. 1–12.

[10] Chou, K. C. (1995): A general solution model for predicting ternary thermodynamics properties. *Calphad*, 19, pp. 315–325.

[11] Chou, K. C., Li, W. C., Li, F., He, M. (1997): Formalism of new ternary model expressed in terms of binary regular-solution type parameters. *Calphad,* 20, pp. 395–406.

[12] Živković, D., Katayama, I., Yamashita, H., Manasijević, D., Živković, Ž. (2006): Investigation of the thermodynamic model and ternary interaction parameter influence for Sn-Ag-Bi liquid alloys. *RMZ - Materials and Geoenvironment,* 53, pp. 155–161.

[13] Marjanović, S., Manasijević, D., Živković, D. Gusković, D., Minić, D. (2009): Calculation of thermodynamic properties for ternary Ag–Cu–Sn system. *RMZ – Materials and Geoenvironment,* 56, pp. 30–37.

[14] Živković, D., Manasijević, D., Mihajlović, I., Živković, Ž. (2006): Calculation of the thermodynamic properties of liquid Ag–In–Sb alloys. *Serb. Chem. Soc.,* 71, pp. 203–211.

[15] Andersson, J. O., Helander, T., Höglund, L., Shi, P., Sundman, B. (2002): Thermo-Calc & DIictra, Computational Tools For Materials Science. *Calphad,* 26, pp. 273–312.

[16] Redlich, O., Kister, A. (1948): Algebraic Representation of Thermodynamic Properties and the Classification of Solutions. *Industrial Engineering Chemistry*, 40, pp. 345–348.

[17] Gandova,V., Vassilev, G. (2013): Comparative analyses of thermodynamic properties assessments, performed by geometric models: application to the Ni–Bi–Zn system. *J. Min. Metall. Sect. B-Metall.,* 49, pp. 347–352.

Original scientific paper

Received: June 16, 2014
Accepted: January 30, 2015

Fragility curves of RC columns estimated by the CAE method

Ocena krivulj ranljivosti AB-stebrov s CAE-metodo

Klemen Sinkovic, Iztok Perus*
University of Ljubljana, Faculty of Civil and Geodetic Engineering, Jamova cesta 2, 1000 Ljubljana, Slovenia
*Corresponding author. E-mail: iperus@siol.net

Abstract

In the paper an alternative empirical approach for the estimation of fragility curves for RC columns is proposed. The CAE (Conditional Average Estimator) method was used. The procedure includes the LHS method, which was applied in order to take into account different uncertainties. The result of the study are estimated fragility curves for typical reinforced concrete (RC) columns (1) designed without seismic detailing, (2) designed according to first seismic codes used in the former Yugoslavia and (3) designed according to Eurocode 8. The obtained results clearly reveal the higher deformation capacity of RC columns, designed according to Eurocode 8. Additionally, the fragility curves related to various damage states, i.e. concrete crushing, longitudinal bar buckling, and longitudinal bar fracture were estimated. It is concluded that the proposed procedure offers a viable alternative to existing approaches.

Key words: CAE method, drift, fragility, RC columns, performance-based earthquake engineering (PBEE)

Izvleček

V prispevku je predlagan alternativni empirični način za oceno krivulj ranljivosti za armiranobetonske (AB) stebre. Uporabljena je bila CAE-metoda s cenilko pogojnega povprečja. Postopek vključuje tudi LHS-metodo, ki je bila uporabljena z namenom upoštevanja različnih negotovosti. Rezultati študije so ocene krivulj ranljivosti tipičnih AB-stebrov treh različnih obdobij, in sicer za (1) AB-stebre, projektirane brez potresnih predpisov, (2) AB-stebre, projektirane v skladu s prvimi potresnimi predpisi v nekdanji Jugoslaviji, in (3) AB-stebre, projektirane v skladu s predpisi Evrokod 8. Dobljeni rezultati jasno kažejo na večjo deformacijsko kapaciteto stebrov, projektiranih po predpisih Evrokod 8. Dodatno so bile krivulje ranljivosti ocenjene tudi za druga stanja poškodovanosti, kot je drobljenje betona, lokalni uklon vzdolžne armature in zlom vzdolžne armature. Mogoče je skleniti, da predlagani postopek ponuja dobro alternativo sedanjim načinom.

Ključne besede: CAE-metoda, zamik, ranljivost, AB-stebri, potresno inženirstvo

Introduction

In contrast to many of the existing models for the prediction of the deformation capacity of RC columns, which provide only deterministic (point) estimations, in the performance-based design of seismic resistant buildings predictive capacity models that are unbiased and explicitly account for all the uncertainties are needed. Only in probabilistic models of capacity is variability explicitly taken into account[1]. The aim of the paper is thus to propose an alternative method for the estimation of fragility curves for RC columns, which is based on the CAE probabilistic drift capacity model.

As well as in performance-based seismic design, fragility curves are very important for the estimation of the overall risk to the civil infrastructure in earthquake-prone areas. They can be used for emergency response and disaster planning by local and national authorities. Insurance companies can use them to make assessments of potential losses due to a particular scenario earthquake. Due to their numerous possible applications, a number of different research projects have been carried out worldwide. For example, Singhal and Kiremidjian[2] presented vulnerability curves and damage probability matrices for low-, mid- and high-rise RC frame structures, using Monte Carlo simulation techniques and non-linear dynamic analyses. Dumova-Jovanoska[3] presented damage probability matrices and damage indices as functions of intensity for different damage states for selected RC frame and RC wall-frame structures. Kappos et al.[4] applied a hybrid approach for the development of vulnerability curves for reinforced concrete and unreinforced masonry structures in terms of peak ground acceleration and spectral displacement. Panagiotakos and Fardis[5] evaluated the performance of generic archetypal RC buildings according to Eurocode 8, using non-linear analyses. This study was later upgraded by the development of corresponding fragility functions[6]. Akkar et al[7] estimated vulnerability curves for low- and mid-rise infilled frame RC buildings. Push-over analyses of a number of existing buildings in Duzce were performed for buildings with a low-level of seismic design, having between two and five storeys. Good agreement of the estimated vulnerability curves with observed damage after the 1999 Duzce earthquake was observed. Rossetto & Elnashai[8] produced vulnerability curves for low-rise infilled RC frames, designed on the basis of the old Italian seismic code. The proposed analytical curves are in reasonable agreement with the empirical curves. There are several other applications. A more detailed survey of works related to fragility can be found in[6], and on the probabilistic approach to capacity models in[9].

Due to the complexity of the problem, fragility studies generally focus on generic types of structures[6]. Consequently, simplified structural models, having properties that account for the uncertainties and randomness in the structural parameters, are used to mathematically represent real buildings. The fragility curves are then presented as a function of different intensity measures, *IM*, (e.g. *PGA*, *PGV*, S_a, S_d) for different types of structures, different numbers of storeys, etc., taking into account different damage states (e.g. yielding, collapse). Fragility curves can be presented for buildings as a whole or for any of their structural elements. In the latter case, demand can also be expressed in terms of deformation, not only in terms of *IM*. This is because the fragility of a structural member is defined as the conditional probability of failure for given values of the selected demand parameter. Hence, fragility curves can be obtained by simulations of the seismic response of structures at varying demand thresholds. Moreover, by ignoring the uncertainty in the demand, each fragility curve can display the probability that the capacity is less than or equal to a particular displacement/drift demand[1].

Empirical, expert opinion based, analytical and hybrid methods can be used for the assessment of fragility curves. In this paper an empirical approach to the estimation of the fragility curves of RC columns using the CAE method is presented. For example, the fragility of a RC column can be defined as the conditional probability of failure (at an ultimate drift defined at a 20 % drop in maximum strength) for given values of drift demand. Additionally, fragility can be derived in terms of other damage states, e.g. concrete crushing, longitudinal bar buckling, longitudinal bar fracture and axial loss

failure. In this paper the CAE method is briefly presented. The different databases used in the study are described. The obtained results are verified by making comparisons with existing solutions from the literature. Fragility curves for typical RC columns, designed without seismic detailing, designed according to the first seismic codes used in the former Yugoslavia, and designed according to EC8, are provided as the results of the study.

Procedure for the estimation of fragility curves

The CAE method

The fragility curves presented in this study are estimated by the CAE method. A detailed description of this method from the engineering point of view is given in Peruš et al.[10]. Here only a brief description is given.

The phenomenon of the capacity of RC columns and then the estimation of the corresponding fragility curves can be described by observing *N* RC column specimens during the experiments. The mathematical description of the observation of one specimen during the experiment is called a model vector. As a result, the whole phenomenon can be described by a finite set of model vectors.

$$\{\boldsymbol{X_1}, ..., \boldsymbol{X_n}, ..., \boldsymbol{X_N}\} \tag{1}$$

It is assumed that the observation of one particular specimen can be described by a number of variables, which are treated as components of a model vector

$$\boldsymbol{X_n} = \{b_{n1}, ..., b_{nl}, ...,b_{nD}, c_{n1}, ..., c_{nk}, ...,c_{nM}\} \tag{2}$$

The vector $\boldsymbol{X_n}$ can be further composed of two truncated vectors $\boldsymbol{B}$ and $\boldsymbol{C}$

$$\boldsymbol{B_n} = \{b_{n1}, ..., b_{nl}, ...,b_{nD}\} \text{ and} \quad \boldsymbol{C_n} = \{c_{nl}, ..., c_{nk}, ...,c_{nM}\} \tag{3a}$$

Vector $\boldsymbol{B_n}$ is complementary to vector $\boldsymbol{C_n}$ and therefore their concatenation yields the complete data model, vector $\boldsymbol{X_n}$. The prediction vector, too, is composed of two truncated vectors, i.e., the given truncated vector $\boldsymbol{B}$ and the unknown complementary vector $\hat{\boldsymbol{C}}$

$$\boldsymbol{B} = \{b_1, ..., b_l, ...,b_D\} \text{ and} \quad \hat{\boldsymbol{C}} = \{\hat{c}_1, ..., \hat{c}_k, ...,\hat{c}_M\} \tag{3b}$$

The problem now is how an unknown complementary vector $\hat{\boldsymbol{C}}$ can be estimated from a given truncated vector $\boldsymbol{B}$ and the model vectors $\{\boldsymbol{X_1}, ..., \boldsymbol{X_n}, ..., \boldsymbol{X_N}\}$, i.e., how the drift capacity δ can be estimated from known input parameters and the available data in the database. By using the conditional probability density function, the optimal estimator for the given problem can be expressed as

$$\hat{\delta} = \sum_{n=1}^{N} \delta_n A_n \tag{4}$$

where

$$A_n = \frac{a_n}{\sum_{i=1}^{N} a_i} \tag{5}$$

and

$$a_n = \frac{1}{(2\pi)^{D/2} w_n^D} \exp\left[-\sum_{l=1}^{D} \frac{(b_l - b_{nl})^2}{2w_n^2}\right] \tag{6}$$

Note that in the above equations *M* is assumed to be 1 and consequently $\hat{c}_1 = \hat{\delta}$.

In equations (4–6) δ is an estimate of the displacement/drift at failure or any other damage state (e.g. flexural and shear failure, defined at a 20 % reduction in lateral strength, axial failure, bar buckling, etc.), δ_n is the same output variable corresponding to the *n*-th model vector in the database, *N* is the number of model vectors in the database, b_{nl} is the *l*-th input variable (e.g. axial load index, P^*, shear span index, L^*) of the *n*-th model vector in the database, and b_l is the *l*-th input variable corresponding to the prediction vector. Note that each model vector corresponds to the results of one experiment from the database. *D* is the number of input variables, and defines the dimension of the sample space. A Gaussian function is used in order to achieve a smooth interpolation between the points of the model vectors. In this context the width w_n is called the "smoothing" parameter that corresponds to *n*-th model vector from the

database. In our case the same width w_n of the Gaussian function is used for all the input variables. It is therefore important that the input parameters in the equation for a_n are normalized, i.e. generally in the range from 0 to 1.

An intermediate result in the computational process is parameter $\hat{\rho}$, which is defined as:

$$\hat{\rho} = \frac{1}{N}\sum_{n=1}^{N} a_n \tag{7}$$

It provides a measure of how the influence of all the model vectors in the database is spread over the sample space, and strongly depends on the smoothing parameter *w*. It helps to detect possible less accurate predictions (indicated by low values of $\hat{\rho}$) due to the manner of data distribution in the database, and due to local extrapolation outside the data range.

When the expression for the displacement/ drift $\hat{\delta}$ at failure (Equation 4) is compared with the expression for the first order moment of the random variable *X*, which corresponds to the mean value m_x

$$E[X] = \sum_{i=1}^{N} x_i p_x(x_i) = m_x \tag{8}$$

the similarity between the two expressions becomes evident[11]. $p_x(x_i)$ is the probability of the random variable $X = x_i$ and corresponds to the weights A_n (Equation 5), which depend on the similarity between the input variables of the prediction vector, and on the corresponding input variables pertinent to the model vectors stored in the database. Also, there is clear similarity when the central second order moment of the probability distribution of the random variable *X*, called its variance, given by the expression

$$\mu_x = Var[X] = \sum_{i=1}^{N} (x_i - m_x)^2 p_x(x_i) \tag{9}$$

is compared with the prediction of so-called "local standard deviation" in the CAE method:

$$\hat{E}_\sigma^2 = \sum_{n=1}^{N} (\delta_n - \hat{\delta})^2 A_n \tag{10}$$

The above interpretation of the CAE equations enables the estimation of the corresponding probability distribution, including the median value, as well as different percentile values. The proposed procedure is demonstrated by the simple example presented in Appendix A.

The LHS method

The LHS (Latin hypercube sampling) method was first described by Mackay et al.[12] and then further elaborated by Iman et al.[13]. The method, which has become increasingly popular, was used in this study in order to take into account different uncertainties (e.g. aleatory and epistemic). Aleatory uncertainties, which are inherent in the phenomenon itself, are irreducible, and cannot be influenced by the observer or the manner of observation. On the other hand, epistemic uncertainties arise from errors in measurement, from the finite size of the available observation data, and from the adopted mathematical model. Note that in the presented study no distinction was made between these two types of uncertainties.

LHS allows the creation of experimental samples with as many points as needed or desired[14]. (Note, however, that the number of samples needed should not be too low[15].) It permits the use of very different statistical assumptions, and is able to treat both small and large design spaces (there are no constraints in terms of the data density and location). Additionally, LHS is flexible. If, for example, a few dimensions have to be dropped out, the resulting design is still a Latin hypercube. Moreover, the existing data can be reused without having to make any reduction in the number of sampled points.

The use of LHS in its basic form does not account for any possible correlations between the variables. However, in earthquake engineering, some of the parameters of the RC structural elements are correlated (e.g. the yield strength of the reinforcement, and the concrete compressive strength), so some authors have made us of more advanced variants of LHS (e.g.[15–17]). In the presented study, however, derived input parameters were used, and since it was assumed that they are independent, a basic variant of LHS was used. This is well-justified since parametric studies (not presented here) have shown that the influence of derived input parameters has only a minor effect on the results presented in this study.

The databases used in the study

The application of the CAE method requires a representative database, many different databases of RC structural elements being presently available (e.g.[1, 10, 18–29]). The deformation capacity expressed in terms of ultimate drift, representing a "near collapse" limit state, which is used in this study, is defined as a drift at a predefined drop below maximum strength. A 20 % drop in maximum strength (i.e. when the restoring force reaches 80 % of its maximum value) is commonly used, although this definition may significantly underestimate the true axial load-carrying capacity of the columns. In other cases, when lateral force resistance in columns is not reached because of premature load reversal, and also in cases, when deformation capacity is not reached because of limitation in the applied maximum displacement, the measured maximum drifts provided a lower bound of the deformation capacity.

For validation and comparison purposes, the first database used in the study was the database on RC columns at axial failure[1]. In this paper it is called the DB1 database, and contains data on 28 RC column specimens. Only two input parameters are considered, namely the normalized axial load and the parameter *s/d*, which is related to the confinement (*s* is the hoop spacing, and *d* is the depth to the centre-line of the outermost tension reinforcement).

For the estimation of fragility curves for RC columns which failed in flexure, the PEER database was used[18]. The same input parameters as proposed by Perus et al.[10] were taken into account (i.e. an axial load index, a shear span index, the concrete compressive strength, the confinement effectiveness factor multiplied by the confinement index and the longitudinal reinforcement index). The effective database was called DB2, and contains data on 156 RC column specimens. In order to develop fragility curves for other damage states, different from flexural or axial failure, an effective database, derived from the PEER database, and called the DB3 database, was used. It contains data on 80, 20 and 38 RC column specimens for which the drift at concrete crushing, longitudinal bar buckling, and longitudinal bar fracture, respectively, was measured.

Fragility curves of RC columns

Comparison with the existing solution

In this section the results obtained by using the proposed procedure are compared with the results of the existing solution. It is assumed that all the random variables which account for different uncertainties in the input parameters (e.g. the material properties and the applied loads) are log-normally distributed.

Fragility curves for axial failure were estimated, using the database DB1. The following two parameters and corresponding coefficients of variation were taken into account:

— the axial load index ($P^* = P/P_o$; [0.07–0.22]): $CoV = 0.11$;
— the parameter *s/d*, related to the confinement [0.6–1.23]: $CoV = 0.02$

Note that the bounds which are used in the normalization process of the CAE method (see[10]) take into account the distribution of the two input parameters in the database DB1.

By means of the LHS method, a database with 500 samples for each of the columns (3CLH18 and 2CLD12) from Zhu et al.[1], taking into account different uncertainties, was prepared. The CAE method was then applied. Due to the small number of input parameters, the smoothing parameter was given values of $w_{min} = 0.05$ and $w_{max} = 0.1$.The drift point estimates (i.e. the mean and the local standard deviation) at axial failure were determined, using Eqs. 4–6 and 10, as a function of the axial load index and the parameter *s/d*. Considering Eqs. 4 and 8–10, the CAE empirical cumulative distribution function (CDF) was determined for each sample from the LHS generated database. The corresponding smoothed CDF for the median drift values, as well as for the 15 % and 85 % bounds, were then calculated. The estimate is based on the counted values obtained from the CAE empirical CDF.

The results presented in Figure 1 indicate relatively good agreement between the CAE approach and the approach proposed by Zhou et al.[1]. The discrepancy between the results can be attributed to the functional form, which is not *a priori* assumed in case of the CAE method. The CAE functional form follows the data more closely, which can, however, in some cases

(e.g. extrapolation) lead locally to illogical results. In the presented case, the ρ value (Equation 7) amounts to 0.6 and 1.2 for both of the RC sample columns, respectively. The relatively high values indicate accurate CAE predictions. The observed discrepancy between the results suggests that the uncertainties may be different (i.e. higher) to those usually estimated.

Fragility curves of flexural failure for different designs of RC columns

Fragility curves corresponding to flexural failure for different designs of RC columns (designed without seismic detailing - NO, designed according to first seismic codes used in the former Yugoslavia – YU, and designed according to Eurocode 8 – EC8) were estimated by CAE, using database DB2. Five input parameters were taken into account, with the following statistical parameters:

- axial load index ($P^* = P/P_o$): $CoV = 0.11$,
- shear span index ($L^* = L_V/h$): $CoV = 0.05$,
- concrete compressive strength ($f_c^{'}$): $CoV = 0.05$,
- confinement index ($\rho_s^* = \rho_s f_{ys}/f_c^{'}$): $CoV = 0.08$
- longitudinal reinforcement index ($\rho_l^* = \rho_l f_{yl}/f_c^{'}$): $CoV = 0.08$.

Fragility curves were estimated for $L^* = 3.5$ and three different values of P^*, which amounted to 0.05, 0.15 and 0.25, respectively. Additionally, in the case of the RC columns designed without seismic detailing, a fragility curve for $P^* = 0.35$ was estimated. (Here it should be noted RC columns in such older buildings are, in many cases, heavily loaded due to the applied vertical loads.) Mean values of other three input parameters were assessed from the collected data on past designs. Note that only data on columns in the first storey, which is usually the critical one, were taken into account. The mean values and corresponding coefficients of variations, which account for different uncertainties, are presented in Table 1.

The results which correspond to fragility curves with an 85 % confidence level are presented in Figure 2. A very small difference in the drift capacity between the RC columns designed without seismic detailing and RC columns designed according to YU codes can be observed. Table 1

Table 1: *Mean values and corresponding coefficients of variation which accounts for different uncertainties*

	NO	YU	EC8
ρ_s^*	0.002 / 0.51	0.002 / 0.51	0.05 / 0.22
ρ_l^*	0.15 / 0.41	0.15 / 0.22	0.2 / 0.22
$f_c^{'}$	20 / 0.21	25 / 0.21	30 / 0.21

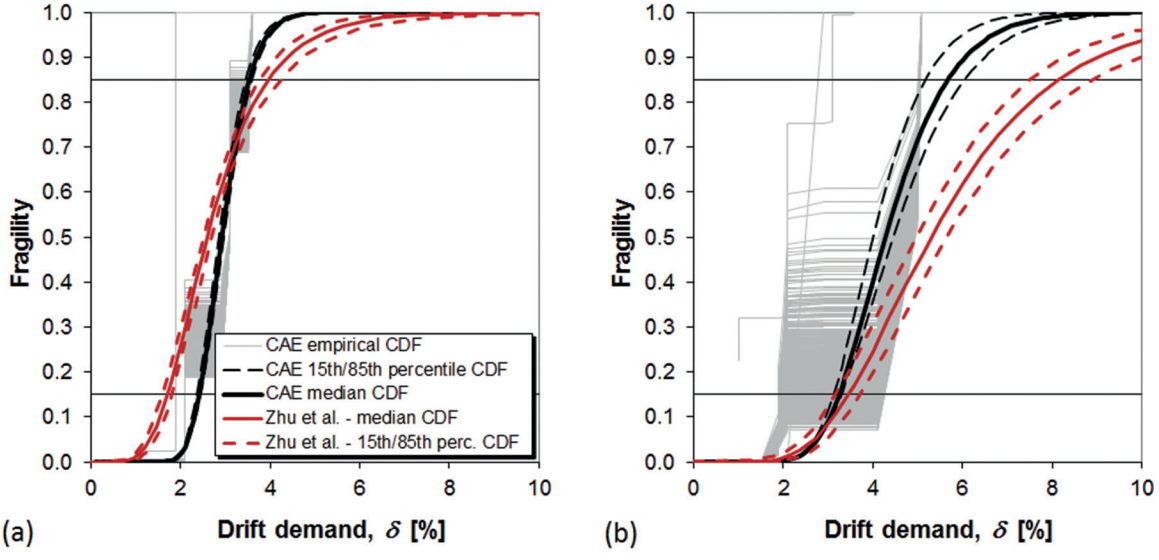

Figure 1: *Fragility estimates for RC columns at axial failure for (a) column 3CLH18 and (b) column 2CLD12[1]. Shown are discrete empirical CDF, obtained by the CAE method and by the corresponding smoothed (log-normal) CDF, and the same estimates, as obtained by Zhu[1].*

reveals, that the most notable change in the input parameters is the increase in concrete compressive strength, which only slightly improves the drift capacity and decreases dispersion. It should be noted, that despite of validation of YU codes for that particular time of being, the requirements for shear reinforcement were insufficient, which can be also observed from the data, taken from actual designs of buildings.

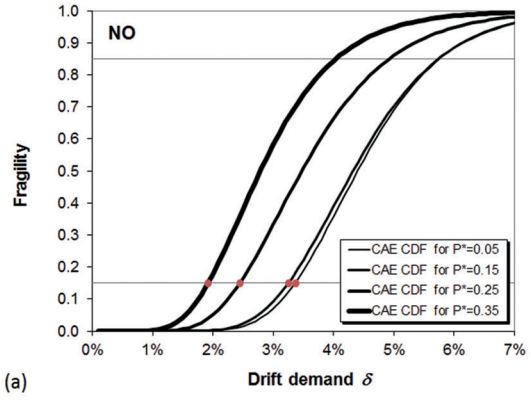

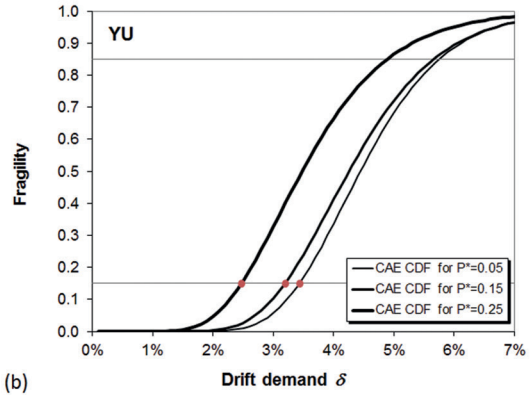

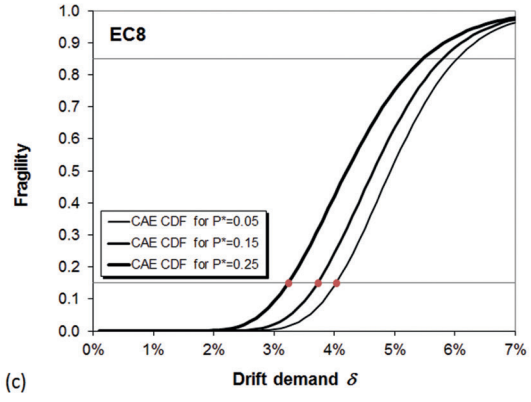

Figure 2: *Fragility curves with an 85 % confidence level for a typical column, designed (a) without seismic codes, (b) according to seismic codes used in the former Yugoslavia, and (c) according to the EC8 code. In all cases L^* amounts to* 3.5.

An important increase in drift capacity can be observed in the case of Eurocode 8, where all three parameters, especially the shear reinforcement which can significantly contribute to the drift capacity, are also increased. RC columns designed without seismic detailing exhibit a surprisingly high drift capacity. In the case of Eurocode 8 the ultimate drift capacity is reduced by a corresponding factor due to poor seismic detailing and the use of smoothed bars. The presented results suggest that a better CAE model should include additional parameters which would take into account proper seismic detailing.

Fragility curves of RC columns for different damage states

Besides the fragility curves corresponding to flexural and axial failure, fragility curves can also be estimated for other damage states, e.g. concrete crushing, longitudinal bar buckling and longitudinal bar fracture. The procedure is the same, only a proper database is required. In order to demonstrate the estimation of fragility curves of RC columns for other damage states, the database DB3 was used. Note that in this case uncertainties were not taken into account. The results are compared with the measured drift obtained in the case of the pseudo-dynamic testing of the 3-storey SPEAR building[30], which is representative building of old constructions in southern European Countries without specific provisions for earthquake resistance. It was designed for gravity loads alone, using the concrete design code applying in Greece between 1954 and 1995, with the construction practice and materials typical of the early 70s: for a concrete a nominal strength f_c' = 25 MPa was assumed while based on the scarcity of the current production, it was only possible to find reinforcement with a characteristics yield strength larger than initially requested $f_y \approx 450$ MPa. The structure is regular in elevation since typical storey height is 3 m. The plan configuration is doubly non symmetric (Figure 3), with 2-bay frames spanning from 3 m to 6 m. Eight out of the nine columns have a square 25 cm × 25 cm cross-section (also the interior column C3), whereas the ninth column has a 25 cm × 75 cm cross section.

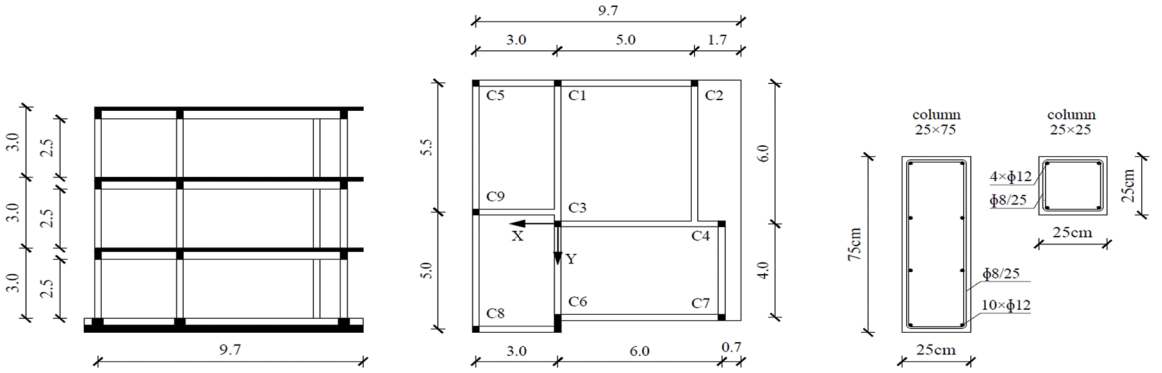

Figure 3: *The elevation view, the plan view and the typical reinforcement in RC columns of the SPEAR building.*

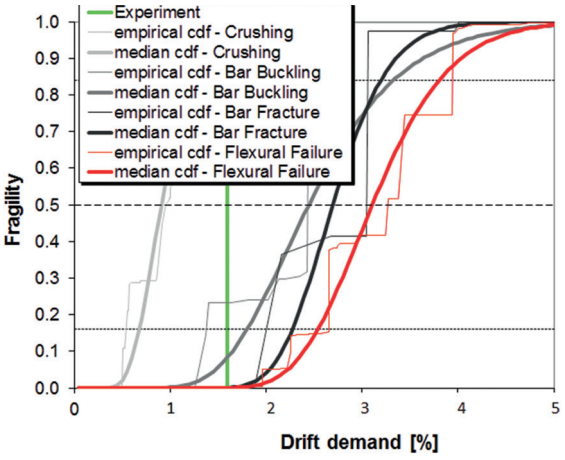

Figure 4: *Fragility curves at an* 85 % *confidence level for column C3 in the first storey of the SPEAR building. Considered are concrete crushing, longitudinal bar buckling, longitudinal bar fracture, and flexural failure of the column, respectively.*

Figure 4 reveals that concrete crushing should occur at early stages of the experiment. Figure 5 confirms the obtained result. Namely, extensive spalling and cracking was observed at the top of the column. The estimated smoothed CDF indicates that neither longitudinal bar buckling, nor longitudinal bar fracture or ultimate drift was achieved. Indeed, the ultimate drift was not achieved, and other heavy damage was not observed. At an 85 % confidence level, longitudinal bar buckling is expected at the increased drift (approx. 1.8 %). This may be followed by longitudinal bar fracture at 2.3 % drift. Flexural failure may be expected at a drift of 2.6 %.

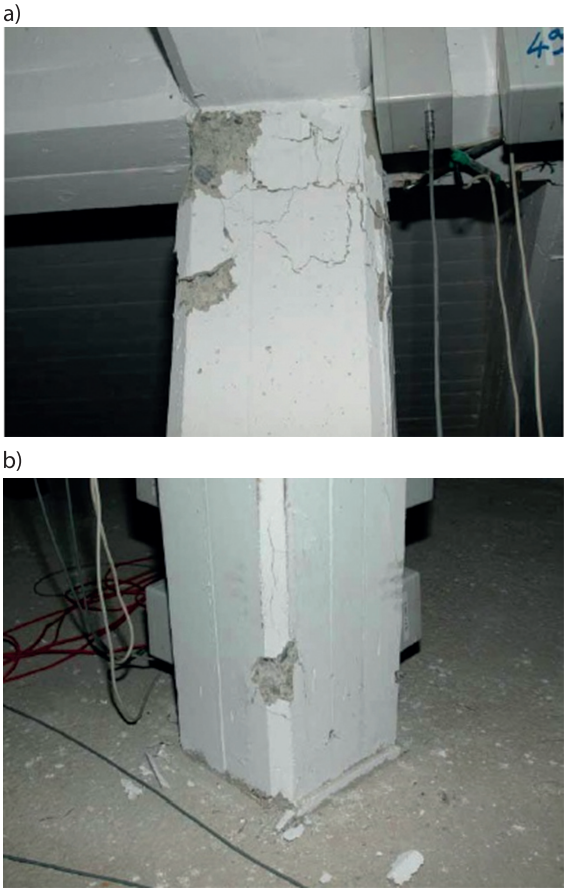

Figure 5: *Damage after the PGA* = 0.2 g *pseudo-dynamic testing of the SPEAR building*[30]*: (a) extensive spalling at the top of the column, and (b) minor damage at the base of the column.*

Conclusions

In the paper an empirical approach to the estimation of fragility curves of RC columns using the CAE method is presented. The LHS method was applied in order to take into account different uncertainties.

As a result of the study fragility curves at an 85 % confidence level for typical RC columns, designed without seismic detailing, according to first seismic codes in the former Yugoslavia, and according to Eurocode 8 were proposed. The resulting increasing trend can be observed, while a small difference in the drift capacity was observed between the RC columns designed without seismic detailing and those designed according to the YU codes. Both types of columns were designed with relatively bad detailing for shear reinforcement and usually with smooth longitudinal reinforcement, which have the biggest role in case of EC8 codes and provide favourable flexural behaviour with adequate deformation capacity of RC columns. One of the possible reasons could be also the fact that the discussed existing buildings are not fully representative for buildings built before and after YU regulations. The other reason can be imperfect CAE model. Those differences were not fully discussed since the primary purpose of the article was to propose a relatively simple method for the determination of the fragility curves. On the other hand an important increase in drift capacity was observed in the case of EC8 codes, especially due to the increase and better detailing of shear reinforcement and also due to better detailing of longitudinal reinforcement with better material characteristics, which typically significantly contributes to the higher deformation capacity of RC columns.

Further research is still needed in order to increase the sample size of existing buildings designed according to YU codes, and to improve the presented CAE model. Obtained conclusions may be very general, but other specific statements could be highly speculative at the moment.

Fragility curves related to other damage states, i.e. concrete crushing, longitudinal bar buckling, and longitudinal bar fracture, were also estimated. It can be concluded that the proposed procedure offers a viable alternative to other procedures, and that there is no need to use closed-form equations for the prediction of point estimates. However, the presented results suggest that a better CAE model is needed to accurately describe the older designs of RC columns. It should include an additional parameter which would account for poor seismic detailing.

Appendix A

In order to better illustrate the use of the CAE method for the estimation the fragility curves, the calculations for the input data P^* = 0.25 and L^* = 3 are shown in Table A1. Note that, for illustration purposes, only two input parameters are considered. The database consists of 7 test samples of RC columns. Equations 1–7 are used, taking into account w = 0.15. It can be clearly seen that the influence of the 7 different input drift values (based on the results of measurements) on the predicted drift value depends on the similarity of the input parameters P^* and L^* between the measured and predicted deformation. The highest weight A_n is assigned to the sample #6 because its values of P^* = 0.27 and L^* = 2.4 are the nearest to the target values P^* = 0.25 and L^* = 3.

In the next step the drifts δ are sorted from the lowest to the highest value, together with the corresponding coefficients A_n (see Table A2). The results are presented in Figure A1, where

Table A1: *An example of the prediction of ultimate drift δ for P^* = 0.5 and L^* = 3 by the CAE method (w = 0.15)*

Sample	P^*	L^*	Norm. P^*	Norm. L^*	δ	a_n	A_n	$\delta_n A_n$	$(\delta_n-\delta)^2 A_n$
#1	0.13	1.50	0.74	0.70	0.034	0.042	0.015	0.000	0.000 006 20
#2	0.35	3.50	0.30	0.30	0.042	0.371	0.129	0.005	0.000 020 22
#3	0.05	2.10	0.90	0.58	0.049	0.016	0.005	0.000	0.000 000 17
#4	0.00	3.30	1.00	0.34	0.078	0.004	0.001	0.000	0.000 000 77
#5	0.18	2.80	0.64	0.44	0.063	0.703	0.244	0.015	0.000 017 46
#6	0.27	2.40	0.46	0.52	0.051	0.789	0.274	0.014	0.000 003 43
#7	0.21	3.15	0.58	0.37	0.057	0.957	0.332	0.019	0.000 002 01
					$\sum \rightarrow$	2.882	1.000	0.0545	0.000 050 26

δ_{mean} = 0.045 45;

$\sigma = \sqrt{0.00005026} = 0.0071$

the dotted line represents the values from the last column in Table A2 (CAE empirical CDF). The corresponding smoothed log-normal cumulative distribution function (smoothed CDF) is estimated from the mean and local standard deviation (δ_{mean} = 0.045 45, σ = 0.007 1), calculated above.

Table A2: *Determination of the CAE empirical and corresponding smoothed lognormal cumulative distribution function (CDF)*

Sample	δ	A_n	$\sum A_n$
#1	0.034	0.014 70	0.014 70
#2	0.042	0.128 61	0.143 31
#3	0.049	0.005 43	0.148 74
#6	0.057	0.273 78	0.422 52
#7	0.063	0.332 18	0.754 70
#5	0.068	0.243 90	0.998 61
#4	0.081	0.001 39	1.000 00

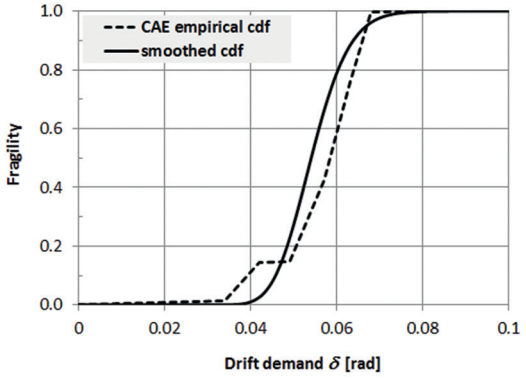

Figure A1: *Fragility function determined from the CAE empirical CDF and the corresponding smoothed lognormal CDF.*

Acknowledgements

The results presented in this paper are based on work supported by the Slovenian Research Agency. The constructive comments provided by Prosessors P. Fajfar and M. Dolšek are greatly appreciated.

References

[1] Zhu, L., Elwood, K. J., Haukaas, T. (2007): Classification and seismic safety evaluation of existing reinforced concrete columns. *Journal of Structural Engineering*, 133 (9), pp. 1316–1330.

[2] Singhal, A, Kiremidjian, A. (1995): *Method for developing motion damage relationships for reinforced concrete frames*, Report #115, Blume Earthquake Engineering Centre, Stanford University, Stanford.

[3] Dumova-Jovanoska, E. (2000): Fragility curves for reinforced concrete structures in Skopje (Macedonia) region. *Soil Dynamics and Earthquake Engineering,* 19 (6), pp. 455–466.

[4] Kappos, A., Panagopoulos, G., Panagiotopoulos, C., Penelis, G. (2006): A hybrid method for the vulnerability assessment of R/C and URM buildings. *Bull. Earthquake Eng.,* 4, pp. 391–413.

[5] Panagiotakos, T. B., Fardis, M. N. (2004): Seismic performance of RC frames designed to Eurocode 8 or to the Greek Codes 2000. *Bulletin of Earthquake Engineering,* 2, pp. 221–259.

[6] Papailia, A. (2011): *Seismic fragility curves for reinforced concrete buildings*. MSc Thesis (Supervisor M. N. Fardis), University of Patras.

[7] Akkar, S., Sucuoglu, H., Yakut, A. (2005): Displacement-based fragility functions for low- and mid-rise ordinary concrete buildings. *Earthquake Spectra*, 21 (4), pp. 901–927.

[8] Rossetto, T., Elnashai, A. (2005): A new analytical procedure for the derivation of displacement-based vulnerability curves for populations of RC structures. *Engineering Structures,* 27 (3), pp. 397–409.

[9] Zhu, L. (2005): *Probabilistic drift capacity models for reinforced concrete columns*. MSc Thesis (Supervisor K. J. Elwood, Co-supervisor T. Haukaas), The University of British Columbia.

[10] Perus, I., Poljansek, K., Fajfar, P. (2006): Flexural deformation capacity of rectangular RC columns determined by the CAE method. *Earthquake Eng. Struct. Dyn.*, 35 (12), pp. 1453–1470.

[11] Perus, I., Dolsek, M. (2009): The error estimation in the prediction of ultimate drift of RC columns for performance-based earthquake engineering. *RMZ-Mater. Geoenviron.*, 56 (3), pp. 322–336.

[12] McKay, M. D., Beckman, R. J., Conover, W. J. (1979): A Comparison of three methods for selecting values of input variables in the analysis of output from a computer code. *Technometrics,* 21, pp. 239–245.

[13] Iman, R. L., Helton, J. C., Campbell, J. E. (1981): An approach to sensitivity analysis of computer models, Part 1. Introduction, input variable selection and preliminary variable assessment. *Journal of Quality Technology,* 13, pp. 174–183.

[14] Viana, F. A. C. (2013): *Things you wanted to know about the Latin hypercube design and were afraid to ask*. 10th World Congress on Structural and Multidisciplinary Optimization, May 19–24, 2013, Orlando, Florida, USA.

[15] Dolsek, M. (2009): Incremental dynamic analysis with consideration of modeling uncertainties. *Earthquake Eng. Struct. Dyn.*, 38, pp. 805–825.

[16] Vorechovský, M., Novak, D. (2009): Correlation control in small-sample Monte Carlo type simulations I: A simulated annealing approach. *Probabilistic Engineering Mechanics,* 24, pp. 452–462.

[17] Dolsek, M. (2012): Simplified method for seismic risk assessment of buildings with consideration of aleatory and epistemic uncertainty. *Structure and Infrastructure Engineering: Maintenance, Management, Life-Cycle Design and Performance,* 8 (10), pp. 939–953.

[18] Berry, M., Parrish, M., Eberhard, M. (2004): PEER structural performance database, User's Manual, Version 1.0, 2004, Pacific Earthquake Engineering Research Center; Available on: < http://www.ce.washington.edu/~peera1/.>

[19] Panagiotakos, T. B., Fardis, M. N. (2001): "Deformations of reinforced concrete members at yielding and ultimate." *ACI Structural Journal*, 98 (2), pp. 135–148.

[20] Biskinis, D. E., Roupakias, G. K., Fardis, M. N. (2004): Degradation of Shear Strength of RC Members with Inelastic Cyclic Displacements. *ACI Structural Journal,* 101 (6), pp. 773–783.

[21] Biskinis, D. E. (2007): *Resistance and Deformation Capacity of Concrete Members with or without Retrofitting*. PhD Thesis (Supervisor M. N. Fardis), Civil Engineering Department, University of Patras, Greece. (in Greek).

[22] Biskinis, D. E., Fardis, M. N. (2010): Deformations at Flexural Yielding of Members with Continuous or Lap-Spliced Bars. *Structural Concrete,* 11 (3), pp. 127–138.

[23] Biskinis, D. E., Fardis, M. N. (2010): Flexure-Controlled Ultimate Deformations of Members with Continuous or Lap-Spliced Bars, *Structural Concrete,* 11 (2), pp. 93–108.

[24] Grammatikou, S. (2013): *Strength, deformation capacity and failure mode of RC walls in seismic loading*. MSc Thesis (Supervisor M. N. Fardis), Civil Engineering Department, University of Patras, Greece. (in Greek).

[25] Lignos, D. G., Krawinkler, H. (2012): *Sidesway collapse of deteriorating structural systems under seismic excitations*. Report No. 177, 2012, The John A. Blume Earthquake Engineering Center, Stanford, CA, USA.

[26] Lignos, D. G., Krawinkler, H. (2013): Development and utilization of structural component databases for performance-based earthquake engineering. *Journal of Structural Engineering*, Special issue 139, pp. 1382–1394.

[27] Poljansek, K., Perus, I., Fajfar, P. (2009): Hysteretic energy dissipation capacity and the cyclic to monotonic drift ratio for rectangular RC columns in flexure. *Earthquake Eng. Struct. Dyn.*, 38 (7), pp. 907–928.

[28] SERIES database (2013): RC column, beam and wall database. Available on: < http://www.dap.series.upatras.gr/>.

[29] Perus, I., Biskinis, D., Fajfar, P., Fardis, M. N., Grammatikou, S., Krawinkler, H., Lignos, D. (2014): *The SERIES database of RC elements*. 2nd European conference on Earthquake Engineering and Seismology, Istanbul, August 2014, Paper #145.

[30] Negro, P., Mola, E., Molina, F. J., Magonette, G. E. (2004): *Full-scale PSD testing of a torsionally unbalanced three-storey non-seismic RC frame*. 13th WCEE, Paper # 968, August 2004, Vancouver, B. C., Canada.

Original scientific paper

Received: December 11, 2014
Accepted: February 2, 2015

Geochemical and isotopic characterization of coalbed gases in active excavation fields at Preloge and Pesje (Velenje Basin) mining areas

Geokemijska in izotopska karakterizacija premogovnih plinov iz aktivnih odkopov rudarskih območij Preloge in Pesje (Velenjski bazen)

Tjaša Kanduč[1,*], Fausto Grassa[2], Jerneja Lazar[3], Simon Zavšek[3]

[1]Jožef Stefan Institute, Jamova cesta 39, 1000 Ljubljana, Slovenia

[2]Istituto Nazionale di Geofisica e Vulcanologia Sezione di Palermo, Via Ugo La Malfa, 153, 90146 Palermo, Italy

[3]Velenje Coal mine, Partizanska 78, 3320 Velenje, Slovenia

*Corresponding author. E-mail: tjasa.kanduc@ijs.si

Abstract

Coalbed gases in excavation fields of mining areas in the Velenje coal basin have been subjected to geochemical and isotopic monitoring since the year 2000, with the aim of obtaining better insights into the origin of coalbed gases. Results from active excavation fields in the mining areas Pesje and Preloge in the year 2013 are presented in this study. Composition and isotopic composition of coalbed gases were determined with methods utilizing mass spectrometry. The chemical and isotopic composition of coalbed gases in the Velenje Basin vary and depend on the composition of the source of coalbed gas before excavation, advancement of the working face, depth of the longwall face, pre-mining activity and newly mined activity. The basic gas components determined in excavation fields are CO_2 and methane. The isotopic composition of deuterium in methane has been determined and used to characterize the origin of methane. The isotopic compositions of carbon and hydrogen in methane in the excavation fields show its biogenic origin, while a high Carbon Dioxide Methane Index indicates the bacterial and endogenic origin of CO_2.

Key words: Characterization of coalbed gases, stable isotopes, excavation fields, Velenje Basin

Izvleček

Geokemijski in izotopski monitoring premogovnih plinov na aktivnih odkopih v rudarskih območjih Velenjskega premogovnega bazena poteka od leta 2000 z namenom pridobiti vpogled v sestavo premogovnih plinov in njihov izvor. V tem prispevku predstavljamo geokemične in izotopske parametre iz aktivnih rudarskih območij Pesje in Preloge v letu 2013. Sestavo in izotopsko sestavo premogovnih plinov smo ugotovili z metodami masne spektrometrije. Premogovni plini v Velenjskem bazenu se spreminjajo po kemijski, kot tudi po izotopski sestavi glede na izvorno sestavo premogovega plina pred odkopavanjem, hitrost odkopavanja, globino odkopnega čela, odkopna čela s predhodno rudarsko aktivnostjo ali na novo odkopana območja. Glavni plinski komponenti na odkopih sta CO_2 in metan. Na novo v tem prispevku predstavljamo rezultate izotopske sestave devterija v metanu, ki se uporablja za popolno karakterizacijo izvora metana. Rezultati izotopske sestave ogljika in vodika v metanu na aktivnih odkopih kažejo na biogeni izvor, medtem ko CO_2 na bakterijski in endogeni izvor, kjer se pojavlja visok indeks CO_2-metan (Carbon Dioxide Methane Index).

Ključne besede: karakterizacija premogovnih plinov, stabilni izotopi, aktivni odkopi, Velenjski bazen

Introduction

Unconventional gas resources, including coal bed methane and shale gas, are a growing part of the global energy mix, which has changed the economic and strategic picture for gas consuming and producing countries, including the USA, China and Australia that, together, are responsible for around half the currently recoverable unconventional gas resources[1]. Some other countries, including Canada, India and Indonesia, are also seeking to develop their CBM (Coalbed Methane) and shale gas resources. Exploration was initially focused on mature coals with high contents of what was thought to be thermogenic gas (e.g. Black Warrior, San Juan and Bowen basins). However, CBM production was often hindered by low permeability and mineralization in cleats and fractures, necessitating the development of cost effective horizontal drilling and completion techniques. CBM exploration then extended beyond the producing fields to lower rank coals and subsequently to less mature coal basins, in which it was thought that higher permeability and greater coal thickness would compensate for lower gas contents (e.g. Illinois, Powder River and Surat basins). Knowledge of the stable isotope geochemistry of coal bed and shale gas and the related production water is essential to determine not only gas origins but also the dominant methanogenic pathway in the case of microbial gas[2].

Evidence for the microbial origin of methane in low rank coals, the presence of secondary microbial gas at shallow levels in higher rank coals and the presence of secondary microbial gas at shallow levels in higher rank coals have been reviewed[3–7], providing an introduction to the use of compositional and isotopic parameters in determining the origin of CBM. However, the timing of methanogenesis, factors governing coal bioavailability and the process of stepwise microbial degradation of coal to methane remain topics of considerable interest to both researchers and industry in the light of possible stimulation of enhanced microbial methane generation from coal[8–10].

In like fashion to CBM, shale gas/coalbed gas can be of thermogenic, microbial or mixed origin, the distinction being made primarily on the basis of the stable isotope compositions of the gases and co-produced waters[11–13]. These studies have shown that the relative proportions of microbial and thermogenic gas are depth related, with deeper locations containing exclusively thermogenic gas and shallower locations a mixture of microbial and thermogenic gases.

The ranges in carbon isotope signatures from different sources (gas, solid and liquid phases) are presented in Figure 1. Microbial methane is enriched with ^{12}C, while methane associated with petroleum is treated as thermogenic in origin and is enriched with ^{13}C. Deep sourced CO_2 has $\delta^{13}C_{CO2}$ values of –7 ‰ (Figure 1). C_3 plants have $\Delta^{13}C$ values ranging from –30 ‰ to –20 ‰ and C_4 plants in the range from –18 ‰ to –10 ‰ (Figure 1). Vienna Pee Dee Belemnite (VPDB) is the reference material used for determining isotopic composition of carbon ($\delta^{13}C$), and has a default δ value of 0 ‰[14].

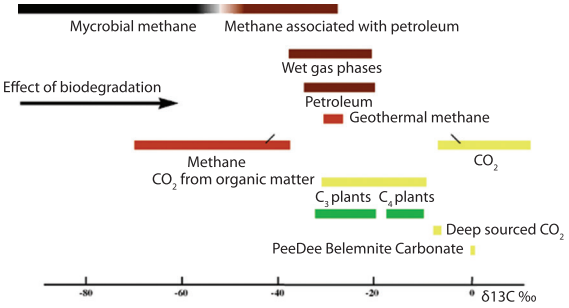

Figure 1: *Ranges in carbon isotope signatures from different sources[15].*

The geochemical and isotopic characterization in the period 2000–2012 of coalbed gases from different excavation fields from Velenje basin have been published[16–20]. Formation waters in Velenje Basin are not trapped in the coal seam, since large amounts of groundwater are extracted from Velenje Basin aquifers to facilitate underground mining of coal. Groundwater recharging the basin is therefore not in direct contact with the coal seam. Hydrogeochemical and isotopic characteristics of Velenje Basin groundwaters and their interactions with surface waters are described in[21].

The aim of this study is to account for the concentration, distribution and origin of coalbed gases ("free gas")[22, 23], including unconventional gas (methane), from the excavation fields

K.-65/F, G3/C, K.-65/B, K.-65/E and K.-65/C in mining areas Preloge and Pesje, based on geochemical and isotopic tracers. The new tracer, isotopic composition of methane (δD_{CH4}) was applied in this study for geochemical characterization of the origin of methane and was compared with values from other worldwide sedimentary basins.

Materials and methods

Coalbed gas was sampled by the operator-miner responsible for underground coalbed gas monitoring. Free gas includes both the volatiles filling the pores and cracks within the coal structure and some gas degassed from the coal during drilling and sampling[23]. Long boreholes (25 m) were used for monitoring coal gas concentration; the design of the borehole is described in[20]. Coalbed gases from the lignite seam were sampled at working faces Pesje K.-65/F, Preloge G3/C, Pesje K.-65/B, Pesje K.-65/E and Pesje K.-65/C and at boreholes jpk 62 + 10°, jpk 56 + 10°, jpk 63 + 10°, jpk 70 + 10°, jpk 73 + 10° (Figure 2). Lignite was produced by the Velenje Longwall Mining Method (VLMM), a longwall top coal caving method, as described in[20].

After drilling, a capillary tube was inserted in boreholes. "Free gas"[23] emitted from the borehole was collected in a plastic syringe 50 ml and transferred to a ampoule 12 ml, which was flushed and filled with coalbed gas under pressure. After sampling the "free gas" from the boreholes, the ampoules were stored under normal atmospheric conditions until analysis. Seven ampoules were filled at each location, the third being analyzed for chemical composition (CO_2, CH_4, O_2, N_2, Ar). The other ampoules were stored for determining the isotope composition of carbon in methane ($\delta^{13}C_{CH4}$), CO_2 ($\delta^{13}C_{CO2}$) and deuterium in methane (δD_{CH4}).

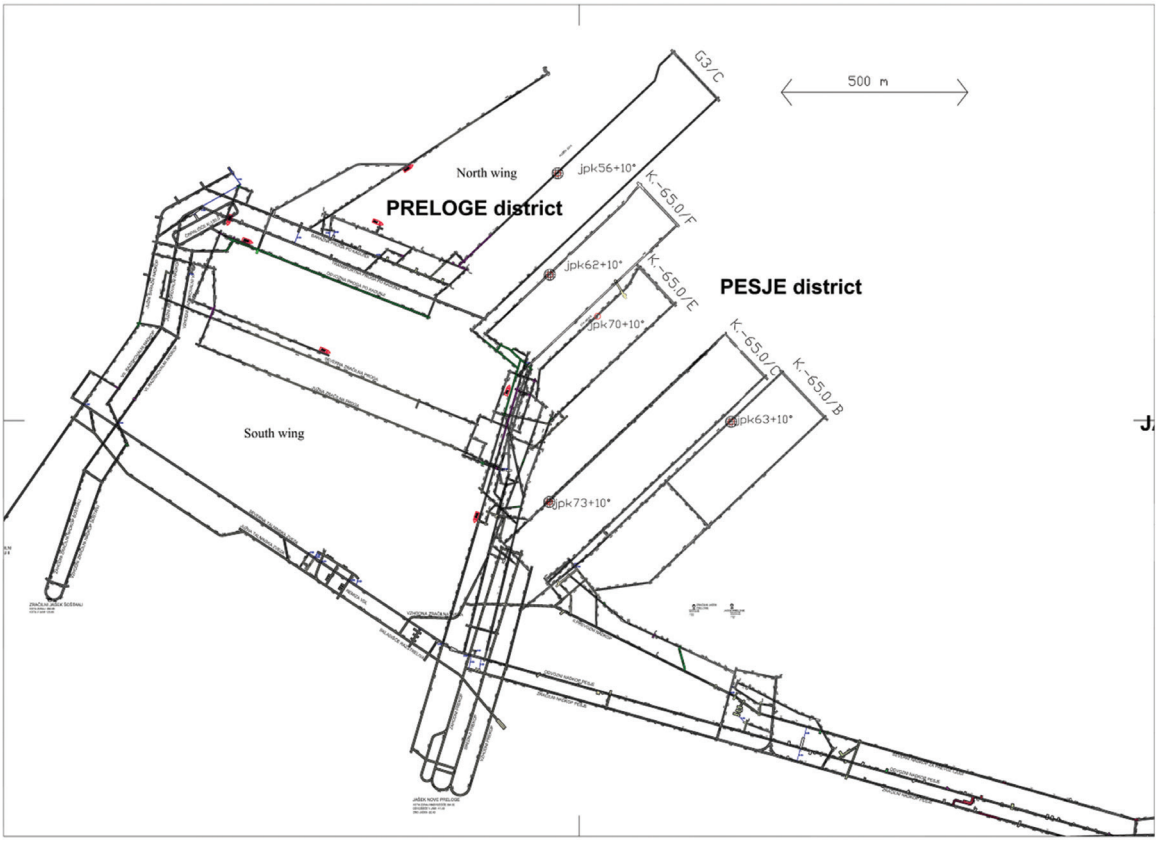

Figure 2: *Map of sampling locations of coalbed gases from the lignite seam at working faces: Pesje -65/F, Preloge G3/C, Pesje -65/B, Pesje -65/E and Pesje -65/C and boreholes: jpk* 62 + 10°, *jpk* 56 + 10°, *jpk* 63 + 10°, *jpk* 70 + 10°, *jpk* 73 + 10°.

Analytical procedure

Concentrations of methane, CO_2, nitrogen, oxygen and argon were determined using a homemade mass NIER spectrometer as described in detail in[18, 20].

The isotope compositions of methane and CO_2 were determined using an Europa 20–20 continuous flow isotope ratio mass spectrometer with an ANCA – TG preparation module. First, water was removed, then CO_2 was analyzed directly for ^{13}C content. For methane measurements CO_2 was removed and methane then combusted over hot 10 % platinum on CuO (1 000 °C). The methane, completely converted to CO_2, was then analyzed directly for the isotopic composition of carbon ($\delta^{13}C$). Working standards calibrated to IAEA (International Atomic Energy Agency) reference materials were used, with values of –4.3 ‰ for CO_2 and –53.4 ‰ for methane relative to Vienna Pee Dee Belemnite (VPDB). The analytical precision for carbon isotope composition is estimated to be ±0.2 ‰ for CO_2 and ±0.6 ‰ for CH_4. The stable carbon isotopes are presented in δ notation relative to VPDB standards and expressed in parts per million[14] as follows[24]:

$$\delta(^{13}C/^{2}H)_s = \frac{R_s - R_{RM}}{R_{RM}} \times 1000\ [‰] \quad (1)$$

Where:

R_s – ratio $^{13}C/^{12}C$ in sample

R_s – ratio $\delta^2H/\delta H$ in sample

R_{RM} – ratio $^{13}C/^{12}C$ and $^{2}H/H$ in reference material

The $^{2}H/H$ ratio of CH_4 was determined using a Thermo Delta XP GC-TC/CF-IRMS coupled to a TRACEGC analyzer at the Istituto Nazionale di Geofisica e Vulcanologia Sezione di Palermo in Italy. The method of $\delta^{13}C_{CH4}$ determination is described in detail in[20].

Results and discussion

Due to air contamination within the boreholes (used for ventilation of the coalmine) and the capillary system, samples were recalculated on an air-free basis. The percentage of oxygen in the sampled ampoules was used to calculate the amount of nitrogen, according to the ratio in air (N_2/O_2), considering Dalton's law[25]: methane migrates faster than CO_2. The major gas components were CO_2 and methane. Of all the samples analyzed (n = 72) in this study, seventeen were in excess in N_2. Concentrations of CO_2 ranged from 36.1 % to 98.2 % and methane from 1.8 % to 63.9 %. Geochemical indices, CDMI ($(CO_2/(CO_2 + CH_4) \times 100$ %) varied from 36.1 % to 98.2 % and stable isotope ratios varied in the following ranges: $\delta^{13}C_{CO2}$ from –11.0 ‰ to 1.9 ‰, $\delta^{13}C_{CH4}$ from –71.8 ‰ to –43.4 ‰, δD_{CH4} from –343.9 to –223.1 ‰ and $a_{CO2\text{-}CH4}$ from 1.040 to 1.071 (Table 1). The calculated gas dryness index ($C_1/(C_2 + C_3)$) ranged from $339.74 \cdot 10^{-6}$ to $23\,272.7 \cdot 10^{-6}$ and the coalbed gas is therefore considered as being dry, i.e. methane is the major gas component. The higher hydrocarbons determined in Velenje Basin were ethane, propane, iso-butane, *n*-butane, iso-pentane, *n*-pentane and hexane[20].

High correlation (R^2 = 0.99) was obtained between methane and CO_2 concentrations (Figure 3) in a lignite seam within boreholes: mining area Pesje K.-65/F, jpk 62 + 10°, mining area Preloge G3/C, jpk 56 + 10°, mining area Pesje K.-65/B 63 + 10°, mining area Pesje K.-65/E, jpk 70 + 10°, mining area Pesje K.-65/C, jpk 73 + 10°. Working faces from different mining areas exhibit different geochemical and isotopic compositions of coalbed gases, which also depend on the depth of the excavation field (Table 1). In addition, the total gas composition at pre-mined longwall panels and, on the other hand, at longwall panels located under fresh overburden can be different. It is known that the highest concentrations of methane gas are found at longwall panels located under fresh overburden. This occurrence is connected with the more rapid migration of CH_4 up through the seam due to its smaller molecular size than that of CO_2 and with the fact that CH_4 is a free gas in the Velenje lignite structure while CO_2 is adsorbed in the matrix of the coal. This fact applies only until the influence of active mining is not shown on the gas composition in the samples.

The high advancement rate of up to 9 m per day constitutes a potential for gas outbursts[18]. The rates of advancement of working faces in this study are as follows: Pesje working face K.-65/F, jpk 62 + 10° from 0.9 m/d to 3.5 m/d,

Preloge working face G3/C, jpk 56 + 10° from 3 m/d to 4 m/d, working face K.-65/B, jpk 63 + 10° from 0.8 m/d to 1.9 m/d, K.-65/E, jpk 70 + 10° from 1.7 m/d to 3.8 m/d and K.-65/C, jpk 73 + 10° 1.3 m/d (Table 1). The rate of advancement of the working face is low (range from 0.8 m to 1.9 m) at working face K.-65/B (mining area Pesje), jpk 63 + 10° due to the high CO_2 concentration and therefore higher risk of outburst generation. The areas of high and low methane concentrations (Figure 3) are in keeping with the physicochemical properties of CO_2 and methane[25]. This pattern is observed for all the excavation fields investigated in this study (Figure 3). Excavation fields K.-65/F, G3/C, K.-65/E and K.-65/C have higher ranges of gas concentrations than excavation field K.-65/B, where higher CO_2 concentration is observed (Figure 3).

Table 1: *Geochemical ccomposition of coalbed gases and isotopic compositions of carbon in CO_2 ($\delta^{13}C_{CO2}$) and methane ($\delta^{13}C_{CH4}$) at working faces K.-65/F, G3/C, K.-65/B, K.-65/E, K.-65/C within boreholes jpk* 62 + 10°, *jpk 56* + 10°, *jpk* 63 + 10°, *jpk* 70 + 10°, *jpk* 73 + 10°. *CDMI index = (CO_2/(CO_2 + CH_4)) × 100 %), δD_{CH4} (isotopic composition of deuterium in methane) and $a_{CH4\text{-}CO2}$ (fractionation factor between CH_4 and CO_2)*

Working face -65F, borehole jpk 62 + 10°, mining area Pesje, z = –74 m									
Date of sampling	**Distance of the working face (m)**	**CH_4 (vol. %)**	**CO_2 (vol. %)**	**N_2 (vol. %)**	**CDMI index (%)**	**$\delta^{13}C_{CO2}$ (‰)**	**$\delta^{13}C_{CH4}$ (‰)**	**δD_{CH4} (‰)**	**$\alpha_{CO2\text{-}CH4}$**
January 4, 2013	190	42.5	57.5	0.0	57.5	–8.9	–52.6	–294.5	1.046
January 9, 2013	174.4	43.3	56.7	0.0	56.7	–8.8	–52.7	–296.3	1.046
January 15, 2013	156.2	43.2	56.8	0.0	56.8	–8.9	–52.3	–296.4	1.046
January 22, 2013	131.3	44.9	55.1	0.0	55.1	–9.1	–52.9	–293.6	1.046
January 28, 2013	112.1	43.3	56.7	0.0	56.7	–9.1	–54.1	–298.8	1.048
February 6, 2013	70.9	42.9	57.1	0.0	57.1	–8.9	–52.9	–294.9	1.046
February 11, 2013	59.8	53.0	47.0	0.0	47.0	–9.2	–53.2	–294.2	1.046
February 19, 2013	34.7	24.5	75.5	0.0	75.5	–9.0	–54.5	–292.6	1.048
February 20, 2013	31.2	24.0	76.0	0.0	76.0	–9.3	–55.0	–291.4	1.048
February 21, 2013	27.4	19.4	80.6	0.0	80.6	–9.1	–54.8	–292.4	1.048
February 22, 2013	25	15.9	84.1	0.0	84.1	–9.2	–55.0	–293.0	1.048
February 23, 2013	21.4	19.7	80.3	0.0	80.3	–9.3	–54.7	–294.0	1.048
February 25, 2013	17.9	19.1	80.9	0.0	80.9	–8.9	–54.3	–293.3	1.048
February 26, 2013	14.4	19.8	80.2	0.0	80.2	–8.6	–53.5	–295.8	1.047
February 27, 2013	11.1	20.4	79.6	0.0	79.6	–8.9	–54.5	–291.8	1.048
March 1, 2013	4.6	17.7	82.3	0.0	82.3	–8.8	–54.3	–294.6	1.048
March 4, 2013	1.8	13.6	86.4	0.0	86.4	–8.5	–53.2	–298.6	1.047

Working face G3/C, borehole jpk 56 + 10°, mining area Preloge, z = –46 m

Date of sampling	Distance of the working face (m)	CH_4 (vol. %)	CO_2 (vol. %)	N_2 (vol. %)	CDMI index (%)	$\delta^{13}C_{CO2}$ (‰)	$\delta^{13}C_{CH4}$ (‰)	δD_{CH4} (‰)	$\alpha_{CO2\text{-}CH4}$
February 22, 2013	189.9	63.6	36.4	0.0	36.4	–5.1	–43.6		1.040
February 25, 2013	179.6	63.9	36.1	0.0	36.1	–2.4	–43.4	–343.5	1.043
March 8, 2013	125.4	22.2	77.8	0.0	77.8	–9.3	–54.5	–294.0	1.048
March 13, 2013	104.9	22.4	77.6	0.0	77.6	–8.8	–53.9	–292.9	1.048
March 27, 2013	60	41.5	58.5	0.0	58.5	–8.9	–52.6	–296.8	1.046
April 4, 2013	37.4	61.9	38.1	0.0	38.1	–5.4	–46.3	–343.9	1.043
April 15, 2013	19.6	36.4	63.6	0.0	63.6	–4.5	–45.6	–333.3	1.043
April 17, 2013	13.9	33.8	66.2	0.0	66.2	–4.0	–48.6	–326.4	1.047
April 19, 2013	7.3	12.0	88.0	0.0	88.0	–11.0	–71.8		1.066
April 22, 2013	3.9	40.8	59.2	0.0	59.2				

Working face -65/B, borehole jpk 63 + 10°, mining area Pesje, z = –67 m

Date of sampling	Distance of the working face (m)	CH_4 (vol. %)	CO_2 (vol. %)	N_2 (vol. %)	CDMI index (%)	$\delta^{13}C_{CO2}$ (‰)	$\delta^{13}C_{CH4}$ (‰)	δD_{CH4} (‰)	$\alpha_{CO2\text{-}CH4}$
March 27, 2013	200	6.0	94.0	0.0	94.0	–2.1	–55.5	–321.3	1.057
May 8, 2013	171.3	5.3	94.7	0.0	94.7	–2.9	–57.1	–310.4	1.057
May 16, 2013	155.5	4.9	95.1	0.0	95.1	–2.8	–55.9	–307.3	1.056
May 22, 2013	145.7	5.9	94.1	0.0	94.1	–2.4	–55.8	–223.1	1.057
May 30, 2013	131.2	4.0	96.0	0.0	96.0	–2.6	–57.9	–301.3	1.059
June 6, 2013	115.3	4.1	95.9	0.0	95.9	–2.5	–58.7	–299.2	1.060
June 12, 2013	103.8	4.5	95.5	0.0	95.5	–2.3	–58.8	–301.7	1.060
June 20, 2013	89.4								
July 5, 2013	64.4	4.3	95.7	0.0	95.7	1.9	–64.4	–279.6	1.071
July 9, 2013	59.1	3.8	96.2	0.0	96.2	–2.1	–64.1	–269.2	1.066
July 10, 2013	56.5	4.0	96.0	0.0	96.0	–2.1			
July 15, 2013	48.3	3.6	96.4	0.0	96.4	–2.0	–64.2	–273.3	1.067
July 16, 2015	45.6	3.8	96.2	0.0	96.2	–2.1	–64.2	–271.5	1.066
July 17, 2013	44	2.2	97.8	0.0	97.8	–2.0	–64.0	–271.4	1.066
July 18, 2013	41	3.7	96.0	0.0	96.3	–2.0	–63.0	–272.0	1.065
July 19, 2013	37.5	4.1	95.9	0.0	95.9	–2.1	–63.4	–277.2	1.065
July 22, 2013	33.2	4.5	95.5	0.0	95.5	–2.0	–62.9	–278.4	1.065
July 23, 2013	31.9	4.0	96.0	0.0	96.0	–1.8	–62.3	–291.7	1.064
July 24, 2013	29	2.7	97.3	0.0	97.3	–2.1	–62.2	–285.4	1.064
July 25, 2013	27	4.2	95.8	0.0	95.8	–0.3	–51.2	–263.7	1.054
July 26, 2013	24.2	7.5	92.3	0.2	92.3	–2.0	–65.6	–258.6	1.068
July 29, 2013	21.7	1.8	98.2	0.0	98.2	–2.1	–65.9	–255.3	1.068

Working face -65/E, borehole jpk 70 + 10°, mining area Pesje, z = –78 m

Date of sampling	Distance of the working face (m)	CH_4 (vol. %)	CO_2 (vol. %)	N_2 (vol. %)	CDMI index (%)	$\delta^{13}C_{CO2}$ (‰)	$\delta^{13}C_{CH4}$ (‰)	δD_{CH4} (‰)	$\alpha_{CO2\text{-}CH4}$
October 3, 2013	152.4	57.6	42.2	0.2	42.3	–8.8	–50.3	–301.1	1.044
October 8, 2013	138.5	57.5	42.5	0.0	42.5	–8.4	–50.2	–300.1	1.044
October 15, 2013	123.1	6.8	93.2	0.0	93.2	–8.3	–52.0	–319.8	1.046
October 22, 2013	105.1	58.5	41.5	0.0	41.5	–8.7	–50.9	–300.9	1.044
November 5, 2013	76.7	56.8	41.7	1.5	42.3	–8.5	–50.5	–298.8	1.044
November 8, 2013	65.0	55.1	43.9	1.0	44.3	–8.8	–50.3	–299.2	1.044
November 12, 2013	55.1	55.6	44.1	0.3	44.2	–8.3	–50.9	–297.9	1.045

November 14, 2013	48.6	59.9	38.9	1.2	39.4	–8.2	–51.2	–298.7	1.045
November 18, 2013	37.2	51.8	45.1	3.1	46.5	–8.2	–50.8	–300.0	1.045
November 19, 2013	33.4	54.5	44.2	1.3	44.8	–8.2	–50.8	–300.5	1.045
November 20, 2013	30.3	51.1	46.6	2.3	47.7	–8.4	–50.8	–300.4	1.045
November 21, 2013	27.9	43.2	56.2	0.6	56.5	–8.4	–50.6		1.044
November 22, 2013	26.7	35.2	63.6	1.2	64.4	–8.4	–50.6	–299.7	1.044
November 25, 2013	20.9	21.6	77.7	0.7	78.2	–8.8	–50.4	–300.2	1.044
November 26, 2013	19.2	11.7	87.4	0.9	88.2	–8.6	–50.7	–303.7	1.044
November 27, 2013	17.4	13.5	84.9	1.6	86.3	–8.3	–50.5	–301.0	1.044
November 28, 2013	15.0	12.5	87.5	0.0	87.5	–8.6	–50.1	–305.4	1.044
November 29, 2013	12.2	10.9	89.1	0.0	89.1	–8.5	–49.9	–300.0	1.044
December 2, 2013	9.0	15.4	83.5	1.1	84.4	–8.4	–52.3	–299.4	1.046
December 3, 2013	6.5	46.2	53.8	0.0	53.8	–9.2	–47.4	–295.8	1.040
December 4, 2013	3.2	25.6	74.4	0.0	74.4	–8.5	–52.3	–286.5	1.046

Working face -65/C, borehole jpk 73 + 10°, mining area Pesje, z = –69 m

Date of sampling	Distance of the working face (m)	CH_4 (vol. %)	CO_2 (vol. %)	N_2 (vol. %)	CDMI index (%)	$\delta^{13}C_{CO2}$ (‰)	$\delta^{13}C_{CH4}$ (‰)	δD_{CH4} (‰)	$\alpha_{CO2\text{-}CH4}$
November 20, 2013	152.4	46.2	53.8	0.0	53.8	–8.4	–50.2	–298.9	1.044
December 5, 2013	133.8	7.5	91.7	0.8	92.4	–8.8	–52.4	–293.4	1.046

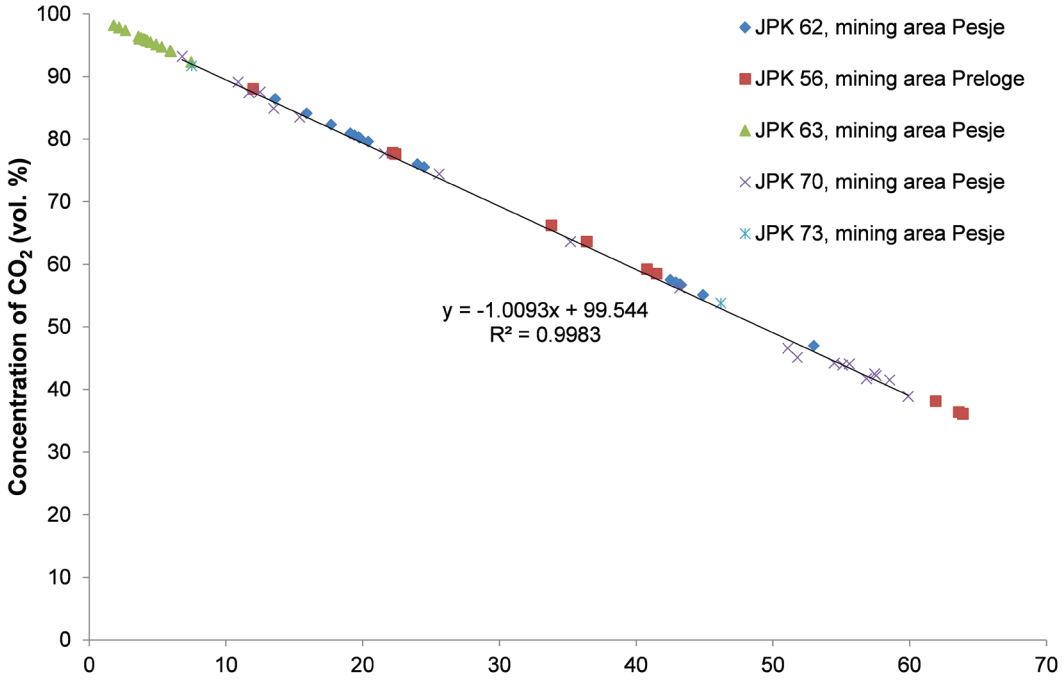

Figure 3: *Concentration of CO_2 versus concentration of methane in lignite seams in advancement of the working faces (see Figure 1) within boreholes: jpk 62, mining area Pesje, jpk 56, mining area Preloge, jpk 63, mining area Pesje, jpk 70, mining area Pesje, jpk 73 mining area Pesje.*

Approaching of the working face also influences the stress situation at working faces. During the excavation of lignite, secondary fissures are generated due to rearrangement of primary stress conditions, enabling release of coalbed gas preserved in pores of the coalbed reservoir[18]. The results of temporal variations of CO_2 and methane within boreholes at working faces 120/B, G2/C and–50/B[18] and working faces K.-5/A, G2/C, K. -130/A, K. -50/C[20] reveal similar trends. The observed maximum concentrations of methane at distances of 177 m and 122 m from the working face coincide with the minimum concentrations of CO_2, but the differences found in coalbed gas composition are due to location of the longwall panels that underlie the unmined area or previously mined areas[20]. No trend is observed in CO_2 and methane concentrations in the advancement of the longwall K.-65/F (jpk 62 + 10°) at a distance of longwall 120 m, as is usually observed when investigating coalbed gas concentrations in advancement of a working face. Overall, high CH_4 gas content (up to 53 vol. %) was observed at the longwall panel K.-65/F, which can be explained by the longwall panel position just under fresh overburden. The highest concentrations of CO_2 and minimal concentrations of methane are observed at a distance of the longwall K.-65/F of 40 m (Figure 4). Maximum CO_2 concentration is observed at a distance of 120 m from the longwall face G3/C (jpk 56), coinciding with the minimum CH_4 concentration, while the maximum CH_4 concentration is observed at a distance of around 40 m from the longwall and another maximum of CO_2 is observed at the distance of the longwall 20 m (Figure 4). At the excavation field K.-65/B, jpk 63 + 10° there is no change in CO_2 and methane concentrations in advancement of the working face; no data concerning gas concentration is available between distances of 110 m and 70 m to allow a clearer interpretation. This excavation field lies in an area of pre-mined excavation and has a high CDMI index (Figure 4). Data relating to the coalbed gas composition in advancement of the working face -65/C (Figure 4) are not presented since only 2 values of gas concentration were obtained. The first maximum of CO_2 concentration (minimum of meth-

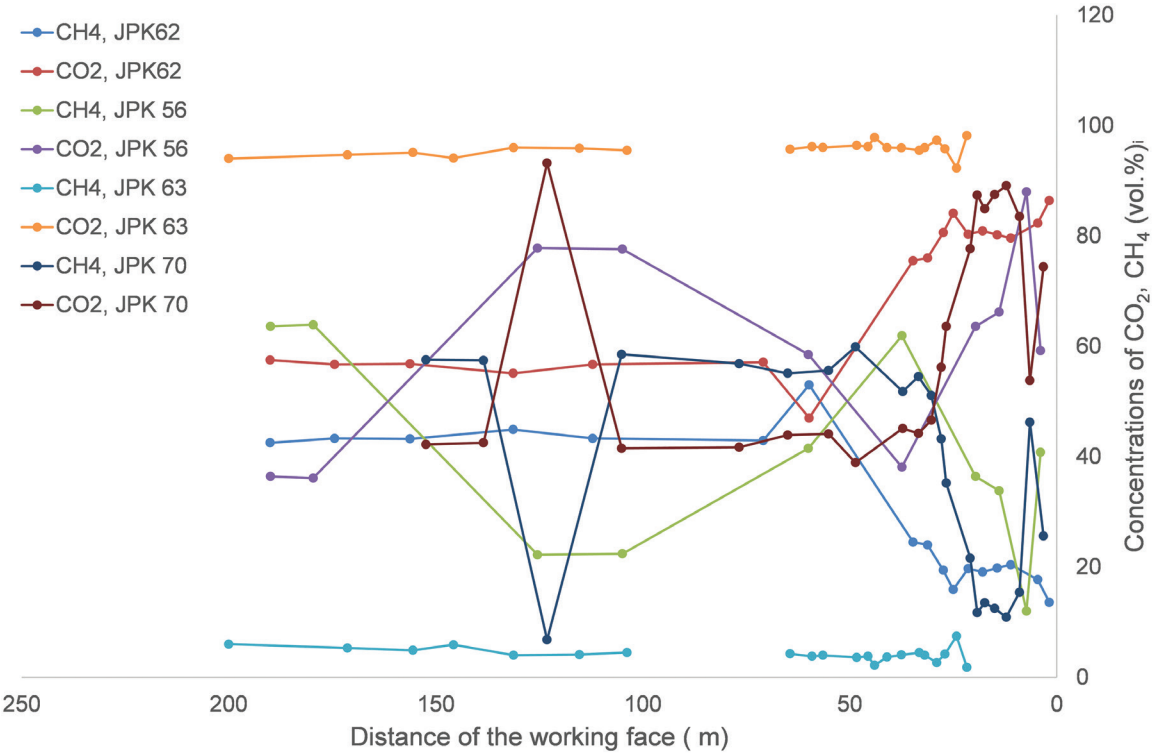

Figure 4: *Concentration of methane and CO_2 versus distance from the longwall of the working faces (-65/F, G3/C, -65/B, -65/E, -65/C) in boreholes jpk 62, jpk 56, jpk 63 and jpk 70.*

ane concentration) occurs at a distance of 120 m from the working face (K.-65/E, jpk 70), and, at 30 m from the working face, lignite structure was demolished (Figure 4). The longwall panel in this case was excavated under fresh overburden, which explains the high methane content compared with that of the longwall panels G3/C and K.-65/B. The methane gas content was high at 59.9 vol. %. Results from previous studies investigating coalbed gases from Velenje Basin showed that CH_4 desorbs more quickly than CO_2, but this is not the case from the observations of gas composition at excavation fields in this study.

The reaction mechanisms of methane and CO_2 generation in natural and coalbed gases are described elsewhere[3, 4, 18]. The products of these reactions support a variety of methanogens. For Velenje Basin it is known that the basin was formed in a Ca-alkaline rich environment[26], which enabled the operation of bacteria (aerobic and anaerobic), with the generation of coalbed gas in lignite (organic rich matrix).

The plots of $\delta^{13}C_{CH4}$ versus $\delta^{13}C_{CO2}$ and $\delta^{13}C_{CH4}$ versus δD_{CH4} (Figures 5, 6) were used to explain the origin of methane. Figures 4 and 5, in the Velenje Basin, indicate the consecutive origins of methane: microbial CO_2 reduction with $\delta^{13}C_{CH4}$ values from –40 ‰ to –50 ‰, microbial acetate fermentation with $\delta^{13}C_{CH4}$ less than –50 ‰ and mixed origin between these two[5]. Enrichment with ^{13}C in methane could be also due to microbial oxidation of methane, which results in enrichment of residual methane with the ^{13}C isotope and depletion of ^{12}C in generated CO_2 (Figure 5).

The method for determining the origin of methane and for distinguishing pathways of microbial methane generation (i.e. acetate fermentation from CO_2 reduction) was proposed by[3] and uses the $\alpha^{13}C_{CO2\text{-}CH4}$ fractionation factor; this was also applied in our study at five excavation fields to distinguish between the two pathways. The $\alpha^{13}C_{CO2\text{-}CH4}$ values indicate that methane was generated via both these processes at all five excavation fields investigated (K.-65/F, G3/C, K.-65/B, K.-65/E and K.-65/C) since the calculated $\alpha_{CO2\text{-}CH4}$ values were below 1.06 (Table 1). Altogether, 13 samples out of a total of 72 with low values of $\delta^{13}C_{CH4}$ (>–60 ‰), and

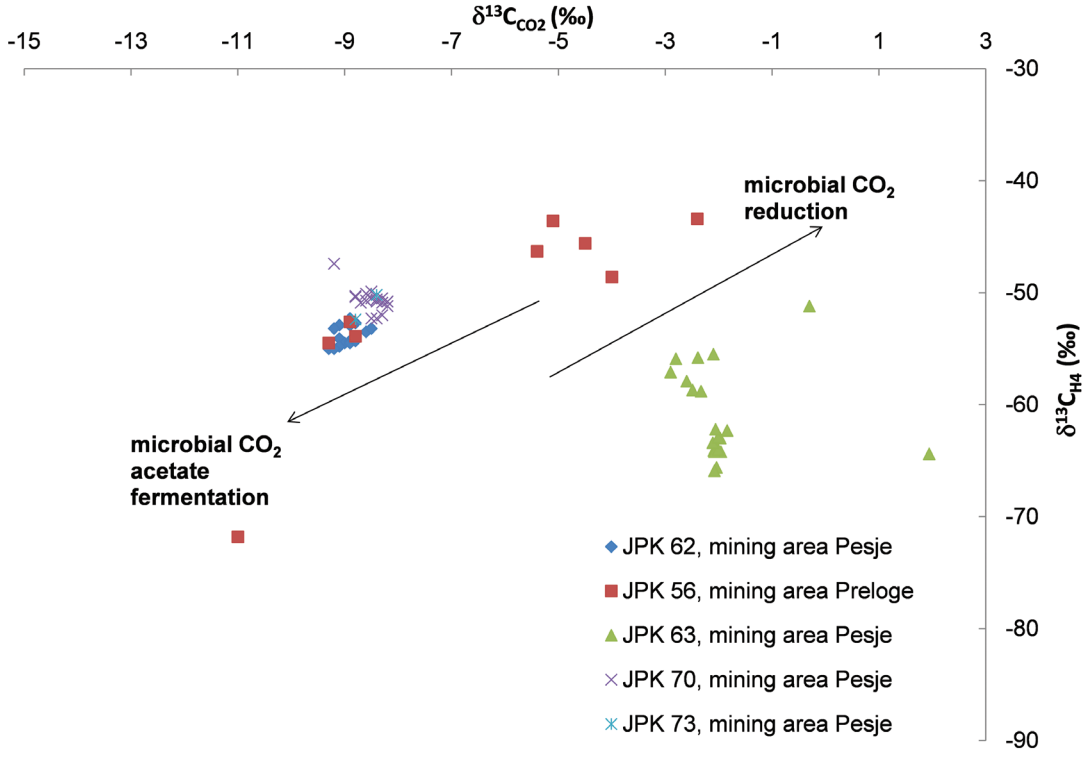

Figure 5: *Interpretation of the origin of methane in the Velenje basin using $\delta^{13}C_{CH4}$ versus $\delta^{13}C_{CO2}$ in a lignite seam at boreholes (jpk 62, jpk 56, jpk 63, jpk 70 and jpk 73) ahead of the working faces (-65/F, G3/C, -65/B, -65/E, -65/C).*

corresponding values of $\delta^{13}C_{CO2}$ from –12 ‰ to 0 ‰, indicate that the methane originates from microbial CO_2 reduction. Following[3, 4] and using $\alpha_{CO2\text{-}CH4}$ as a parameter, most of the samples investigated in our study have $\alpha_{CO2\text{-}CH4} < 1.06$, which is characteristic of acetate fermentation. When interpreting digenetic methanogenic pathways, it should be emphasized that the threshold for acetate fermentation/CO_2 reduction was –50 ‰. We obtained ranges of $\delta^{13}C_{CH4}$ and $\delta^{13}C_{CO2}$ for Velenje basin similar to those obtained for Sydney and Bowen basins (Figure 1).

To obtain a better geochemical characterization of methane in Velenje Basin, we used δD_{CH4} tracer (Figure 6). For coalbed gases from excavation fields K.-65/F, G3/C, K.-65/B, K.-65/E and K.-65/C we conclude that parameters $\delta^{13}C_{CH4}$ and δD_{CH4} both reveal microbial methane and mixing and none of the samples investigated in this study from excavation fields have the value for thermogenic methane (Figure 6).

Plots of $\delta^{13}C_{CH4}$ versus δD_{CH4} from the excavation fields K.-65/F, G3/C, K.-65/B, K.-65/E and K.-65/C (Figure 7) show that coalbed samples for Velenje Basin are similar to those for Powder River, Bowen Basin, Antrim/New Albany shales and Appalachian shales, and indicate fields of microbial methane and mixing, with values of methane enriched with ^{13}C (values of thermogenic methane). From the study of coalbed gases[20] from years 2010 to 2012 from Velenje Basin it was found that the characteristics of methane from the Velenje Basin are similar to those from low rank coal basins such as Powder River Basin and the San Juan Basin, USA, while completely distinct from those of the Lower and Upper Silesian Basins, Poland.

The origin of CO_2 is interesting for its relation to outbursts in coalmines. It is known that high concentrations of carbon dioxide in seam gases in Australian coals occur in regions of igneous activity and associated faulting and this component has been described as being of presumed pneumatolytic origin[33]. We used the plot of $\delta^{13}C_{CO2}$ versus CDMI (Figure 8) to explain the origin of CO_2 at the working faces investigated: K.-65/F, G3/C, K.-65/B, K.-65/E and K.-65/C (Figure 8). Samples from excavation field -65/B are seen to have values of $\delta^{13}C_{CO2}$ indicative of endogenic origin, while samples from excavation fields -65/F, G3/C, -65/E and -65/C have values characteristic of endogenic and bacterial

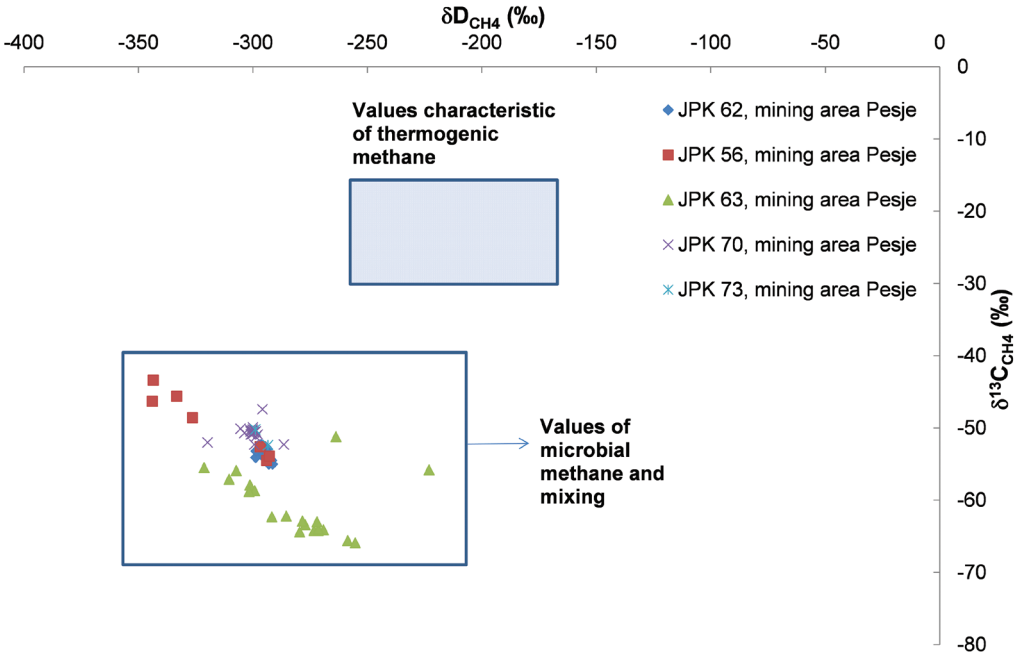

Figure 6: *Interpretation of the origin of methane using $\delta^{13}C_{CH4}$ versus δD_{CH4} in a lignite seam in boreholes (jpk 62, jpk 56, jpk 63, jpk 70 and jpk 73) ahead of the working faces (K.-65/F, G3/C, K.-65/B, K.-65/E, K.-65/C).*

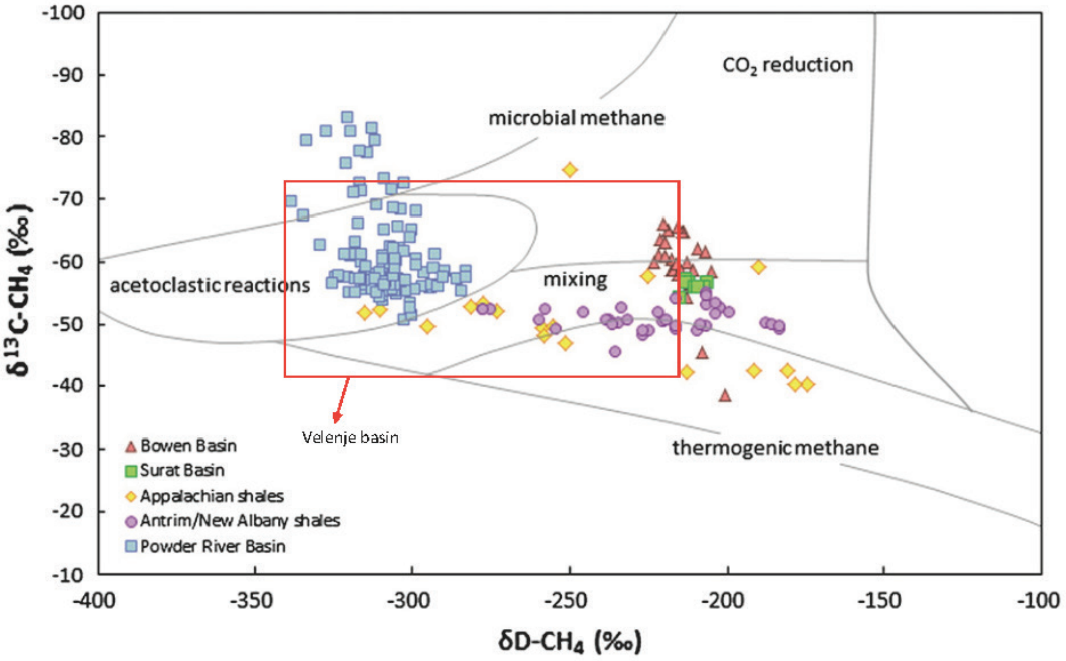

Figure 7: *Isotopic composition of methane ($\delta^{13}C_{CH4}$) versus that of deuterium in methane (δD_{CH4}) in coalbed seam in coalmines from Bowen and Surat basins (Moranbah Gas Project[27]; Oaky Creek[2]; Avon Downs[28]. Gas samples from Powder River basins[29, 30], Antrim and New Albany shales[11, 31] and organic rich shales from North Appalachi basin[32]. In the frame, results of $\delta^{13}C_{CH4}$ and δD_{CH4} (see Table 1 for results) from this study (excavation fields: -K.65/F, G3/C, K.-65/B, K.-65/E, K.-65/C within boreholes: jpk 62, jpk 56, jpk 63, jpk 70, jpk 73) are presented.*

gas formed via CO_2 reduction. Typical endogenic values of $\delta^{13}C_{CO2}$ are about –7 ‰[23] and areas of high CDMI index could be related to tectonics of the Šoštanj and Smrekovec faults systems at the time of formation of the basin[18]. The CDMI index is used as the crucial parameter for excavation fields prone to outburst generation, especially in combination with other factors such as fault zones, detrital lignite, etc.

Previous studies have shown that shale gas can be of thermogenic, microbial or mixed origin, the distinction being made on the basis of the stable isotope composition of the gases and co-produced water e.g. Antrim Shale, Michigan Basin[11, 12], Barnett Shale, Fort Worth Basin, Appalachian Basin[32] and other basins studied such as New Albany Shale, Illinois Basin, Colorado Group, Western Canada Sedimentary Basin[2]. All these studies showed that the relative proportions of microbial and thermogenic gas are depth related; deeper locations contain exclusively thermogenic gas, while shallower locations contain a mixture of microbial and thermogenic methane. In the Velenje Basin, gas concentration, $\delta^{13}C_{CH4}$ and $\delta^{13}C_{CO2}$ also differ with the depth level of excavation fields (Figure 9).

For Velenje Basin it is very important which excavation fields underlie the unmined or previously mined areas[20]. A high CDMI index, with values in the range of 92.5 % to 98.2 %, was observed at the excavation field K.-65/B, jpk 63 + 10° that lies under a pre-mined area. G3/C (jpk 56 + 10°) excavation field is the shallowest field to be investigated and has a larger range of all measured parameters (CO_2, CH_4, $\delta^{13}C_{CO2}$ and $\delta^{13}C_{CH4}$) in comparison to the other excavation fields observed in this study – K.-65/F, K.-65/E, K.-65/C (Figure 9 A-D). The $\delta^{13}C_{CO2}$ values show that the deepest excavation fields (K.-65/E - jpk 70, K.-65/F - jpk 62, mining area Pesje) have typical endogenic CO_2 with CO_2 reduction values. The excavation field G3/C, jpk 56, located at z [–46 m], had the broadest range of $\delta^{13}C_{CO2}$, indicating biogenic and endogenic CO_2. We have not enough data to make a clear interpretation for K.-65/C, jpk 73 + 10° (mining area Pesje). A similar pattern for $\delta^{13}C_{CH4}$ values versus depth is observed, the widest range being for G3/C, [z = –46 m] (Figure 9 C).

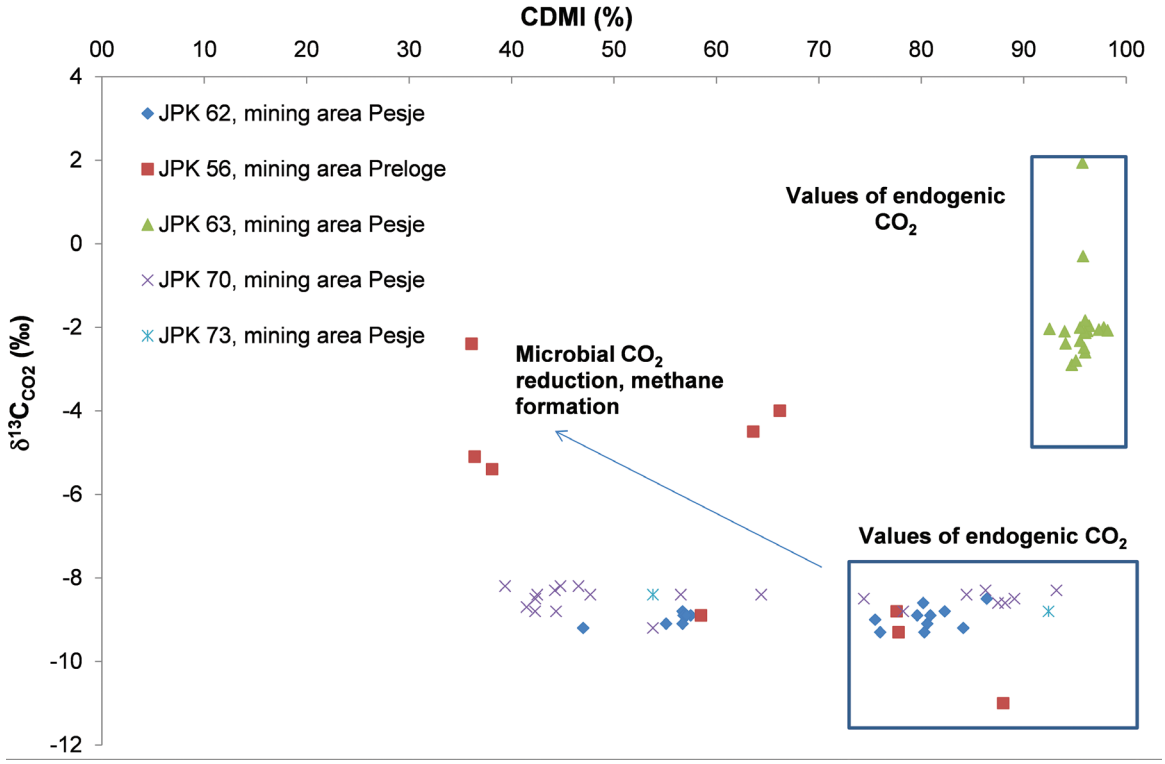

Figure 8: *Interpretation of the origin of CO_2 at working faces using $\delta^{13}C_{CO2}$ versus CDMI index in a lignite seam in boreholes (jpk 62, jpk 56, jpk 63, jpk 70 and jpk 73) ahead of the working faces (K.-65/F, G3/C, K.-65/B, K.-65/E, K.-65/C).*

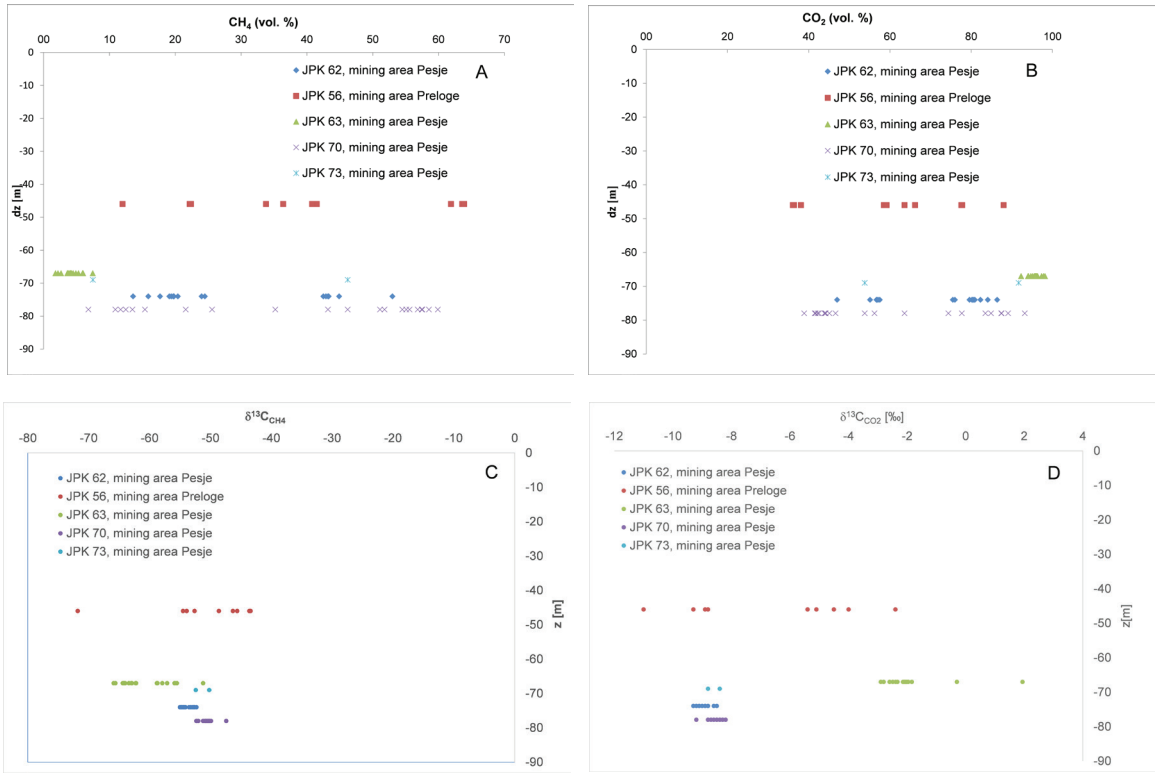

Figure 9: *Concentrations of CH_4 (A), CO_2 (B), $\delta^{13}C_{CH4}$ (C) and $\delta^{13}C_{CO2}$ (D) as a function of depth (m) for excavation fields K.-65/F, jpk 56 + 10°, z [–74 m] , G3/C, jpk 56 + 10°, z [–46 m], K.-65/B, jpk 63 + 10°, z [–67 m], K.-65/E, jpk 70 + 10°, z [–78 m] K.-65/C, jpk 73 + 10° and z [–69 m]).*

Conclusions

Geochemical (CH_4, CO_2, N_2) and isotopic ($\delta^{13}C_{CO2}$, $\delta^{13}C_{CH4}$, δD_{CH4}) tracers have provided a geochemical and isotopic characterization of coalbed gases from five excavation fields at Preloge and Pesje (Velenje Basin) during the year 2013. Isotopic composition of deuterium of methane (δD_{CH4}) has been used to determine the origin of methane. Further, these characteristics of methane have been compared with those observed in other coal sedimentary basins worldwide.

In shallower working faces (Preloge G3/C, jpk 56 ([z = –46 m]) and in the deepest working face (jpk 70, mining area Pesje K.-65/E, [z = –78 m]) larger ranges of methane and CO_2 concentrations have been observed. The concentrations of CO_2 and CH_4 are relatively constant at the excavation field K.-65/B (jpk 63 + 10°). At the deepest excavation field K.-65/E, jpk 70, depth [z] = –78 m, $\delta^{13}C_{CO2}$ values denote an endogenic origin of CO_2 while methane, with $\delta^{13}C_{CH4}$ values corresponding to thermogenic methane, probably results from CO_2 reduction. The wider range of $\delta^{13}C_{CH4}$ (biogenic and thermogenic isotopic values) and $\delta^{13}C_{CO2}$ (biogenic and endogenic isotopic values) are observed at the shallower excavation field G3/C, jpk 56, mining area Preloge [depth –46 m].

Each excavation field appears to be specific in terms of the geochemical characteristics of coalbed gases, making it necessary to carry out such a geochemical and isotopic investigation of coalbed gases in order to more fully understand the origin of gases, especially methane, which is considered as a greenhouse and unconventional gas. Such investigations are relevant to the development of clean coal technologies such as CBM (coalbed methane), which could have great potential when cessation of underground coal excavation is being considered.

The determination of concentrations and stable isotope patterns of coalbed gases at working faces has enabled an interpretation of the origin of coalbed gases in the Velenje basin. From the results of this and previous studies, it can be concluded that coalbed CO_2 from these working faces is endogenic and of bacterial origin. Measurements of $\delta^{13}C_{CH4}$ and δD_{CH4} have led to the conclusion that methane from Velenje Basin has a microbial origin, formed through microbial fermentation and/or CO_2 reduction, and of mixed origin, both thermogenic and biogenic, since some $\delta^{13}C_{CH4}$ values are enriched with ^{13}C isotope. Secondary processes like migration, adsorption/desorption and mixing of gases of different origin during excavation complicate the interpretation of gas origin and have been neglected in interpretations of the origin of coalbed gases.

Acknowledgements

This study was conducted in the framework of project L1-5451 funded by the Slovenian Research Agency (ARRS) and Velenje Coalmine d.d. The authors are grateful to Mr. Ivo Zadnik for technical support and assistance in the field sampling.

References

[1] International energy agency (2011): Golden rules for a golden age of gas. *World Energy Outlook Special Report on Unconventional Gas*, 143 p.

[2] Golding, S. D., Boreham, C. J., Esterle, J. S. (2013): Stable isotope geochemistry of coal bed and shale gas and related production waters: A review. *International Journal of Coal Geology*, 120, pp. 24–40.

[3] Whiticar, M. J. (1996): Stable isotope geochemistry of coals, humic kerogens and related natural gases. *International Journal of Coal Geology*, 32, pp. 191–215.

[4] Whiticar, M. J. (1999): Carbon and hydrogen isotope systematics of bacterial formation and oxidation of methane. *Chemical Geology,* 161, pp. 291–314.

[5] Clayton, J. L. (1998): Geochemistry of coalbed gas – A review. *International Journal of Coal Geology,* 35, pp. 159–173.

[6] Faiz, M, Hendry, P. (2006): Significance of microbial activity in Australian coal bed methane reservoirs-a review. *Bull. Can. Pet. Geol.,* 54, pp. 261–272.

[7] Strapoć, D., Mastalerz, M., Dawson, K., Macalady, J., Callaghann, A. V., Wawrick, B., Turich, C., Ashby, M. (2011): Biogeochemistry of microbial coal-bed methane. *Ann. Rev. Earth Planet. Sci.,* 39, pp. 617–656.

[8] Scott, A. R. (1999): Improving gas recovery with microbially enhanced coalbed methane. In: Mastalerz, M., Glikson, M., Golding, S. D. (Eds.), Coalbed Methane: Scientific Environmental and Economic Evaluation. Kluwer, Dordrecht, pp. 89–110.

[9] Furmann, A., Schimmelmann, A., Brassell, S. C., Mastalerz, M., Picardal, F. (2013): Chemical compound classes supporting microbial methanogenesis in coal. *Chemical geology,* 339, pp. 226–241.

[10] Penner, C. J., Foght, J. M., Budwill, K. (2010): Microbila diversity of western Canadiansubsurface coal beds and methanogenic coal enrichment cultures. *International Journal of Coal Geology,* 82, pp. 81–93.

[11] Martini, A. M., Walter, L. M., Budai, J. M., Ku, T. C. W., Kaiser, C. J., Schoell, M. (1998): Genetic and temporal relations between formation waters and biogenic methane: Upper Devonian Antrim Shale, Michigan Basin, USA. *Geochimica Cosmochimica Acta,* 62, pp. 1699–1720.

[12] Martini, A. M., Walter, L. M., Budai, J. M., McIntosh, J. C., Schoell, M. (2003): Microbial production and modification of gases in sedimentary basins: a geochemical case study from a Devonian shale gas play, Michigan basin. *AAPG Bull.,* 87, pp. 1355–1375.

[13] Schlegel, M. E., McIntosh, J. C., Bates, B. I., Kirk, M. F., Martini, A. M. (2011): Comparison of fluid geochemistry and microbiology of multiple organic-rich reservoirs in the Illinois Basin, USA: evidence for controls on methanogenesis and microbial transport. *Geochimica Cosmochimica Acta,* 75, pp. 1903–1919.

[14] Coplen, T. B. (1996): New guidenices for reporting stable hydrogen, carbon and oxygen isotopes ratio data. *Geochimica Cosmochimica Acta*, 60, pp. 390–3360.

[15] PETROLEUM GEOCHEMISTRY GROUP, CSIRO [online]. Gas composition and isotope geochemistry. [cited 6/12/2000]. Available on: <http://www.dpr.csiro.au/reaearch/erp/gcig.html>.

[16] Kanduč, T. (2004): *Isotopic characteristics of coalbed gases in Velenje Basin*. Master Thesis, Ljubljana, University of Ljubljana, pp. 78 (in Slovene).

[17] Kanduč, T., Pezdič, J. (2005): Origin and distribution of coalbed gases from the Velenje Basin, Slovenia. *Geochemical Journal*, 39, pp. 397–409.

[18] Kanduč, T., Žula, J., Zavšek, S. (2011): Tracing coalbed gas dynamics and origin of gases in advancement of the working faces at mining areas Preloge and Pesje, Velenje basin. *RMZ-Mater. Geoenvironment,* 58, pp. 373–288.

[19] Kanduč, T., Markič, M., Zavšek, S., McIntosh, J. (2012): Methanogenesis in the Pliocene Velenje Coal Basin, Slovenia, inferred from stable carbon isotopes. *International Journal of Coal Geology,* 89, 70–83.

[20] Lazar, J., Kanduč, T., Jamnikar, S., Grassa, F., Zavšek, S. (2014): Distribution, composition and origin of coalbed gases in excavation fields from the Pesje mining areas, Velenje Basin, Slovenia, *International Journal of Coal Geology*, 131, pp. 363–377.

[21] Kanduč, T., Grassa, F., McIntosh, J., Stibilj, V., Ulrich-Supovec, M., Supovec, I., Jamnikar, S. (2014): A geochemical and stable isotope investigation of groundwater/surface-water interactions in the Velenje Basin, Slovenia. *Hydrogeology Journal,* 22, pp. 971–984.

[22] Kotarba, M. (1990): Isotopic geochemistry and habitat of the natural gases from the Upper Carboniferous Zacler coal – bearing formation in the Nowa Ruda coal district (Lower Silesia, Poland). *Organic Geochemistry,* 16, pp. 549–560

[23] Kotarba, M. J. (2001): Composition and origin of coalbed gases in the Upper Silesian and Lublin basins, Poland. *Organic Geochemistry,* 32, pp. 163–180.

[24] O'Neil, J. R. (1979): *Stable Isotope Geochemistry of Rocks and Minerals.* - V: Lectures in Isotope Geology, Jager, E., Hunzinger, J. C., (Eds). - Springer Verlag, Berlin, 235–263.

[25] Atkins, P. W. (1994): *Physical Chemistry*, fifth ed. Oxford Univ. Press, Oxford, 1031 p.

[26] Markič, M., Sachsenhofer, R. F. (1997): Petrographic composition and depositional environments of the Pliocene Velenje lignite seam (Slovenia). *International Journal of Coal Geology,* 33, pp. 229–254.

[27] Kinnon, E. C. P., Golding, S. D., Boreham, C. J., Baublys, K. A., Esterle, J. S. (2010): Stable isotope and water quality analysis of coal bed methane roduction waters and gases from the Bowen Basin, Australia. *International Journal of Coal Geology, 82,* pp. 219–231.

[28] Draper, J. J., Boreham, C. J. (2006): Geological controls on exploitable coal seam gas distribution in Queensland. *Aust. Prod. Pet. Explor. Assoc. J*., 46, pp. 343–366.

[29] Bates, B. I., McIntosh, J. C., Lohse, K. A., Brooks, P.D. (2011): Influence of groundwater flowpaths, residence times, and nutrients on the extent of microbial methanogenesis in coal beds: Powder River Basin, USA. *Chemical geology*, 284, pp. 45–61.

[30] Flores, R. M., Rice, C. A., Stricker, G. D., Warden, A., Ellis, M. S. (2008): Methanogenic pathways of coal-bed gas in Powder River Basin, United States: the geological factor. *International Journal of Coal Geology,* 76, pp. 52–75.

[31] McIntosh, J. C., Walter, L. M., Martini, A. M. (2002): Pleistocene recharge to mid-continent basins: effects on salinity structure and microbial gas generation. *Geochimica Cosmochimica Acta,* 66, pp. 1681–1700.

[32] Osborn, S. G., McIntosh, J. C. (2010): Chemical and isotopic tracers of the contribution of microbial gas in Devonian organic-rich shales and reservoir sandstones, northern Appalachian Basin. *Applied Geochemistry,* 25, pp. 456–471.

[33] Smith, J. W., Gould, K. W. (1980): An isotopic study of the role of carbon dioxide in outbursts in coal mines. *Geochemical Journal*, 14, pp. 27–32.

Original scientific paper

Received: November 26, 2014
Accepted: February 2, 2015

Indicator Kriging porosity maps of Upper Miocene sandstones, Sava Depression, Northern Croatia

Indikatorsko krigiranje poroznosti zgornjemiocenskih peščenjakov v Posavski kadunji v severni Hrvaški

Tomislav Malvić[1], Karolina Novak[2,*], Kristina Novak Zelenika[1]

[1]INA-Industry of Oil Plc., Šubićeva 29, Zagreb, Croatia

[2]INA-Industry of Oil Plc., Av. V. Holjevca 10, Zagreb, Croatia

[3]Faculty of Mining, Geology and Petroleum Engineering, Pierottijeva 6, Zagreb, Croatia

*Corresponding author. E-mail: karolina.novak@ina.hr

Abstract

There are geologically and geostatistically analysed two, presently, the most interesting Upper Miocene sandstone Croatian hydrocarbon reservoirs in the Sava Depression regarding injection of carbon-dioxide. The intention is increasing oil recovery and, simultaneously, keeps part of injected CO_2 permanently in depleted reservoirs. Lithologically, both reservoirs are dominantly fine to medium-grained sandstones, with very restricted pelitic content, where silt, clay and marl fractions are increased only in laterally marginal parts. Lithostratigraphically (informally) those two reservoirs are named as "Gamma 3" (older, here analysed as reservoir "A") and "Gamma 4" (younger, here as reservoir "B"), both belonging to the Iva Member, i.e. the Ivanić Grad Formation. Indicator Kriging had been used to map probabilities to obtain different porosities that indicated on different lithofacies.

Key words: sandstones, Indicator Kriging, porosity, Upper Miocene, Sava Depression, Croatia

Izvleček

V dveh na Hrvaškem sedaj najobetavnejših zgornjemiocenskih rezervoarjih ogljikovodikov so geološko in geostatistično preiskali možnost vtiskanja ogljikovega dioksida. Cilj je bil povečati izkoristek črpanja nafte, hkrati pa v izpraznjenih rezervoarjih trajno uskladiščiti del vtisnjenega CO_2. Litološko sta oba rezervoarja v pretežno drobno do srednjezrnatih peščenjakih z zelo podrejenim pelitskim deležem, pri čemer so meljaste, glinene in laporne frakcije znatneje zastopane le bočno v obrobnih delih. Na osnovi litostratigrafije so rezervoarja neformalno poimenovali "Gama 3" (starejši, označen kot rezervoar "A") in "Gama 4" (mlajši, označeni kot rezervoar "B"). Oba pripadata členu Iva, tj. Ivanićgradski formaciji. Za kartiranje verjetnosti nastopanja različnih poroznosti, ki indicirajo različne litofaciese, so uporabili metodo indikatorskega krigiranja.

Ključne besede: peščenjaki, indikatorsko krigiranje, poroznost, zgornji miocen, Posavska kadunja, Hrvaška

Introduction

In Croatia, the projects for CO_2 transport and storage can be successfully applied in order to (a) increase oil recovery from "mature" sandstone reservoirs and on a commercial basis, (b) permanent store CO_2 with the purpose of greenhouse gas (abbr. GHG) emission reduction. The CO_2 generated from combustion of fossil fuels or produced during production of oil or natural gas is injected into hydrocarbon reservoirs with the aim of increasing oil recovery for more then 30 years, where recovery could be averagely increased for 10–14 %[1, 2]. Currently several dozen of the Enhanced Oil Recovery (abbr. EOR) projects are operating worldwide[3–5].

The CO_2 trapping in the subsurface depends on reservoir pressure, temperature and properties of cap rock. Reservoirs suitable for application of the EOR methods could be described by the following characteristics[6–8]: (a) oil viscosity < 12 mPa s, (b) oil density 825–865 kg/m^3, (c) residual oil saturation, Sor > 25 %, (d) initial reservoir pressure > 100 bar. In addition CO_2 mineral trapping can increase volume of trapped gas for few percentages[9]. Generally, sediments deeper than 800 m provide natural reservoir pressure sufficient to keep the CO_2 in supercritical state. The quality of cap rocks is very important factor for fluid storage into subsurface reservoirs[10].

Assessment of applicability of CO_2 injection into Croatian oil fields was conducted in the '70s and '80s of the last century, mostly through a pilot project on limited part of the Ivanić Field[11–13]. Its results led to a decision on implementation of the EOR project, but also initiated further geological modelling of sandstone reservoirs possibly and partially saturated with CO_2. In the case of the Ivanić Field considered are medium to fine-grained sandstone reservoirs, more than 10 m thick, and still in production as oil reservoirs (but largely exhausted). The age is Upper Pannonian. There is planned to inject 400 000 m^3/d of CO_2 collected onto gas-processing plant Molve. The results could be twofold: (a) enhanced oil recovery and (b) reducing of CO_2 emission[14, 15].

A model of injected gas behaviour is based on an analysis of several geological variables, including fluid properties and chemical reactions. However, it is important to understand distribution of porosity and permeability, as probably two important variables, within the reservoir. Geostatistical methods for reservoir mapping could be divided into deterministical and stochastical ones. Deterministical provide "the most probable" solution from available data, sometimes described like in Kriging based simulation as the median or "zero-realisation" when it is later applied in simulation. The most probable means that there are also other possibilities in representation of surface, which are "located" in uncertainty range typical for input dataset. It resulted in set of equiprobable realisations where selection of representative ones is based on several techniques, but no one of them favour any realisation as more probable.

This study shows applications of Indicator Kriging (abbr. IK) probability maps, as deterministical method, in estimation of porosity and permeability. Such data are derived from Upper Miocene sandstone reservoirs into the Ivanić Field, planned for injection of CO_2. Presented models are the first of such estimation made for those sandstones and consequently this is the first application of indicator transformation into analyses of CO_2 target reservoirs in Croatia.

Geological description of the study area within the Sava Depression

During Late Pannonian and Early Pontian many depressional areas along the entire Pannonian Basin System were re-extended due to the thermal subsidence as result of 2nd transtensional phase[16–18]. Depositional spaces for the accommodation of a huge volume of sandy material were created, and the main sandstone hydrocarbon reservoirs were deposited[19]. Turbidites were dominant clastic transport mechanism in the Croatian part of the Pannonian Basin System (abbr. CPBS) during that time, originated from the Eastern Alps and transported through the Vienna Basin, the Styrian Basin and the Mura Depression, more to the east in several re-deposition phases, when it eventually entered into the Sava Depression[4, 17, 20–22]. Due to long transport only the medium and fine-grained sands and silts reached the depression, where in the calm periods, when turbiditic cur-

rents were not active, typical calm deep-water calcite rich mad (later marls) were deposited. However, the CPBS was characterised with several prominent, even present-day, mountains that existed during entire Miocene like uplifted palaeorelief. Probably some of them were isolated islands in the Central Paratethys and, later, the Lake Pannon and, eventually, the Sava Lake, giving small part of sandy and silty detritus into dominant turbiditic and basin deposits[6, 23]. Study area is located in the northwestern part of the Sava Depression (Figure 1). Present-day the Ivanić Field is asymmetrical brachianticline, with longer axis of northwest-southeast strike, slightly pronounced top in the southern part, and series of NW-SE faults extended along the western part (Figure 2).

Lithologically, reservoir rocks are mostly medium and fine-grained sandstones, i.e. lithoarenites, in vertical alternation with marls (Figure 3). Sandstone and marl layers are not always laterally continuous, i.e. rather they pinch out or could be eroded. As results, some sandstones deposited in separate events could be in direct contact, i.e. amalgamated.

The reservoir "series" (i.e. set of connected depositional events) were classified as Upper Pannonian (9.3–7.1 Ma[16]). Reservoirs are elongated along NW-SE direction and represented fast gravitationally dropped sediment, into "strike-slip" area as depositional minimum. Such areas were characteristic for the entire CPBS during Upper Miocene[17], and typical sedimentation model for such sediments in the western Sava Depression had been described for the Kloštar Field[24, 25]. It assumed that the coarsest

Figure 1: *Location map of the Ivanić Field[12].*

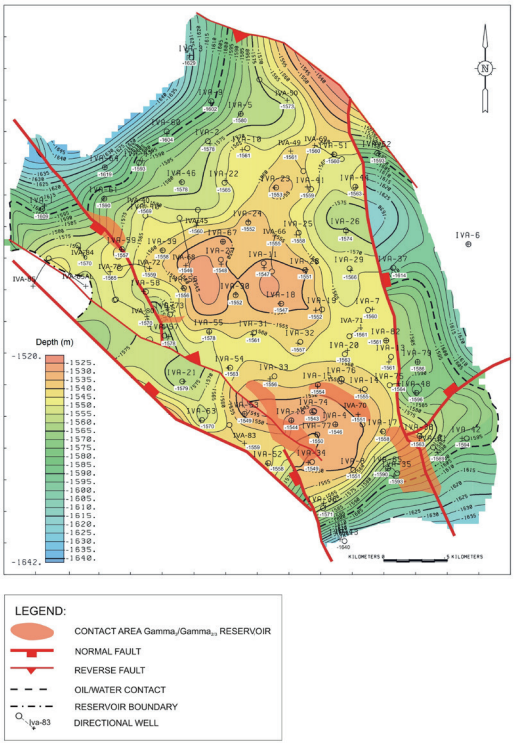

Figure 2: *Structural top map of the reservoir „A" based onto archive maps[12].*

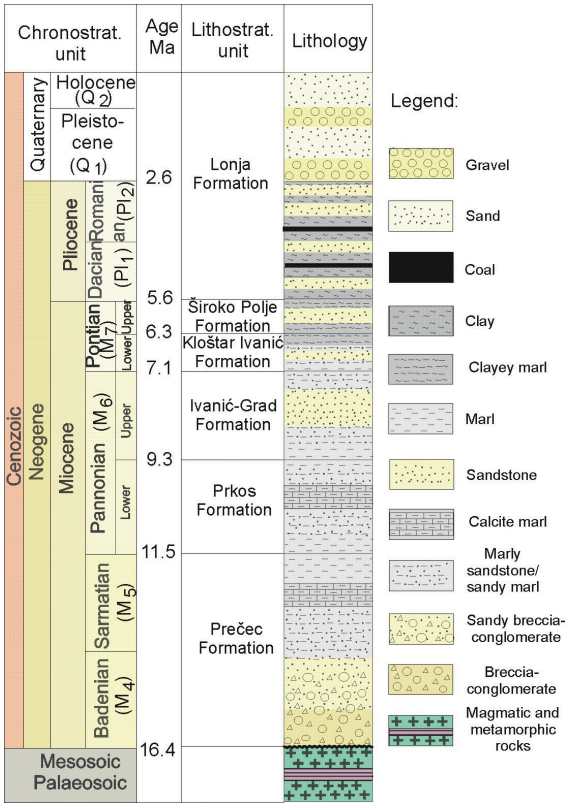

Figure 3: *Schematic geological (lithological, lithostratigraphical and chronostratigraphical) section of the Ivanić Field.*

material had been deposited in the central part of palaeostructure, i.e. main channel(s). Laterally, toward structure borders, depositional lithofacies gradually were replaced with basinal marls.

Basics about applied mapping methods

Deterministical interpolation methods are still commonly used for reservoir characterization and modelling in Croatia[2, 26–30]. However, in several cases stochastical methods are also applied[12] as standard part of geomathematics as it is understood in Croatia[31].

In general, deterministic models for the same input data give always the same results if the analytical method is the same. There are many deterministic interpolation methods, but Kriging is commonly used in geosciences, dealing very well with clustered data and numerical outliers. The goal of the method is to determine spatial relationships between the measured data and the point where value is estimating and it is why a mapping is preceded by variogram (sometimes covariance or madogram) analysis. So, the point's mutual distances, not values, are crucial for interpolation. Moreover, the Kriging is marked with Kriging variance that could be calculated as regional or local. In each case the goal is minimised such variance, i.e. differences between expected and estimated values[32].

Linearity of Kriging estimation could be expresed by Equation 1. It means that value of regionalised variable at selected location (Z_k) is estimated from all surrounding and spatially dependence values (Z_i), using appropriate weighting coefficient (λ_i).

$$Z_k = \sum_{i=1}^{n} \lambda_i \times Z_i \qquad (1)$$

Where are:
Z_k – kriged value,
Z_i – value at location "i",
λ – weighted coefficient.

Such estimation also implies that values Z_i will have normal (Gaussian) distribution. It is conseqeunce of the central limit theorem where is implied that any variable with large number of indenpendent events obtains Gaussian distribution, whatever is probability density function of events[33]. The weighting coefficients in the Kriging are calculated using matrix eqautions[34, 35].

One of the most frequently used Kriging method for facies identification is the Indicator Kriging, i.e. usage of porosity cutoffs. It does not require stationarity assumption of 1st or 2nd degree, or multivariate normality, and is very robust in respect to outliers. In fact, statistics is represented only with variograms, and the originally continuous distribution is discretized using cutoffs, knowing know that at a particular location the value lies in a particular interval.

Indicator approach is used for mapping of two categorical (discrete) values or indicator variable, shown by 0 and 1. Intention is showing two different lithotypes or lithofacies, very often by using the cut-off values for porosity as a geological variable suitable for distinguishing clastic lithofacies[36]. The input values are transformed into indicator ones by using the cut-offs that determine presence or absence of lithofacies. Such method is described with following Equation 2:

$$I(x)_k = \begin{cases} 1 & \text{if } z(x) \le v \\ 0 & \text{if } z(x) > v \end{cases} \qquad (2)$$

Where are:
$I(x)$ – indicator variable,
$z(x)$ – measured value,
v – cut-off.

Calculation of the Indicator Kriging, as each Kriging technique, requires variogram analysis. The special in this technique is that variograms need to be calculating for each cut-off and standardised with sill onto 1. Moreover, recommended number of cut-offs is between 5 and 11, what requires sufficient number of measurements[36]. Indicator maps correspond to continuous assessment of iso-probability lines with values in the interval [0, 1]. Mathematically such maps show the probability of the event $\{z(x) < vk\}$.

Input datasets

Input datasets consisted of 16 wells with porosity and permeability values of the reservoirs "A" and "B" (Table 1 and 2). Porosities were calculated from the log analyses and cored intervals. Permeabilities were obtained by unsteady state method at a constant oil/water viscosity ratio and applying a constant differential pressure across the core samples. After correction for overburden pressure, depth correlation of log analyses and coring data was performed.

Several cut-offs were defined for probability mapping:

— In reservoir "A":
< 15 %, 15–19 %, 19–22 %, 22–24 % and > 24 % for porosity, and < 40 × 10^{-3} μm², 40–50 × 10^{-3} μm², 50–60 × 10^{-3} μm², 60–70 × 10^{-3} μm², 70–80 × 10^{-3} μm² and > 80 × 10^{-3} μm² for permeability.

— In reservoir "B":
< 10 %, 10–15 %, 15–20 %, 20–23 % and > 23 %, and < 1 × 10^{-3} μm², 1–5 × 10^{-3} μm², 5–20 × 10^{-3} μm², 35–75 × 10^{-3} μm² and > 75 × 10^{-3} μm².

Histograms are shown in Figure 4.

Indicator Kriging porosity subsurface maps and correlation between porosity and permeability

Petrophysical parameters were mapped by the Indicator Kriging and obtained are probability maps for certain interval. Porosity intervals 19–22 % for reservoir "A" (Map 1) and 20–23 % for reservoir "B" (Map 2) are chosen as the best representing for extension of medium-grained reservoir sandstones. For reservoir "A" is also derived E-type map that shows the most probable values of porosity (Map 3). Correlation between porosity and permeability was calculated using Pearson's correlation coefficient, and coefficient of determination. The value for the reservoir "A" reservoir is R = 0.76 and R^2 = 0.57 retrospectively (Figure 5) and for reservoir "B" 0.89 and 0.79 (Figure 6).

The both values are qualitatively "high" and can described stronger linear dependence between two analysed variables, especially for reservoir "B". Furthermore, both reservoirs are result of deeper lake sedimentary processes. Later, area was subdued to compaction. However, there were not existed processes that could

Table 1: *Input dataset for the reservoir "A"*

Well	Porosity (%)	Horizontal permeability (10^{-3} μm²)
Well 1	21.03	LIQUIDATED
Well 2	18.68	56.22
Well 3	22.65	76.40
Well 4	18.23	39.90
Well 5	20.20	LIQUIDATED
Well 6	14.32	41.40
Well 7	21.32	52.40
Well 8	18.93	48.09
Well 9	22.03	70.68
Well 10	17.27	60.14
Well 11	24.21	81.01
Well 12	23.13	62.50
Well 13	20.95	49.74
Well 14	22.08	67.20
Well 15	19.80	60.93
Well 16	21.12	58.11

Table 2: *Input dataset for the reservoir "B" reservoir*

Well	Porosity (%)	Horizontal permeability (10^{-3} μm²)
Well 1	1.90	LIQUIDATED
Well 2	0.81	1.39
Well 3	5.10	4.07
Well 4	19.78	32.85
Well 5	0.00	LIQUIDATED
Well 6	0.00	0.91
Well 7	0.00	1.39
Well 8	0.00	1.20
Well 9	8.62	10.39
Well 10	23.76	77.38
Well 11	1.99	2.54
Well 12	23.13	34.36
Well 13	12.07	15.83
Well 14	19.09	29.40
Well 15	0.00	1.63
Well 16	21.27	36.37

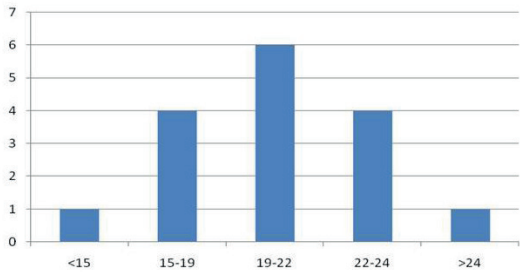

Histogram of number of data in cut-off defined classes of "Gamma 3" porosity
X axis: porosity (%), Y axis: number of data)

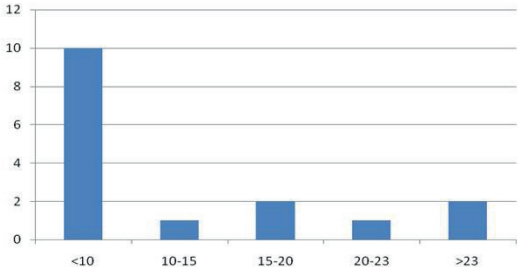

Histogram of number of data in cut-off defined classes of "Gamma 4" porosity
(X axis: porosity (%), Y axis: number of data)

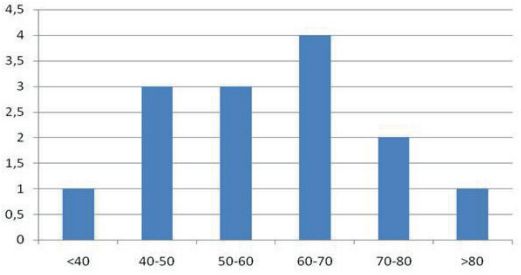

Histogram of number of data in cut-off defined classes of "Gamma 3" porosity
(X axis: permeability (10^{-3} µm^2), Y axis: number of data)

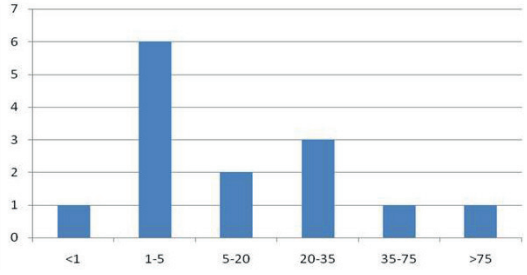

Histogram of number of data in cut-off defined classes of "Gamma 4" porosity
(X axis: permeability (10^{-3} µm^2), Y axis: number of data)

Figure 4: *Histograms of defined classes for the reservoirs "A" and "B" porosity and permeability.*

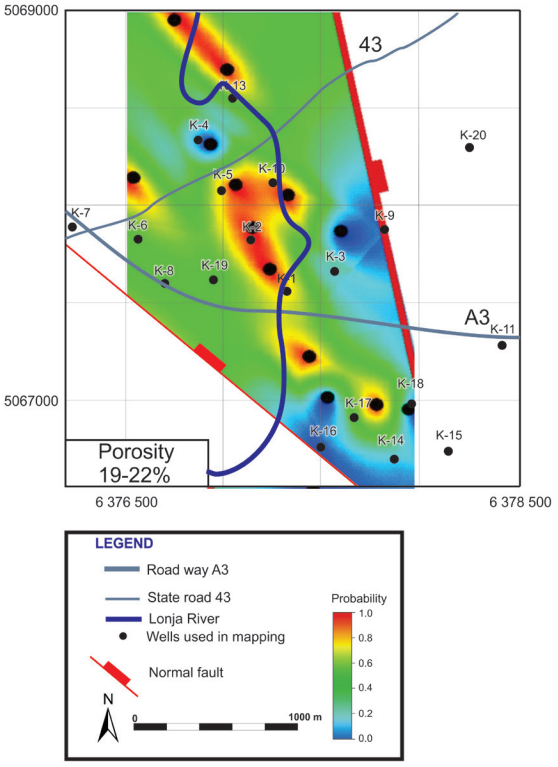

Map 1: *Probability map for the porosity interval* 19–22 % *of reservoir "A" .*

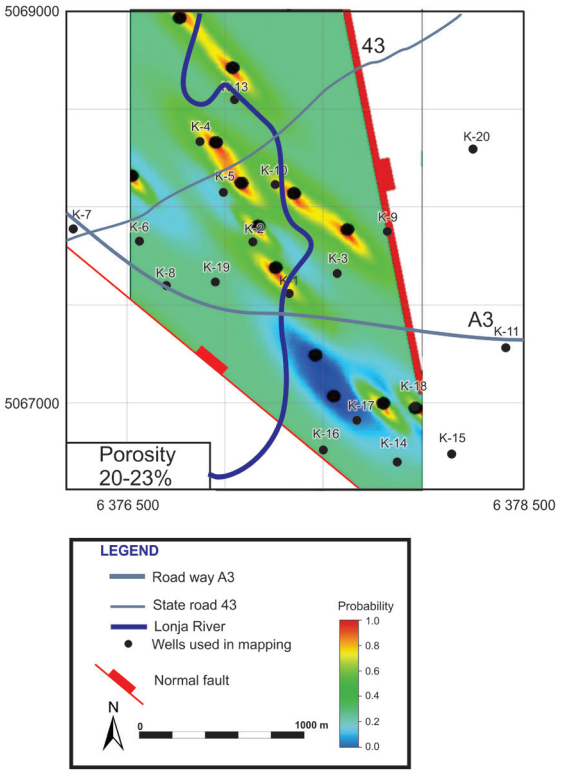

Map 2: *Probability map for the porosity interval* 20–23 % *of reservoir "B".*

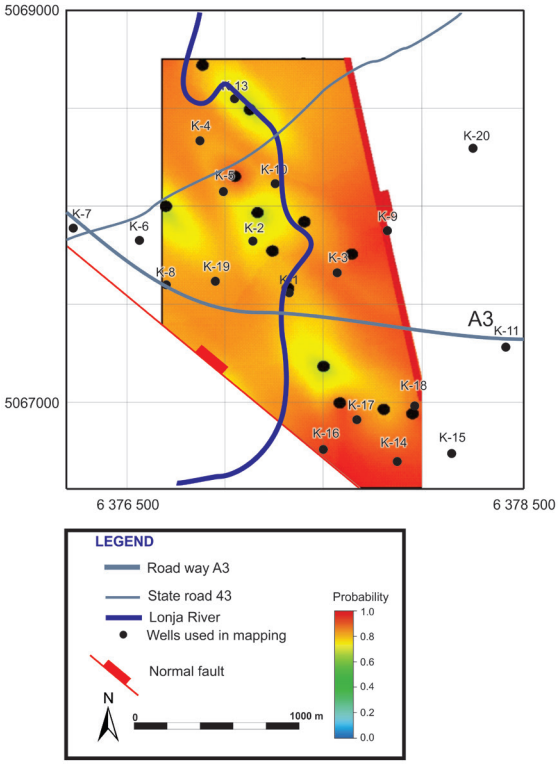

Map 3: *Indicator Kriging E-type map of reservoir "A" porosity, based on the equation of Ordinary Kriging.*

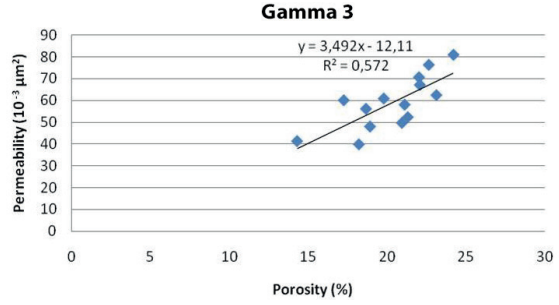

Figure 5: *Porosity and permeability regression line for reservoir "A".*

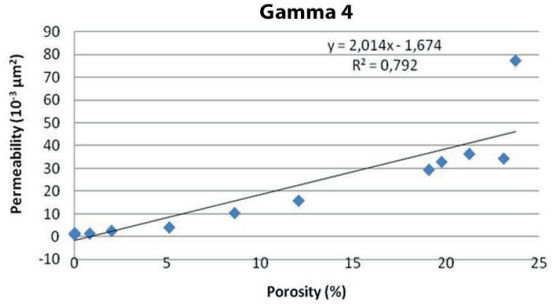

Figure 6: *Porosity and permeability regression line for reservoir "A".*

result in secondary porosity (tectonic caused fracturing) or filling pores with dissolved materials. So, the primary porosity played main role in fluid distribution, what is favourable for linear relation between porosity and permeability. The larger correlation between porosity and permeability in reservoir "B" is probably reflection of generally narrow range of both values in analysed lithological sequence, what is consequence of more uniform depositional environment.

Results and conclusions

Analysed sandstone reservoirs were created in brackish, lacustric depositional environments of the Lake Pannon. The mineral content is represented with quartz, dolomite rock fragments, micas, K-feldspars and cement. The texture is medium to fine-grained with porosity mostly between 15 % and 25 % and average permeability between 50 and 60 × 10^{-3} µm^2. Those values can be considered as typical for the Upper Miocene sandstones in the Sava Depression. Depositional environment included periodically active regional turbidites during Late Pannonian and Early Pontian stages.

However, here are marked intervals between 19 % and 23 % as the most representative for describing depositional area of typical channel, medium-grained sandstone lithofacies. Those are the best lithology for fluid flow and injection into analysed reservoirs. For this purpose those intervals are mapped into two reservoirs planned for CO_2 injection. The results (Maps 1 and 2) shows areas where such turbiditic lithofacies could be certainly followed. However, the maps are biased with elongated "bull-eyes" effect, what is not favourable feature for interpretation. It could be override using approximately omnidirectional variogram model, with larger ranges, but it was not observed in data itself. So, presented Indicator Kriging probability maps are considered as the most representative and useful for planning pilot injection.

The last Map 3 is direct porosity map of the reservoir "A", but interpolated using Ordinary and Indicator Kriging algorithms simultaneously.

It was possible using algorithm that indicator probability maps considered as the "weights" for the more precise application of the Ordinary Kriging.
Interestingly, not each "bull-eye" shape was characterised with maximal probabilities or direct porosity estimated values. It is directed reflection of palaeo-depths of each such "micro" strike-slip on the bottom of the Ivanić Structure during Upper Pannonian, where some of them were deeper and "collected" the coarser detritus (mostly on the east and southeast) then other ones.

Acknowledgments

This work represents part of a multidisciplinary geological research project entitled "Development of geomathematical methods for analysis of Neogene depositional environments in the Croatian part of Pannonian Basin System" (head T. Malvić), financially supported by the University of Zagreb in programme "Supporting of researching 2" in the 2013, the licensed version of WinGslib had been used for mapping.

References

[1] Awan, A. R., Teigland, R., Kleppe, J. (2008): A Survey of North Sea Enhanced-Oil-Recovery Projects Initiated During the Years 1975 to 2005. *SPE Res. Eval. & Eng.,* 11 (3), pp. 497–512.

[2] Balić, D., Velić, J. & Malvić, T. (2008): Selection of the most appropriate interpolation method for sandstone reservoirs in the Kloštar oil and gas field. *Geologia Croatica,* 61 (1), pp. 27–35.

[3] Bennaceur, K., Monea, M., Sakurai, S., Gupta, N., Ramakrishnan, T. S., Whittaker, S., Randen, T. (2004): CO_2 capture and storage a solution within. *Oilfield Review*, 16 (3), pp. 44–61.

[4] Ma, J., Morozov, I. (2010): AVO modeling of pressure-saturation effects in Weyburn CO_2 sequestration. *The Leading Edge*, 29 (2), pp. 178–183, doi: 10.1190/1.3304821.

[5] White, D. (2009): Monitoring CO_2 storage during EOR at the Weyburn-Midale Field. *The Leading Edge*, 2 (7), pp. 838–842, doi: 10.1190/1.3167786.

[6] Sarapa, M. (1981): *Utjecaj ugljičnog dioksida na svojstva i iscrpak nafte* (Influence of carbon-dioxide on oil properties and recovery) Mag. Thesis. University of Zagreb: Faculty of Mining, Geology and Petroleum Engineering 1981; 171 p.

[7] Sečen, J. (2006): *Enhance oil recovery methods (Metode povećanja iscrpka nafte) (1st ed.*). Zagreb: INA-Industry of Oil Plc 2007, pp. 273–364.

[8] Stalkup, F.I. (1980): Carbon Dioxide Miscible Flooding: Past, Present, And Outlook for the Future. *Journal of Petroleum Technology,* 30 (8), 1102–1112, doi: 10.2118/7042-PA.

[9] Lu, J., Wilkinson, M. & Haszeldine, R. S. (2011): Carbonate cements in Miller field of the UK North Sea: a natural analogue for mineral trapping in CO_2 geological storage. *Environmental Earth Sciences,* 62 (3), pp. 507–517.

[10] Bauer, S., Class, H., Ebert, M., Gotze, H., Holzheid, A., Kloditz, O., Rosenbaum, S., Rabbel, W. & Schafer, D. (2012): Modelling, Parameterization, and Evaluation of Monitoring Methods for CO_2 Storage in Deep Saline Formations the CO_2 MoPa Project. *Environmental Earth Sciences,* doi: 10.1007/s1266-012-1707-y.

[11] Goričnik, B., Domitrović, D. (2003): Laboratorijska istraživanja primjenjivosti CO_2 procesa na naftnim poljima u Republici Hrvatskoj (Laboratory researching of applicability of CO_2 processes in oil fields in Republic of Croatia). *Naftaplin,* 1, pp. 5–12.

[12] Novak, K., Malvić, T., Velić, J., Simon, K. (2013): Increased hydrocarbon recovery and CO_2 storage in Neogene sandstones, a Croatian example: part II. *Environ Earth Sciences,* 71 (8), pp. 1866–6280, doi:10.1007/s12665-013-2756-6.

[13] Perić, M., Kovač, S. (2003): Simulacijska studija procesa povećanja iscrpka nafte (EOR-procesa) istiskivanjem ugljik-dioksidom primjenom višekomponentnog modela COMP III (Simulation Study of Enhanced Oil Recovery Process by CO_2 injection Applying a Multi-component COMP III). *Naftaplin,* 1, pp. 13–25.

[14] Novak Zelenika, K., Velić, J., Malvić, T. (2013): Local sediment sources and palaeoflow directions in Upper Miocene turbidites of the Pannonian Basin System (Croatian part), based on mapping of reservoir properties. *Geological quarterly,* 57 (1), pp. 17–30.

[15] Novosel, D. (2005): Rezultati projekta pokusnog istiskivanja nafte utiskivanjem ugljičnog dioksida na Naftnom polju Ivanić (The project results of

test oil replacement by carbon dioxide on the Ivanić oil field). *Naftaplin,* 1, pp. 51–60.

[16] Haq, B. U., Eysinga, F. W. B. (1998): *Geological Time Table* (5th ed.). Amsterdam: Elsevier Science, (Wall Chart).

[17] Malvić, T. (2012): Review of Miocene shallow marine and lacustrine depositional environments in Northern Croatia. *Geological Quarterly,* 56 (3), pp. 493–504.

[18] Malvić, T., Velić, J. (2011). *Neogene Tectonics in Croatian Part of the Pannonian Basin and Reflectance in Hydrocarbon Accumulations.* In: New Frontiers in Tectonic Research: At the Midst of Plate Convergence, Schattner, U. (eds.), InTech, Rijeka 2011, pp. 215–238.

[19] Velić, J. (2007): *Geologija ležišta nafte i plina (Geology of oil and gas reservoirs)*. Faculty of Mining, Geology and Petroleum Engineering, University of Zagreb 2007; 342 p.

[20] Rögl, F. (1998): *Palaeographic Consideration for Mediterranean and Paratethys Seaways (Oligocene to Miocene).* Ann. Naturhist. Mus. Wien 99A 1998; pp. 279–310.

[21] Vrbanac, B. (1996): *Palaeostructural and sedimentological analyses of Upper Pannonian sediments Ivanić Grad Formation in the Sava Depression*. Doctoral Thesis. University of Zagreb: Faculty of Mining, Geology and Petroleum Engineering 1996; 121 p.

[22] Vrbanac, B., Velić, J., Malvić, T. (2010): Sedimentation of deep-water turbidites in the SW part of the Pannonian Basin. *Geologica Carpathic,* 61 (1), 55—69, doi: 10.2478/v10096-010-0001-8.

[23] IEA GHG Weyburn CO2 Monitoring & Storage project Summary Report 2000–2004. Petroleum Technology research Centre, Regina 2004. Available on: <http://www.ptrc.ca/siteimages/Summary_Report_2000_2004.pdf>.

[24] Novak Zelenika, K., Cvetković, M., Malvić, T., Velić, J. & Sremac, J. (2013): Sequential Indicator Simulations maps of porosity, depth and thickness of Miocene clastic sediments in the Kloštar Field, Northern Croatia. *Journal of Maps,* 9 (4), pp. 550–557.

[25] Novak Zelenika, K. (2012): *Deterministički i stohastički geološki modeli gornjomiocenskih pješčenjačkih ležišta u naftno-plinskom polju Kloštar* (Deterministic and stohastic geological models of Upper Miocene sandstones reservoirs at the Kloštar oil and gas field). Doctoral Thesis, University of Zagreb: Faculty of Mining, Geology and Petroleum Engineering 2012, 190 p.

[26] Cvetković, M., Velić, J., Malvić, T. (2009): Application of neural networks in petroleum reservoir lithology and saturation prediction. *Geologia Croatica,* 62 (2), pp. 115–121.

[27] Malvić, T. (2005): Rezultati geostatističkog kartiranja poroznosti polja zapadnog dijela Dravske depresije (Molve, Kalinovac, Stari Gradac). *Nafta*, 56 (12), pp. 472–476.

[28] Malvić, T. (2006): Middle Miocene Depositional Model in the Drava Depression Described by geostatistical porosity and thickness maps (case study: Stari Gradac-Barcs Nyugat Field). *Rudarsko-geološko-naftni zbornik,* 18, pp. 63–70.

[29] Malvić, T., Balić, D. (2009): Linearnost i Lagrangeov linearni multiplikator u jednadžbama običnoga kriginga (Linearity and Lagrange Linear Multiplicator in the Equations of Ordinary Kriging). *Nafta,* 60 (1), pp. 31–43.

[30] Malvić, T., Đureković, M. (2003): Application of methods: Inverse distance weighting, ordinary kriging and collocated cokriging in porosity evaluation, and comparison of results on the Beničanci and Stari Gradac fields in Croatia. *Nafta,* 54 (9), pp. 331–340.

[31] Lapaine, M., Malvić, T. (2009): Geomathematics between Mathematics and Geosciences. *Annual of the Croatian Academy of Engineering,* 12, pp. 51–67.

[32] Isaaks, E., Srivastava, R. (1989): *An Introduction to Applied Geostatistics*. New York: Oxford University Press Inc. 1989; 580 p.

[33] Geiger, J. (2006): *The behaviour of Sequential Gaussian Simulation in the limits*. Xth Congress of Hungarian Geomathematics, (May 18–20. 2006), Morahalom, Hungary.

[34] Deutsch, C. V., Journel, A. G. (1997): *GSLIB: Geostatistical Software Library and User's Guide (2nd ed.)*. New York: Oxford University Press Inc. 1997; 369 p.

[35] Hohn, M. E. (1988): *Geostatistics and Petroleum Geology*. New York: Van Nostrand Reinhold 1998; 400 p.

[36] Novak Zelenika, K., Malvić, T. & Geiger, J. (2010): Mapping of the Late Miocene sandstone facies using Indicator Kriging. *Nafta,* 61 (5), pp. 225–233.

Professional paper

Received: October 25, 2014
Accepted: January 20, 2015

Design of product properties by suitable planning of a cold forging process

Oblikovanje lastnosti izdelka z ustreznim načrtovanjem procesa hladnega kovanja

Vid Krušič*, Martin Fabjan
MAHLE Letrika, d. o. o., Polje 15, 5290 Šempeter pri Gorici, Slovenia
*Corresponding author. E-mail: vid.krusic@si.mahle.com

Abstract

One of the main advantages of the cold forming technology is improvement of mechanical properties such as tensile strength and hardness. At cold metal forging the hardness increases by plastic deformation, also known as work hardening. The degree of plastic deformation is represented by equivalent plastic strain. It is generally accepted that the mechanical property such as hardness are directly related to equivalent plastic strain. If the operating sequence to manufacture a certain product by cold forging is suitably planned, the required value of equivalent strain or appropriate hardness in the product's cross-section is achieved. The paper deals with planning of mechanical properties in manufacture of antivibration elements for the needs of the automotive industry and hubs of magnetic ignition systems for the motorcycle industry. At the production of antivibration elements the resistance to permanent plastic deformation in the case of axial dynamic loading of a product have to be assured, while in the case of hubs of magnetic ignition systems the appropriate hardness in the product's cross-section has to be achieved. A reliable design of the desired mechanical properties of products is assured by suitable planning of the forming processes in the virtual environment with the support of numerical simulations.

Key words: cold forging, product property design, hardness, FE simulation

Izvleček

Ena izmed glavnih prednosti hladnega preoblikovanja je izboljšanje mehanskih lastnosti izdelka, kot sta natezna trdnost in trdota. Pri hladnem preoblikovanju trdota narašča s plastično deformacijo, kar je poznano kot hladno utrjevanje. Stopnja plastične deformacije je izražena z ekvivalentno plastično deformacijo. Splošno je znano, da je mehanska lastnost, kot je trdota, direktno povezana z ekvivalentno plastično deformacijo. Če je preoblikovalno zaporedje za izdelavo izdelka ustrezno načrtovano, lahko dosežemo zahtevano ekvivalentno deformacijo oziroma ustrezno trdoto po prerezu izdelka. Članek podaja načrtovanje mehanskih lastnosti pri izdelavi antivibracijskih izdelkov za potrebe avtomobilske industrije ter pest magnetnih vžigalnikov za potrebe industrije motornih koles. Pri antivibracijskih elementih moramo zagotoviti odpornost proti trajni plastični deformaciji v primeru aksialne dinamične obremenitve izdelka, medtem ko pri pestih magnetnih vžigalnikov z ustrezno trdoto po prerezu izdelka zagotavljamo obratovanje pri visokih vrtljajih. Zanesljivo oblikovanje želenih mehanskih lastnosti izdelkov lahko zagotovimo z načrtovanjem preoblikovalnih procesov v virtualnem okolju ob podpori numeričnih simulacij.

Ključne besede: hladno preoblikovanje, oblikovanje lastnosti izdelka, trdota, simulacija z MKE

Introduction

From the perspective of production processes, cold forming (CF) is one of the most important technologies which enable production of geometrically demanding and accurate products. The CF technology aims at plastic deformation of a blank from simple initial forms by the forming process to a product of a complex form and dimensions. The main reasons for using the CF technology mostly in the automotive industry are as follows[1–3].

- Great accuracy of dimensions and good surface qualities in mass manufacture of products,
- Efficient material use; generally smaller refinishing operations, including machining, are required,
- Improved mechanical properties as a result of hardening in cold, the fibres flow is uninterrupted and adjusted to the product loading, which enables the products to withstand greater dynamic loads and to be lighter accordingly,
- Technology is economical and environment friendly.

In cold plastic deformation, the material is hardened. This causes structural changes of material. Grains are elongated in the direction of the main deformation. Owing to the material hardening, there are changes of mechanical, physical and chemical properties of metal (Figure 1). By greater deformation, true stress, tensile strength, material hardness, and electrical resistance increase. At the same time reduction of elongation, contraction, impact toughness, resistance to corrosion, heat conductivity and elasticity module occur.

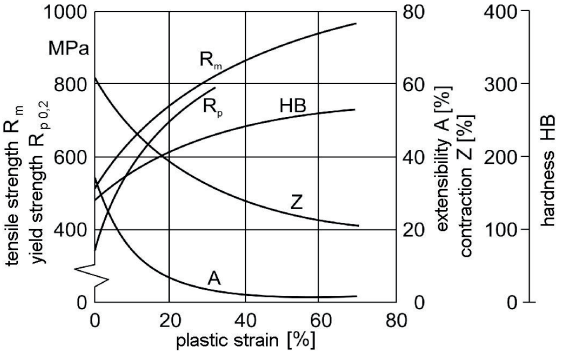

Figure 1: *Changes of mechanical properties as a consequence of cold forming process.*

Up to now many researches have been made towards predictions of mechanical properties of a product. If we are familiar with the ratio between the hardness and effective strain of the formed part material and the strain flow of the formed part, we can predict the course of hardness of a cold-formed part. Kim et al. performed a pressure test by the help of an experiment and FE simulation for the steel AISI 1010[4]. Hardness values regarding pressure test and effective deformations from the FE simulations have been analysed in the same point of a formed-piece. The curve and/or ratio between the hardness and the effective strain were acquired by a regression analysis. In the next study, a similar analytical model for hardness prediction of a formed piece was presented, which is based upon the known effective strain that was achieved by the FE analysis of a formed-piece[5]. The model was confirmed by an experiment, so that hardness prediction of a formed-piece is quite accurate. Tekkaya[6] carried out an analysis of final imprinting in a cold-formed part in order to find equivalent Vickers hardness and to gain the ratio between the Vickers hardness and the flow stress. Mechanical properties of a product like hardness, yield stress, elongation, residual ductility and tensile test depend directly on the equivalent deformation caused in cold forming. The article by K. Osakada and J. Yanagimoto[7] emphasizes that distribution of an equivalent deformation of the formed-piece is gained through the FE simulation and in this way we can – by a suitable ratio – define the course of mechanical properties of a product. D. Biermann et al. recommended a new way of product manufacture, which already at the planning stage considers the real material properties defined by a production process (Figure 2), while the classical way of a product planning considers only ideal material properties[8]. In this way, knowledge on local material properties are gained in tensile tests, damages, other stress, textures and micro structures used already in the process of planning, what enables product manufacture true to size. Safety factor and product weight are in this way substantially reduced, which results in reduced consumption of energy in primary production of materials as well as in the later use of a product.

Hardening in cold forming can be used to one's advantage in product manufacture, where specific product properties like a defined hardness in the product cross-section or specified tensile stress are required. By suitable planning of the forming operation sequence required for a product manufacture, we can achieve the specified mechanical properties of a product. Schematic course of the process steps for a suitable planning of mechanical properties of a product with the forming process is shown in Figure 3. In this kind of planning of the specified mechanical properties, one has to pay attention to obtain a healthy product in the cross section cut, which means there are no damages of the product.

The purpose of this paper is to show planning of the specified mechanical properties in the products by the cold forming technology for the needs of the automotive and motorcycle industries. First example shows planning of manufacture of the automotive antivibration bush, where in case of axial dynamic loading of a product resistance to permanent plastic deformation is required. The second example shows manufacture of a hub of magnetic ignition system for the needs of motorcycles with the requirement for a suitable tensile stress in the product cross-section. We can assure a reliable planning of the desired mechanical properties of products by creating the forming processes in the virtual environment with the support of numerical simulations.

Requirements for the manufacture of an antivibration busch

During driving, the car is subject to various vibrations both for external impacts, caused by the roadway, and internal impacts resulting from various drive elements. The external impacts caused by the roadway can be insulated by tyres with mufflers and dumpers, while the internal vibrations are insulated by antivibration elements. Figure 4 shows over 20 different antivibration elements, which are built into a car in order to insulate vibrations. These are elements that are used as vibration insulation as for example in vibrations from an engine, exhaust system, suspension etc. Usually these are steel, tube-like parts, whose external surface if potted by rubber. In MAHLE Letrika we make various tube-like elements for the needs of antivibration elements (Figure 5(a))[9]. These metal tube-like elements are made by the cold forming technology. The product requirements include a specific form and resistance to permanent plastic deformation. Such form and resistance can be achieved only by the cold forming technology. Figure 5 (b) shows the allowed plastic deformation in case of axial dynamic loading of a bush.

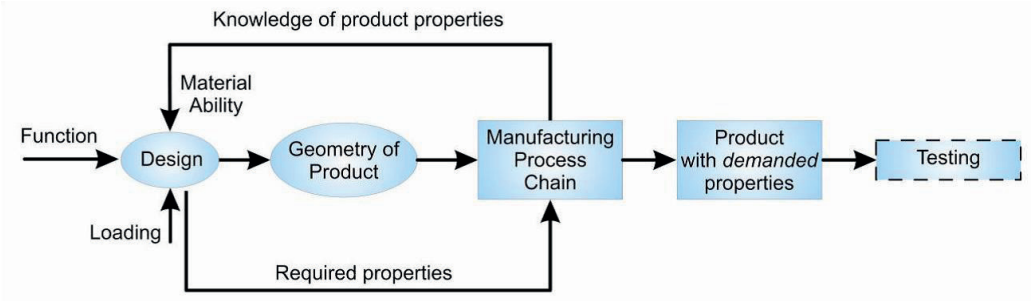

Figure 2: *New approach in designing and manufacturing products*[8].

Figure 3: *A flow chart for design product properties by suitable planning of the cold forging process.*

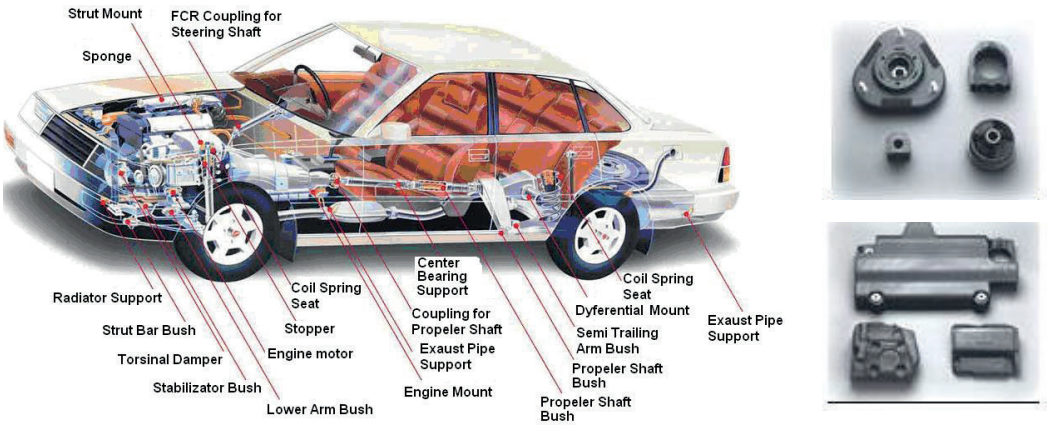

Figure 4: *Various antivibration elements built in a car.*

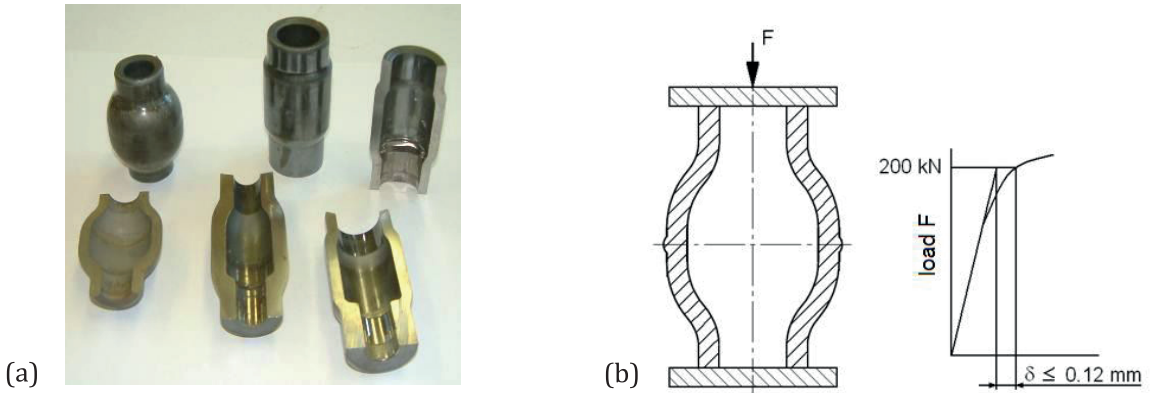

Figure 5: *(a) metal tube-like parts of antivibration elements, (b) allowed plastic deformation in loading of an antivibration bush.*

Planning of antivibration busch by CF technology

To make a steel Ck 25 (DIN) bush, double passing through the press is required. In the first passing, operations follow in the sequence from (a) to (d) as shown in Figure 6. First, we plan the initial blank, which has previously been annealed and surface-treated by a phosphate and molybdenum disulphide, to a suitable external diameter. Then, the subsequent operations follow: centring, backward extrusion and bottom punching. After the first passing, the formed-piece is annealed properly and again surface-treated. In the last operation (e), reduction/narrowing of the upper part of the pre-form to the appropriate final form is made. We planned the operation sequence and metal flow during the pre-forming operation by the help of the programme DEFORM 2D[10].

The final bush form and material hardening during the forming process have to ensure the requirements regarding the plastic deformation in case of an axial loading (Figure 5(b)). Figure 7 (a) shows the flow of effective deformations in the product cross-section simulated by the FE method. The upper curve in the diagram (Figure 8) shows the impact of loading on the permanent plastic deformation analysed in the virtual environment. A cold formed bush achieves permanent plastic deformation of a few hundredths of a millimetre in case of loading by 200 kN, which is within the limits of the allowed deformation 0.12 mm. The results have been confirmed also by physical tests in production. We were interested also in what would the resistance be if a bush was made by the machining procedure and/or in the non-hardened condition (Figure 7 (b)). In this case, we exceed the permanent plastic deformation already at loading of 120 kN as shown in the lower curves in the diagram (Figure 8). Even at full non-hardened bush (Figure 7 (c)) the situation is essentially the same as at non-hardened bush. A critical section is the same in both bushes.

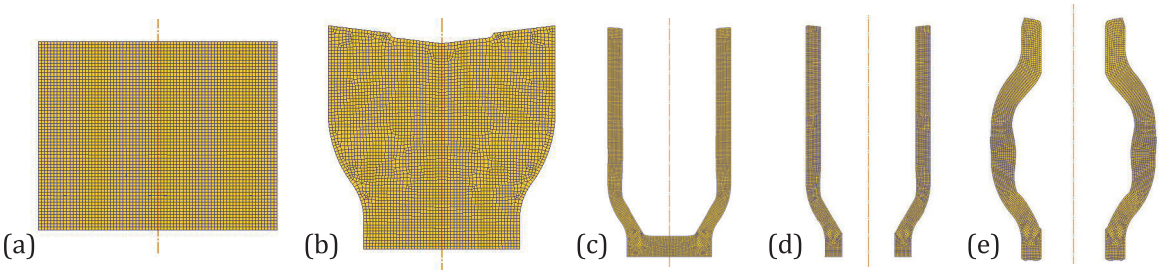

Figure 6: *Operational plan of the forming operation sequence for manufacture of a bush.*

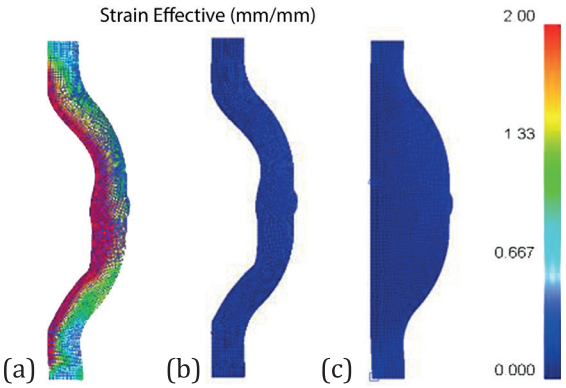

Figure 7: *(a) CF bush - hardening in the cross-section, (b, c) non-hardened bush.*

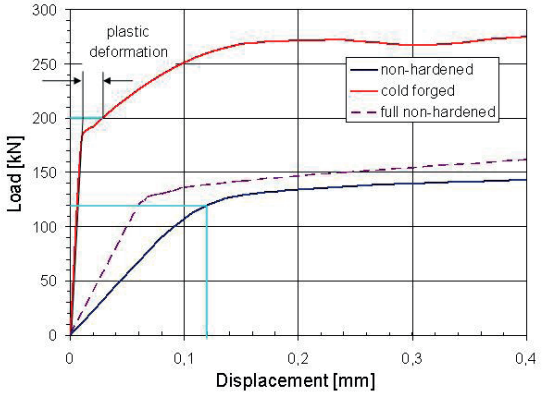

Figure 8: *Plastic deformation of a bush in dependence on loading.*

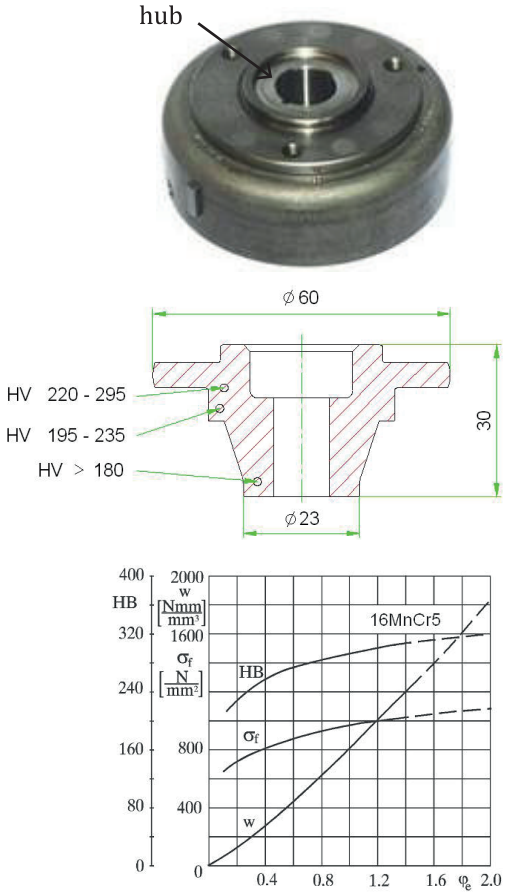

Figure 9: *The flywheel, hub of magnetic ignition system and hardness in dependence on the true strain for steel 16MnCr5.*

Requirements for a hub of magnetic ignition system

The next example of improved mechanical properties is shown in manufacture of a hub of magnetic ignition system. A hub is a component element of the magnetic ignition system, which is used in motorcycles (Figure 9). The hub's job is to transfer the torque from the shaft to the flywheel at a high rotational speed. A basic requirement of a hub made of steel 16MnCr5 is that it has a suitable hardness in the cross-section, which in this way ensures product hardness. An appropriate hardness in the product cross-section is achieved when a hub is made by the cold forming technology. The forming processes have to be planned so that they ensure a suitable deformation in the desired product points. Bigger deformation at the same time denotes greater hardness as shown in the diagram in Figure 9. Attention has to be paid so that deformation does not exceed the critical limit, which could cause material damage.

Planning of an appropriate hardness in the hub cross-section

As already described in the introduction, the cold forming technology enables improvement of mechanical properties due to material hardening during a forming process. Planning of an appropriate hardness in the product cross-section by the cold forming technology depends on the following factors:

- It is necessary to have data on the forming properties of a material at disposal. Figure 9 shows the curve of the flow stress σf, the curve of the hardness HB and the specific forming work w from the size of the true strain ϕe for steel 16MnCr5[11],
- Available hardware such as presses, number of forming operations that can be carried out in one passing through the press,
- Software to make simulations of material flow and hardening during the forming process. Experimental appraisal of hardness is connected to great costs in respect of tool making, test implementation on a press, measurement of hardness in the formed-piece cross-section etc.
- Knowledge and experience in the field of CF metals. Definition of optimum sequence of forming operations is required, which on one hand enables achieving of the suitable hardness in the product cross-section and on the other hand as long tool life as possible, automatic operating of the formed pieces during passing through the press etc.

The forming process is planned at the end, i.e. from the final form to the initial blank. First, we design a suitable pre-form for the final operation. In Figure 10 (a), (b) two pre-forms are made and flow of an appropriate effective strain of a product gained by the FE simulation. Based on the comparison we can make an analysis about the pre-form (a) causing bigger effective deformations on the final product, while the pre-form (b) ensures a more homogeneous deformation, which pretty well meets the requirements regarding the distribution of the required hardness in the product cross-section. However, to optimize a suitable pre-form more FE simulations have been made, Figure 10 show only two of them.

Figure 11 shows the sequence of the forming operations gained by the FE simulation method. The machined-piece with a suitable product weight is first surface treated. The forming operations follow from operations (a)–(c) for the first passing through a vertical mechanical stress 630 t. Heat treatment follows, then the pre-form (c) process annealing and surface treatment, and the second passing through the press for operations (d)–(g). The simulated hardness flow in the product cross-section is shown in Figure 12. The highest hardness is achieved in the lower and upper side of the flange and in the inside of the hub hole.

The hardness flow meets the hardness of the product requirements. Approval of suitable planning of the forming operation sequences and hardness in the hub cross-section is acquired only in the product mass production. Inspection of cold-formed hubs showed that hardness meets the planned/required hardness in the product cross-section well. An accurate analysis of the product micro-structure is required in order to determine possible material damages due to local hardening and/or forced flow of material.

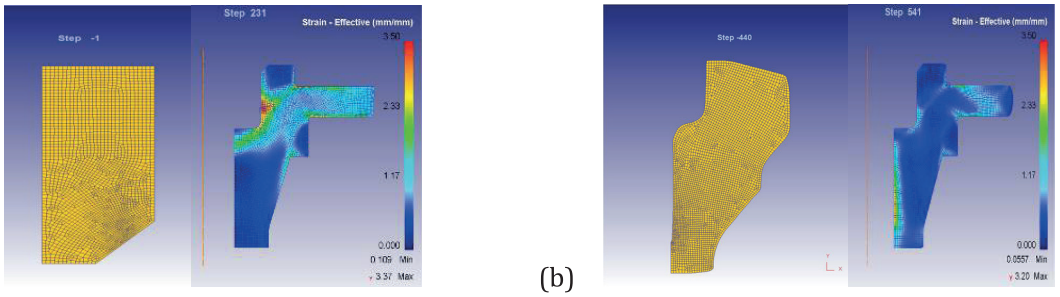

Figure 10: *(a), (b) various pre-forms and flow of the effective strain in the product final form.*

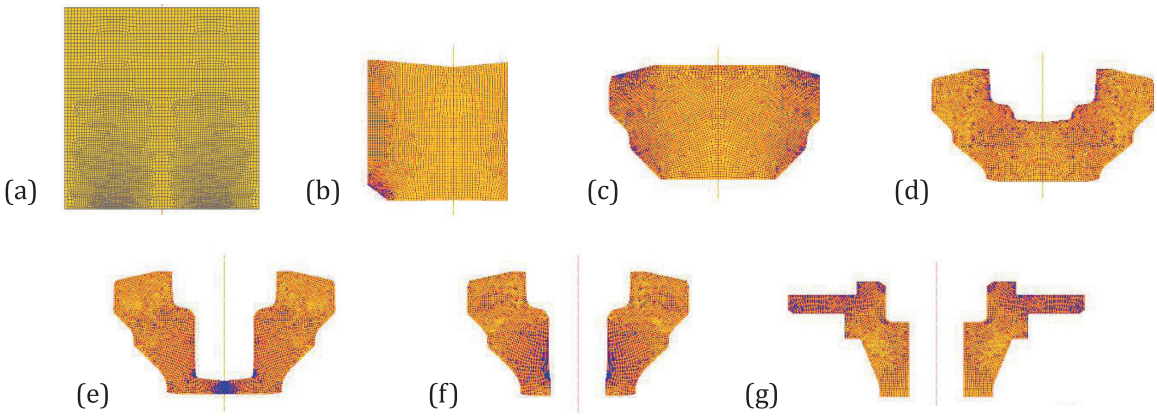

Figure 11: *Sequence of the forming operations for the manufacture of the hub of magnetic ignition system.*

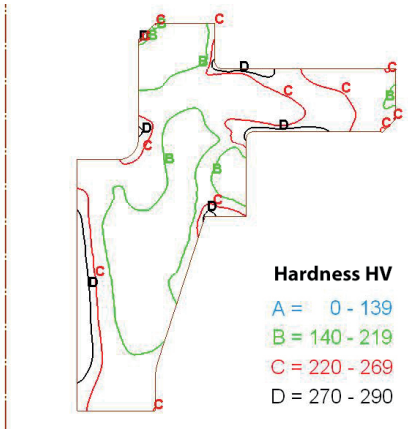

Figure 12: *The hardness flow in the hub cross-section simulated by the help of FE simulation.*

Conclusions

The paper deals with planning of suitable mechanical properties in a product by the CF technology. Two examples of product manufacture for the needs of the automotive industry and industry of motorcycles are shown, in which the functional requirement is a product resistance against the permanent plastic deformation in case of an axial loading and distribution of suitable hardness in the product cross-section. By the support of a FE simulation and suitable planning of the forming operations sequence we can ensure the specified functional requirements in the products and thus make a good use of the advantages offered by the CF technology.

Acknowledgements

The article was published in Conference Proceedings: New Developments in Forging Technology, Editor Prof. Dr. M. Liewald MBA, Institute for Metal Forming Technology, University of Stuttgart, Fellbach, Germany, 2013.

References

[1] Gologranc, F. (1991): *Forming, part 1*. University of Ljubljana, Faculty of Mechanical Engineering, Ljubljana, (in slovene), p. 250.

[2] Altan, T., Ngaile, G., Shen, G. (2005): *Cold Forging Fundamentals and Applications*. ASM International, Materials Park, OH, p. 341.

[3] Lange, K. (1985*): Handbook of Metal Forming*, McGraw-Hill Book Company, New York, p. 1176.

[4] Kim, H., Lee, S. M., Altan, T. (1996): Prediction of hardness distribution in cold backward extruded cups. *Journal of Materials Processing Technology,* 59, pp. 113–121.

[5] Sonmez, F. O., Demir, A. (2007): Analytical relations between hardness and strain for cold formed parts. *Journal of Materials Processing Technology,* 186, pp.163–173.

[6] Tekkaya, A. E. (2001): Improved relationship between Vickers hardness and yield stress for cold forming materials. *Steel Research,* 72 (8), pp. 204–310.

[7] Osakada, K., Yanagimoto, J. (2010): *Prediction of Property of Metal Forming Product by the Finite Element Method*. Proceedings of the 1st International conference on product property prediction, Ed; D. Biermann, A. E.Tekkaya, W. Tillman, Technische Univertaet Dortmund, pp. 155–167.

[8] Biermann, D., Tekkaya A. E., Tillmann, W. (2010): *Tailor Made Properties – Visions for the future of Manufacturing.* Proceedings of the 1st International conference on product property prediction, Ed; D. Biermann, A. E. Tekkaya, W. Tillman, Technische Univertaet Dortmund, pp. 77–91.

[9] Krušič, V., Mašera, S. (2009): *Improvement of mechanical characteristics of products by cold forming technology*. 9th conference and exhibition Innovative Automotive Technology IAT'09, Ed; M. Fajdiga, J. Klemenc, F. Trenc, Nova Gorica, (in slovene), pp. 385–392.

[10] SFTC (2007): *Deform 2/3D*, Ver. 8.1, User Manual, Columbus, Ohio, 2007.

[11] Kuzman, K. (1989): *Exercises in forming techniques*. University of Ljubljana, Faculty of Mechanical Engineering, Ljubljana, (in slovene), p. 71.

Professional paper

Received: July 12, 2014
Accepted: February 11, 2015

Petrophysical evaluation of reservoirs in 'y' prospect Niger delta

Petrofizikalna ocena rezervoarjev na raziskovalnem območju 'y' v delti Nigra

Yemisi. C. Ajisafe
Ekiti state University, Faculty of Science, Department of Geology, Ado Ekiti, Nigeria
Corresponding author. E-mail: tuaseyemi@yahoo.co.uk

Abstract

A suite of well logs of two wells (1 and 2) from 'Y' Prospect Niger Delta were evaluated using GeoGraphix software, with the aim of computing the petrophysical characteristics of the reservoirs as well as identify reservoir lithology within and between wells for information on stratigraphic and lithological parameters of the wells. Three reservoirs were correlated at depth range of 1 524 m to 1 800 m, with thicknesses of 10–45 m. Cross plot of neutron porosity and density porosity were used to discriminate the fluid types. Computation of petrophysical properties and reservoir evaluation were carried out to determine recoverable hydrocarbon in place in the reservoirs. Well log data shows that area was characterized by sandy shale interbeds. Porosity values for the reservoir ranged from 30–40 %, water saturation 30–45 % and hydrocarbon saturation 65–80 %. Gas zone of economic importance was detected in reservoir L300 in well 2. The reservoir properties of the wells showed that they could be fair to very good for hydrocarbon accumulation.

Key words: petrophysical properties, hydrocarbon reservoir, GeoGraphix, Nigeria

Izvleček

Karotažne podatke iz dveh vrtin (1 in 2) v raziskovalnem območju 'Y' v delti Nigra so ovrednotili z GeoGraphixovimi programi z namenom izračunati petrofizikalne značilnosti rezervoarjev ogljikovodikov, opredeliti litološke lastnosti v vrtinah in med njima ter dobiti ustrezne podatke o stratigrafskih in litoloških parametrih. V globini med 1 524 m in 1 800 m so povezali prereze treh rezervoarjev debeline od 10 m do 45 m. Tipe fluidov v plasteh so določili iz podatkov o nevtronsko ugotovljeni poroznosti in gostoti. Količine pridobljivih ogljikovodikov v rezervoarjih so ocenili iz izračunanih petrofizikalnih lastnosti in značilnosti rezervoarjev. Karotažni podatki nakazujejo prisotnost peščeno-muljastih vmesnih plasti. Vrednosti poroznosti v rezervoarjih se gibljejo med 30 % in 40 %, nasičenosti z vodo med 30 % in 45 % in nasičenosti z ogljikovodiki med 65 % in 80 %. Navzočnost ekonomsko pomembnih zalog plina so ugotovili v rezervoarju L300 v vrtini 2. Lastnosti rezervoarjev v vrtinah pričajo o dobri do zelo dobri sposobnosti za nakopičenje ogljikovodikov.

Ključne besede: petrofizikalne lastnosti, rezervoar ogljikovodikov, GeoGraphix, Nigerija

Introduction

A well log can be defined as an indirect record showing the rock and fluid properties along borehole. Such physical properties include electrical, radioactive, and some special kinds of measurements like electrical resistivity, spontaneous potential, gamma ray intensity, density, acoustic velocity etc.[1]. Most quantitative log analyses are aimed at defining petrophysical parameters, but only few of these parameters(-Formation lithology, thicknesses and depths of the reservoirs and even non-reservoirs) can be measured directly. Others have to be derived or inferred from the measurement of other physical parameters of the rocks. Three basic logs (lithology, resistivity and porosity logs) are needed for proper formation evaluation. One is required to indicate permeable zones; another is needed to measure the resistivity of the formation, while the third is important for estimating porosity values.

Well logs furnish the data necessary for the quantitative evaluation of hydrocarbon in-situ. From the view point of decision making, well logging is the most important aspect of drilling and completion process[2]. The information obtained from these logs can be used to interpret geology in general and in reservoir, identify productive zones, and estimate hydrocarbon reserves.

This study therefore assesses the reservoir quality of two wells: well 1 and well 2 (Figure 1) using GeoGraphix Software. The main focus is to determine some reservoir properties with a view to ascertaining if the results generated make possible to predict economic saturation and production.

Geology of the study area

The Niger Delta (Figure 2) is a regressive sequence of clastic sediments developed in series of offlap cycles[3]. The base of the sequence consists of massive and monotonous marine shales. These grade into interbedded shallow-marine and fluvial sands, silts, and clays, which form the typical paralic facies portion of the delta[3]. The uppermost part of the sequence is a massive non-marine sand section. The established Cainozoic sequence in the Niger delta consists, in ascending order of the marine shales (Akata Formation), paralic clastics (Agbada Formation), and continental sands (Benin Formation)[4]. Akata Formation is composed of shales, clays and silts at the base of the delta sequence. They contain a few streaks of sand, possibly of turbiditic origin, and were deposited in holomarine (delta-front to deeper marine) environments. Agbada Formation forms the hydrocarbon perspective sequence in the Niger delta. It is represented by an alternation

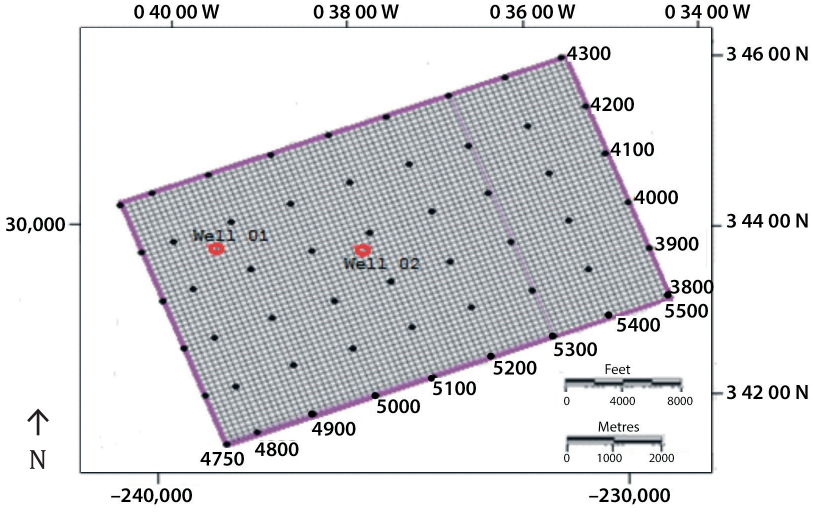

Figure 1: *Base map of "Y" prospect, showing the positions of the two wells (well 1 and 2) and 3D seismic survey.*

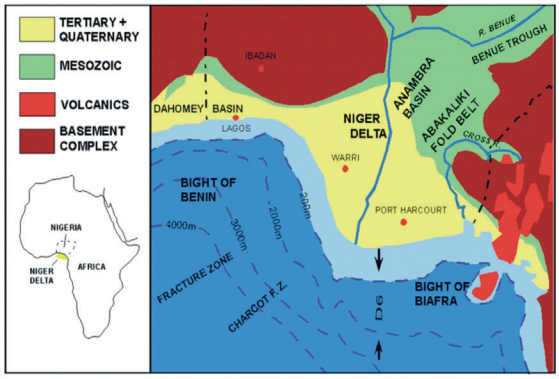

Figure 2: *A geological map showing the Niger delta*[13].

of sands, silts, and clays of various proportions and thicknesses, representing cyclic sequences of offlap units. The shallowest part of the sequence is composed almost entirely of non-marine sand. It was deposited in alluvial or upper coastal plain environments following a southward shift of deltaic depobelts (structural and stratigraphic belts)[5]. This mechanism, called the escalator regression model, postulated that the base of the Benin Formation in any of the six depobelts is coeval with the Agbada Formation in the adjacent depobelt to the south.

This principle implies an abrupt shift in the age of the base of the Benin Formation across the bounding faults of depobelts and had been used to define the Northern limit of the Northern Delta depobelt[6]. Weber[7] discussed in detail the sedimentology, growth faults dynamics and hydrocarbon accumulation in the Niger Delta. Short[8] and Avbovbo[9] also, studied the hydrocarbon potentials of the Niger Delta using well data. Oomkens[10] discussed lithofacies relations in the late Quaternary period. The stratigraphy, sedimentation and structure of Niger Delta was reviewed by Schlumberger[11].

The importance of longshore drift and submarine canyons and fans in the development of the basin has been emphasized by Burke[12].

Method of study

Two wells namely well 1 and well 2 exist in "Y" Prospect. Well 1 is a vertical well with a total depth of 2 332 m, and gamma-ray (GR) log, deep laterolog (LLD), compensated sonic log (BCSL), and compensated formation density log (FDC) were used in this well.

Well 2 is also a vertical well with a total depth of 2 160 m. The logs used in this well include, caliper log (CALI), gamma-ray (GR) log deep, laterolog (LLD), compensated sonic log (BCSL), and compensated formation density log (FDC).

Petrophysical Evaluation: The analysis of the data was done using GeoGraphix software. The data consist of logs (from two wells) namely the caliper log, the gamma ray log (GR), deep laterolog, and porosity logs (sonic, density and neutron logs).

Identification and Delineation of Lithologies: The *GR* log was used to identify the permeable and impermeable beds. *GR* values greater or equal to 75 API° were identified as shale beds while zones with *GR* readings below 75 API° were identified as sandstones. Intervals where the caliper logs read values lower than 24 cm were considered as permeable zones. This is because reduction in borehole diameter is indicative of the build-up of mudcake in permeable zones.

Identification of Fluids: Fluids in the permeable beds were identified, using the deep laterolog resistivity logs and a combination of the neutron and density logs. High resistivity values of deep-reading resistivity log in permeable beds are indicative of either the presence of hydrocarbon or fresh water.

Determination of Volume of Shale: The presence of shale in a reservoir can adversely affect the correct evaluation of petrophysical parameters particularly resistivity, porosity and water saturation. Hilchie[13] notes that the most important effect of shale in a formation is to reduce the resistivity contrast between oil or gas and water. With sufficient shale in a reservoir, it becomes very difficult to detect a productive zone[14]. Porosity and water saturation values must be corrected for shale effect to allow for a reliable formation evaluation. The first step in making this correction is to determine the volume of shale present in the reservoir.

For this study, shale volume was determined using the GR_{log}. The Gamma Ray Index (I_{GR}) was calculated first from the log using the formula[15];

$$I_{GR} = \frac{GR_{\log} - GR_{\min}}{GR_{\max} - GR_{\min}} \quad (1)$$

Where are;
$GR_{\log}$ = gamma ray reading of formation.
$GR_{\min}$ = minimum gamma ray reading (clean sand)
$GR_{\max}$ = maximum gamma ray reading (shale)

Subsequently, the calculated I_{GR} was used in the formula[10] for Cainozoic unconsolidated rocks to determine the volume of shale (V_{sh}).

$$V_{sh} = 0.083(2^{3.7 \times I_{GR}} - 1) \quad (2)$$

The calculated volumes of shale are expressed in percentage.

Determination of Porosity: Porosity values were obtained from sonic log, density log and a combination of neutron and density logs. Sonic porosity values were calculated using the formula proposed by Dewan[2] for undercompacted sandstones:

$$\phi_s = 0.63\left(1-\left(\frac{54}{\Delta t}\right)\right) \quad (3)$$

The calculated sonic porosity was subsequently corrected for both shale and hydrocarbon effects.
The density porosity (ϕ_D) was computed from eqn. 4;

$$\phi_D = \frac{\rho_{ma} - \rho_b}{\rho_{ma} - \rho_{fl}} \quad (4)$$

Where are:
ρ_{ma} = matrix (sandstone) density = 2.638 g/cm^3
ρ_b = formation bulk density
ρ_{fl} = fluid density

The 3.5 p.u (0.035) is subtracted from the calculated density porosity to convert from apparent limestone porosity unit to apparent sandstone porosity unit. Shale effect was subsequently corrected for to give the effective density porosity (PhiDe or ϕ_{De}).
Correcting for shale effect;

$$\phi_{De} = \phi_D - V_{sh} \times \phi_{D_{sh}} \quad (5)$$

Where are:
ϕ_{De} = effective density porosity
V_{sh} = volume of shale = 8.26 %
$\phi_{D_{sh}}$ = density porosity of adjacent shale = 0.10

The neutron log values were in API Neutron Unit and had to be converted to apparent limestone porosity. The values obtained were converted to apparent sandstone unit by the addition of 3.5 p. u (0.035). Shale effect was also corrected for to obtain the effective neutron porosity (PhiNe or ϕ_{De}).

Porosity values were also computed from a combination of neutron and density logs as follows.

$$\phi_{NDe} = \frac{\phi_{Ne} + \phi_{De}}{2} \quad \text{(for oil zones)} \quad (6)$$

$$\phi_{NDe} = \sqrt{\frac{\phi_{Ne}^2 + \phi_{De}^2}{2}} \quad \text{(for gas zones)} \quad (7)$$

Where are:
ϕ_{NDe} = effective neutron-density derived porosity
ϕ_{Ne} = effective neutron porosity
ϕ_{De} = effective density porosity

Determination of Formation Water Saturation and Hydrocarbon Saturation
The water saturation of the uninvaded zone (S_w) was computed from

$$S_w = \sqrt{\frac{R_0}{R_t}} \quad [11] \quad (8)$$

The hydrocarbon saturation (S_{hc}) was calculated from the equation;

$$S_{sh} = 1 - S_w \quad (9)$$

The water saturation of the flushed zone (S_{xo}) was estimated from the Archie's formula;

$$S_{x0} = \sqrt{\frac{FR_{mf}}{R_{x0}}} \quad (10)$$

The other saturation values calculated are the Moveable Hydrocarbon Saturation (*MHS*) and the Residual Hydrocarbon Saturation (*RHS*).

$$MHS = S_{x0} - S_w \quad (11)$$
$$RHS = 1 - S_{x0} \quad (12)$$

Tables 1 and 2 show the calculated parameters at sampled intervals for the calculated reservoirs.

Table 1: *Statistical data derived from GeoGraphix software for Well 1*

DEPTH	*PHIN*	*RHOB*	*PHID*	*DT*	*PHIA*	*GR*	V_{shl}	*PHIE*	*RT*	*Ro*	*SwA*	*BVW*
4 060	0.414 9	2.158	0.311	128.86	0.363	85.7	0.821	0.064 8	1.56	9.54	1	0.064 8
4 070	0.350 4	2.109	0.34	146.48	0.345	57.2	0.465	0.184 5	4.39	1.18	0.518	0.095 5
4 080	0.349 3	2.119	0.334	146.63	0.342	62.5	0.532	0.16	4.04	1.56	0.621	0.099 5
4 090	0.294 4	2.118	0.335	141.96	0.315	32.2	0.152	0.266 7	13	0.56	0.208	0.055 5
4 100	0.308 3	2.061	0.368	127	0.338	31.2	0.141	0.290 8	0.68	0.47	0.835	0.242 8
4 110	0.329 8	2.113	0.337	126.89	0.333	38.1	0.227	0.257 9	0.75	0.6	0.896	0.231
4 120	0.366 2	2.108	0.341	132.88	0.353	53.9	0.423	0.203 9	0.85	0.96	1	0.203 9
4 130	0.337 7	2.025	0.39	135.53	0.364	38.7	0.234	0.278 5	0.64	0.52	0.895	0.249 3
4 140	0.334 7	2.129	0.328	133.92	0.331	38.7	0.234	0.253 7	0.77	0.62	0.9	0.228 5
4 150	0.349 9	2.091	0.351	127.07	0.35	34	0.175	0.288 9	0.74	0.48	0.807	0.233 1
4 160	0.401 2	2.249	0.257	123.31	0.329	95.1	0.939	0.020 1	1.4	99.45	1	0.020 1
4 170	0.486 8	2.259	0.251	133.41	0.369	93.7	0.922	0.028 9	1.25	47.8	1	0.028 9
4 180	0.273 4	2.121	0.333	146.24	0.303	35.8	0.198	0.243 3	6.83	0.68	0.315	0.076 5
4 190	0.277	2.093	0.35	172.96	0.313	34.5	0.181	0.256 4	50.55	0.61	0.11	0.028 1
4 200	0.313 5	2.063	0.367	152.52	0.34	38.4	0.231	0.261 9	36.9	0.58	0.126	0.032 9
4 210	0.39	1.984	0.414	147.52	0.402	56.3	0.454	0.219 6	3.53	0.83	0.485	0.106 5
4 220	0.373 7	2.196	0.288	121.78	0.331	89.6	0.87	0.042 9	1.04	21.77	1	0.042 9
4 230	0.345	2.179	0.298	122.71	0.322	75.7	0.696	0.097 7	1.24	4.19	1	0.097 7
4 240	0.377 1	2.03	0.387	137.36	0.382	53.3	0.416	0.223 1	0.83	0.8	0.983	0.219 3
4 250	0.394 2	2.186	0.294	129.94	0.344	65.1	0.564	0.150 1	0.92	1.77	1	0.150 1
4 260	0.387 9	2.122	0.332	131.27	0.36	65.7	0.571	0.154 3	0.78	1.68	1	0.154 3
4 270	0.341 8	2.066	0.365	122.53	0.354	34.2	0.177	0.291	0.68	0.47	0.833	0.242 4
4 280	0.315 2	2.116	0.336	118.99	0.326	28.1	0.102	0.292 5	0.73	0.47	0.803	0.234 8
4 290	0.346 2	2.05	0.375	125.45	0.36	49.5	0.369	0.227 6	0.69	0.77	1	0.227 6
4 300	0.427 7	2.141	0.321	128.93	0.374	61.7	0.522	0.179	0.84	1.25	1	0.179
4 310	0.322 2	2.085	0.354	122.46	0.338	38.6	0.233	0.259 4	0.82	0.59	0.853	0.221 2
4 320	0.379 5	2.064	0.367	130.16	0.373	59.4	0.492	0.189 3	0.7	1.12	1	0.189 3
4 330	0.298 2	2.184	0.295	119.78	0.297	65	0.563	0.129 7	0.95	2.38	1	0.129 7
4 340	0.279 3	2.106	0.341	119.1	0.31	31.4	0.143	0.266 1	0.77	0.56	0.856	0.227 9
4 350	0.350 5	2.137	0.323	118.23	0.337	32.8	0.16	0.283 1	0.82	0.5	0.78	0.220 8
4 360	0.320 6	2.121	0.333	121.58	0.327	56.2	0.452	0.178 9	0.89	1.25	1	0.178 9
4 370	0.328 4	2.078	0.359	123.19	0.344	39.8	0.248	0.258 4	0.68	0.6	0.939	0.242 7
4 380	0.344 1	2.037	0.383	127.57	0.364	47.7	0.346	0.237 8	0.64	0.71	1	0.237 8
4 390	0.381 5	2.313	0.219	116.05	0.3	95	0.937	0.018 9	1.25	111.6	1	0.018 9
4 400	0.358	2.25	0.256	118.82	0.307	88.1	0.851	0.045 6	1.2	19.26	1	0.045 6
4 410	0.374 4	2.134	0.325	124.35	0.35	88.5	0.856	0.050 2	0.86	15.86	1	0.050 2
4 420	0.295 9	2.108	0.341	121.8	0.318	30.6	0.133	0.276 1	0.78	0.52	0.823	0.227 1
4 430	0.302 7	2.046	0.377	127.43	0.34	30.3	0.129	0.296 3	0.63	0.46	0.85	0.251 9
4 440	0.429 4	2.307	0.222	119.7	0.326	82.2	0.778	0.072 3	1.01	7.66	1	0.072 3
4 450	0.383	2.321	0.214	112.16	0.299	95.5	0.943	0.016 9	1.53	139.39	1	0.016 9
4 460	0.450 9	2.242	0.26	123.42	0.356	94.7	0.934	0.023 5	1.24	72.26	1	0.023 5
4 470	0.347 2	2.039	0.381	131.02	0.364	43	0.287	0.259 7	21.09	0.59	0.168	0.043 5
4 480	0.298 8	2.043	0.379	132.67	0.339	38.2	0.228	0.261 7	27.5	0.58	0.146	0.038 1
4 490	0.343 4	2.054	0.373	131.13	0.358	29.4	0.118	0.315 9	15.21	0.4	0.162	0.051 3
4 500	0.333 1	2.12	0.333	124.25	0.333	44	0.3	0.233 3	0.7	0.73	1	0.233 3

PHIN – Neutron Porosity *RHOB* – Bulk Density *DT* - Sonic log *PHIND* – Density Porosity *PHIA* – Average Porosity *GR* – Gamma Ray V_{shl} – Volume of Shale *PHIE* – Effective Porosity *RT* – True Resistivity *Ro* – Wet Resistivity *SwA* – Average Water Saturation

Table 2: *Statistical data derived from GeoGraphix software for Well 02*

DEPTH	*PHIN*	*RHOB*	*PHID*	*DT*	*PHIA*	*GR*	V_{shl}	*PHIE*	*RT*	*Ro*	*SwA*	*BVW*
4 600	0.46	2.21	0.28	115.63	0.37	93.03	0.913	0.032 2	1.22	38.54	1	0.032 2
4 610	0.157	2.07	0.364	121.66	0.261	41.38	0.267	0.191	106.67	1.1	0.101	0.019 4
4 620	0.131	2.1	0.348	126.12	0.24	45.25	0.316	0.164	30.77	1.49	0.22	0.036 1
4 630	0.259	2.19	0.289	124.21	0.274	75.92	0.699	0.082 5	5.13	5.87	1	0.082 5
4 640	0.48	2.14	0.32	147.01	0.4	90.64	0.883	0.046 8	2.39	18.26	1	0.046 8
4 650	0.129	2.03	0.39	143.56	0.26	61.89	0.524	0.123 6	26.89	2.62	0.312	0.038 6
4 660	0.135	2.18	0.297	142.82	0.216	45.7	0.321	0.146 7	21.77	1.86	0.292	0.042 9
4 670	0.232	2.06	0.369	136.74	0.301	78.5	0.731	0.0808	3.14	6.13	1	0.080 8
4 680	0.195	2.07	0.362	137.64	0.279	52.89	0.411	0.164 3	10.7	1.48	0.372	0.061 1
4 690	0.058	1.95	0.434	137.59	0.246	52.09	0.401	0.147 2	13.22	1.85	0.374	0.055
4 700	0.208	2.09	0.354	133.05	0.281	39.91	0.249	0.210 9	57.14	0.9	0.125	0.026 5
4 710	0.199	2.13	0.327	131.45	0.263	42.75	0.284	0.188 1	18.82	1.13	0.245	0.046 1
4 720	0.166	2.04	0.384	135.5	0.275	62.98	0.537	0.127 2	5.83	2.47	0.651	0.082 8
4 730	0.043	1.86	0.488	139.37	0.265	45.33	0.317	0.181 2	533.33	1.22	0.048	0.008 7
4 740	0.03	1.85	0.496	151.07	0.263	47.36	0.342	0.173 1	57.14	1.34	0.153	0.026 5
4 750	0.214	2.19	0.292	142.68	0.253	38.34	0.229	0.195 2	200	1.05	0.072	0.014 1
4 760	0.018	1.9	0.465	131.11	0.241	52.89	0.411	0.142 2	24.81	1.98	0.282	0.040 2
4 770	0.197	2.02	0.393	136.45	0.295	51.5	0.394	0.179	10.67	1.25	0.342	0.061 2
4 780	0.24	2.05	0.377	152.03	0.308	42.09	0.276	0.223 3	31.37	0.8	0.16	0.035 7
4 790	0.066	1.92	0.453	147.89	0.259	53.05	0.413	0.152 2	25	1.73	0.263	0.04
4 800	0.026	1.82	0.511	140.37	0.269	45.69	0.321	0.182 4	39.51	1.2	0.174	0.031 8
4 810	0.408	2.2	0.283	131.81	0.346	96.41	0.955	0.015 5	1.08	166	1	0.015 5
4 820	0.048	1.97	0.42	125.08	0.234	56.06	0.451	0.128 7	25.4	2.42	0.308	0.039 7
4 830	0.061	1.95	0.433	137.63	0.247	50.88	0.386	0.151 5	72.73	1.74	0.155	0.023 5
4 840	0.046	1.98	0.415	128.52	0.231	46.25	0.328	0.155 1	31.37	1.66	0.23	0.035 7
4 850	0.338	2.13	0.33	130.21	0.334	76.42	0.705	0.098 3	7.05	4.14	0.766	0.075 3
4 860	0.182	2.05	0.373	133.48	0.278	75.23	0.69	0.086	4.96	5.41	1	0.086
4 870	0.442	2.08	0.355	143.16	0.399	101.48	1	0	1.95			
4 880	0.117	1.97	0.424	131.52	0.27	50.59	0.382	0.166 9	19.39	1.44	0.272	0.045 4
4 890	0.021	1.94	0.442	129.29	0.232	44.78	0.31	0.16	34.41	1.56	0.213	0.034 1
4 900	0.093	1.98	0.418	135.37	0.256	42.72	0.284	0.183 1	42.1	1.19	0.168	0.030 8
4 910	0.04	1.96	0.428	136.79	0.234	50.56	0.382	0.144 5	106.67	1.92	0.134	0.019 4
4 920	0.282	2.18	0.299	134.6	0.29	83.52	0.794	0.059 8	3.11	11.18	1	0.059 8
4 930	0.013	1.82	0.512	133.72	0.263	40.2	0.253	0.196 5	228.57	1.04	0.067	0.013 2
4 940	0.125	2.01	0.396	123.34	0.261	61.94	0.524	0.124 1	13.01	2.6	0.447	0.055 5
4 950	0.04	2.03	0.386	122.22	0.213	37.39	0.217	0.166 7	118.51	1.44	0.11	0.018 4
4 960	0.034	1.9	0.467	129.7	0.251	50.23	0.378	0.155 8	61.54	1.65	0.164	0.025 5
4 970	0.246	2	0.403	137.19	0.325	81.81	0.773	0.073 8	6.28	7.35	1	0.073 8
4 980	0.08	1.96	0.426	135.98	0.253	59.89	0.499	0.126 9	20.25	2.48	0.35	0.044 4
4 990	0.348	2.21	0.282	123.25	0.315	90.98	0.887	0.035 5	2.09	31.78	1	0.035 5
5 000	0.082	2	0.404	129.35	0.243	48.86	0.361	0.155 4	10.03	1.66	0.406	0.063 1

PHIN – Neutron Porosity *RHOB* – Bulk Density *DT* - Sonic log *PHIND* – Density Porosity *PHIA* – Average Porosity *GR* – Gamma Ray V_{shl} – Volume of Shale *PHIE* – Effective Porosity *RT* – True Resistivity *Ro* – Wet Resistivity *SwA* – Average Water Saturation

Reserve Estimation

The volumes of hydrocarbons in place were estimated from the following formulae;

$$OIP = 7758\phi(1 - S_w)Ah \quad (13)$$

$$GIP = 43560\phi(1 - S_w)Ah \quad (14)$$

Where are:
OIP = oil in place (barrels)
GIP = gas in place (cubic feet)
The constants 7 758 and 43 560 are conversion factor for oil and gas barrels or cubic meter respectively.
ϕ = porosity (decimal)
S_w = formation's water saturation (decimal).
Area = area of the reservoir (in acres)
h = net thickness of reservoir (wet with oil or gas) (in feet)

Discussion of results

Gamma-ray (GR) logs were used to identify the lithology in both wells penetrated. The lithology was identified by defining shale base line (Figure 3), which is a constant line in front of the shale and in front of the sand. Thick sand at a depth of 304.8 m to 926.7 m (1 000–3 040 ft) was delineated in well 1. Well 2 contain thick sand layer at a depth of 100 m to 914.4 m (328–3 000 ft). At a depth of 1 237.5 m to 1 371.6 m (4 060–4 500 ft), and 1 402.1 m to 1 524 m (4 600–5 800 ft) thick sand (identified reservoir sand) was also observed in well 1 and well 2 respectively. Figure 3 shows the stratigraphic cross section within the study area. The major lithologies encountered in the study area were basically shale and sand, some of which occurs as interbeds. The reservoir sandstone was evaluated quantitatively for effective porosity, water & hydrocarbon saturation and net pay (Tables 3 and 4).

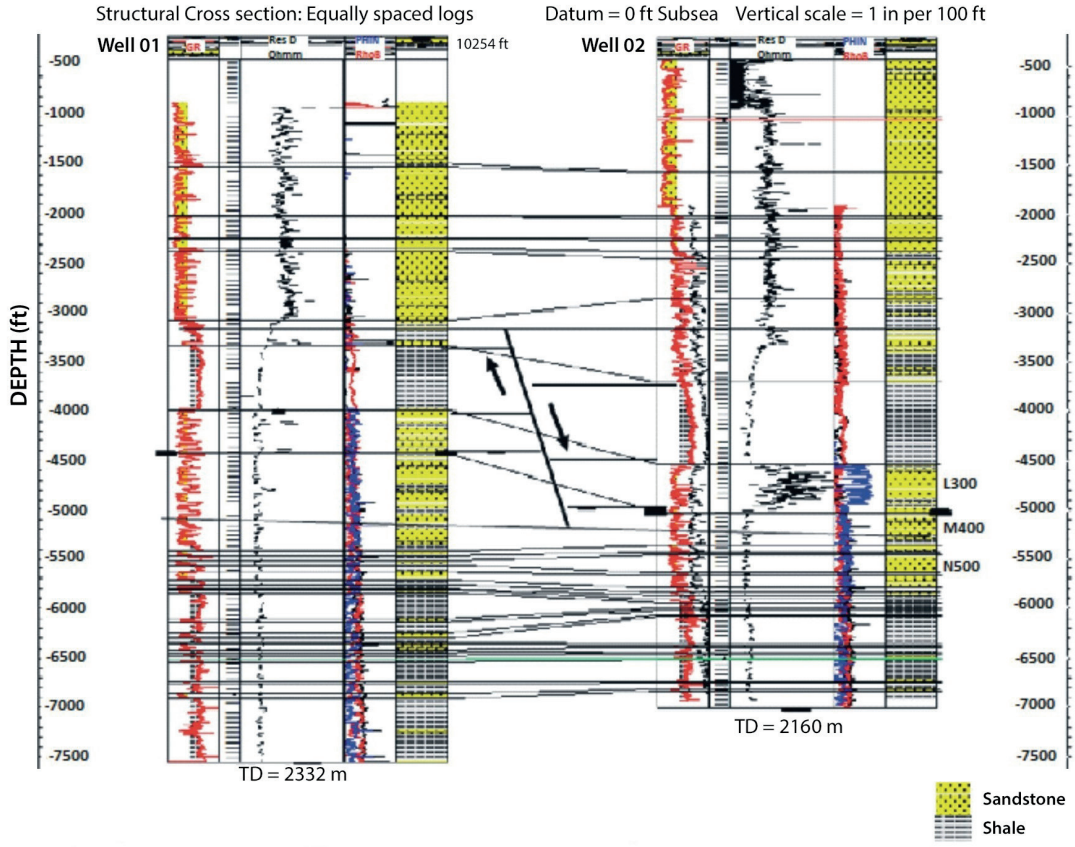

Figure 3: *Correlation across the wells of "Y" Prospect showing mapped sands.*

Table 3: *Petrophysical Parameters for Well 01*

SANDS	ZONE	TOP *MD*/m	BASE *MD*/m	*PHIE*/%	S_w/%	S_{hc}/%	GROSS (m)	Net sand thickness (m)	*NTG*	*PAY*/m
L300	1	1 240.54	1 524	19.95	48.5	51.5	283.46	43.65	0.154	22.9
M400	2	1 539.24	1 630.68	21.56	76.91	23.1	91.44	14.08	0.154	0.87
N500	3	1 685.54	1 699.25	12.25	98.52	1.48	13.72	3.88	0.283	–

MD – Measured Depth PHIE – Effective Porosity S_w – Water Saturation S_{hc} – Hydrocarbon Saturation *NTG* – Net-to-Gross

Table 4: *Petrophysical Parameters for Well 02*

SANDS	ZONE	TOP *MD*/m	BASE *MD*/m	*PHIE*/%	S_w/%	S_{hc}/%	GROSS (m)	Net sand thickness (m)	*NTG*	*PAY*/m
L300	1	1 402.08	1524	13.46	30.82	69.18	121.92	101.07	0.829	80.75
M400	2	1 542.88	1 615.44	17.73	55.78	44	73.15	8.266	0.113	1.37
N500	3	1 676.4	1 706.88	20.26	92.38	7.62	30.48	6.858	0.225	0.14

MD – Measured Depth PHIE – Effective Porosity S_w – Water Saturation S_{hc} – Hydrocarbon Saturation NTG – Net-to-Gross

Neutron density logs were used to define hydrocarbon type (gas) present in "Y" Prospect. Petrophysical analysis of the reservoir bed was based on examination of the well logs. The combination of neutron and density logs was used for reservoir L300 in both wells to detect gas zone. At these intervals, density porosity was observed to be greater than neutron porosity and the curves cross over each other, therefore were identified as gas bearing zones (Figure 4). This is because gas in pores causes the density porosity to read very high values (gas has a lower density than oil or water) and causes the neutron porosity to be too low (there is a low concentration of hydrocarbon atoms in gas than in oil and water). Figure 5 shows the crossplot of neutron porosity with *RhoB* (Formation Bulk Density).

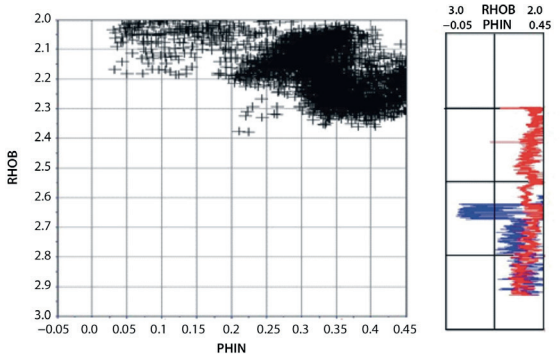

Figure 4: *Pickett crossplot of Neutron porosity(PHIN) with Bulk Density (RhoB).*

Gas has a very marked effect on both density and neutron logs. If it is assumed that the formation fluid is water and the invasion zone is shallow, then gas will result in a lower bulk density (note on the cross plot, this results in a point higher on the *y*-axis), and a lower apparent neutron porosity (Figure 6).

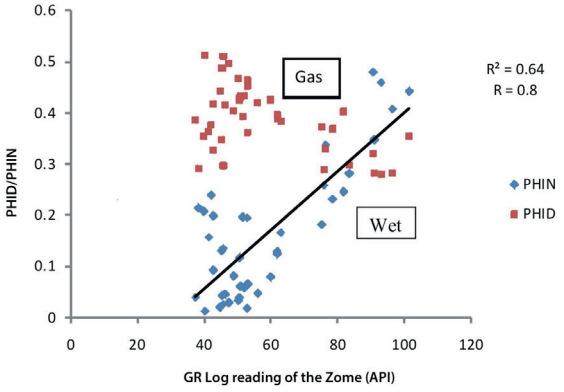

Figure 5: *Crossplot of Neutron Porosity (PHIN) with Density Porosity (PHID).*

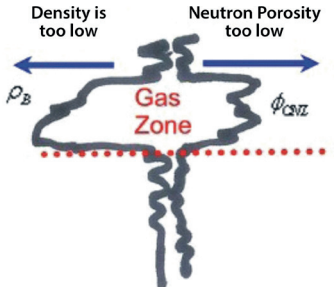

Figure 6: *Typical log curve showing gas zone and its effect on density and neutron.*

Conclusion

Reservoir evaluation is an attempt to find appropriate reservoir rocks and then to estimate the porosity, permeability and water saturation. In Niger Delta sands more than 15 m thick in most places represent composite bodies, and may consist of two to three stacked channels. They are poorly consolidated and have porosities as high as 40 % in oil- bearing reservoirs. Porosity reduction is gradual. All sands shallower than 3 000 m have porosities of more than 15 %, but below 4 000 m only a few sands have more than 15 % porosity. Gross, net and net-to-gross values for sandstones in well -1 are 13.72–283.46, 3.88–43.65 and 0.154–0.283, while those for well - 2 are 30.48–121.92, 6.858–101.07 and 0.113–0.829 respectively. Reservoir which contain hydrocarbon is referred to as pay zone and the porosities range 20–40 %. The average porosity (*PHIA*) which is the average porosity within the net is 0.23 (23 %) for well 01, it is 0.28 (28 %) for well 2. The porosity values are within the porosities of producing reservoirs in the Niger Delta. Water saturation is generally low in hydrocarbon bearing zone ranging from 1–30 % thereby implying high hydrocarbon saturation. The water saturation, values in "Y" Prospect at well 1 and well 2 are 0.85 (85 %), and 0.62 (62 %) respectively. The reservoir properties evaluated for the wells showed that they could be fair to very good for hydrocarbon accumulation.

Acknowledgements

The author wishes to express her sincere appreciation to Mobil Producing Nigeria Unlimited for the provision of the data used for this work. Also I am thankful to the Landmark for the licensed GeoGraphix software which was used for the well evaluation.

References

[1] Sheriff, R. E. (1992): Basic petrophysics and geophysics. *Reservoir Geophysics*, No. 7, Society of exploration Geophysicists, Tulsa, pp. 37–49.

[2] Dewan, J. T. (1983): *Essentials of Modern Open-Hole Log Interpretation*; Tulsa, Oklahoma, U.S.A, p. 244.

[3] Evamy, D. W., Haremboure, J., Kamerling, P., Knaap, W. A., Molloy, F. A., Rowlands, P. H. (1978): Hydrocarbon habitat of Tertiary Niger Delta. *AAPG Bulletin*, 62 (1), pp. 1–39.

[4] Knox, G. J., Omatsola, E. M. (1989): *Development of the Cenozoic Niger Delta in terms of the "escalator regression" model and Impact on hydrocarbon distribution*; in W. J. M., van der Linden et al., eds, 1987 Proceedings KNGMG Symposium on Coastal Lowlands, geology, and Geotechnology: Dordrecht, the Netherlands, Klumer Academic Publishers, pp. 181–202.

[5] Weber, K. J. (1971): Sedimentological aspects of oil fields in the Niger Delta. *Geologic en Mijnbouw*, 50, pp. 559–576.

[6] Ekweozor, C. M., Daukoru, E. M. (1994): *Northern Delta depobelt portion of the Akata-Agbada, petroleum system, Niger Delta, Nigeria*; in L. B. Magoon and W. G. Dow, eds, The petroleum system - from source to trap: AAPG Memoir, pp. 599–613.

[7] Weber, K. J., Daukoru, E. M. (1975): *Petroleum Geology of the Niger Delta*; Proceedings of the Ninth World Petroleum Congress, Tokyo, Japan, 2, pp. 209–221.

[8] Short, K. C., Stauble, A. J. (1967): Outline of the Geology of Niger Delta. *AAPG Bulletin*, 51, pp. 761–779.

[9] Avbovbo, A. A. (1978). Tertiary Lithostragraphy of the Niger Delta. *AAPG*, 62 (2), pp. 295–300.

[10] Oomkens, E. (1974): Lithofacies relations in the late Quaternary Niger Delta complex. *Sedimentology*, 2, pp. 195–222.

[11] Schlumberger (1991): *Log interpretation principles/ applications*; Houston, Schlumberger educational services, pp. 26–41.

[12] Burke, K. (1972): Longshore drift, submarine canyons, and submarine fans in development of Niger Delta. *AAPG Bulletin*, 59 (3), pp. 414–419.

[13] Hilchie, D. W. (1978): *Applied Openhole Log Interpretation*; Golden, Colorado, D. W. Hilchie. Inc., pp. 10–65.

[14] Asquith, G., Krygowski, D. (2004): *Basic Well Log Analysis*; 2nd edition, AAPG, Tulsa, Oklahoma, U.S.A, p. 244.

[15] Schlumberger, (1989): *Log interpretation principles/ applications*; Houston, Schlumberger educational services, pp.13–19.

Instructions to Authors
Navodila avtorjem

RMZ – MATERIALS & GEOENVIRONMENT (RMZ – Materiali in geookolje) is a periodical publication with four issues per year (established in 1952 and renamed to RMZ – M&G in 1998). The main topics are Mining and Geotechnology, Metallurgy and Materials, Geology and Geoenvironment.
RMZ – M&G publishes original scientific articles, review papers, preliminary notes and professional papers in English. Only professional papers will exceptionally be published in Slovene. In addition, evaluations of other publications (books, monographs, etc.), in memoriam, presentation of a scientific or a professional event, short communications, professional remarks and reviews published in RMZ – M&G can be written in English or Slovene. These contributions should be short and clear.
Authors are responsible for the originality of the presented data, ideas and conclusions, as well as for the correct citation of the data adopted from other sources. The publication in RMZ – M&G obligates the authors not to publish the article anywhere else in the same form.

RMZ – MATERIALS AND GEOENVIRONMENT (RMZ – Materiali in geookolje), kratica RMZ – M&G je revija (ustanovljena kot zbornik 1952 in preimenovana v revijo RMZ – M&G 1998), ki izhaja vsako leto v štirih zvezkih. V reviji objavljamo prispevke s področja rudarstva, geotehnologije, materialov, metalurgije, geologije in geookolja.
RMZ – M&G objavlja izvirne znanstvene, pregledne in strokovne članke ter predhodne objave samo v angleškem jeziku. Strokovni članki so lahko izjemoma napisani v slovenskem jeziku. Kot dodatek so zaželene recenzije drugih publikacij (knjig, monografij …), nekrologi In memoriam, predstavitve znanstvenih in strokovnih dogodkov, kratke objave in strokovne replike na članke, objavljene v RMZ – M&G v slovenskem ali angleškem jeziku. Prispevki naj bodo kratki in jasni.
Avtorji so odgovorni za izvirnost podatkov, idej in sklepov v predloženem prispevku oziroma za pravilno citiranje privzetih podatkov. Z objavo v RMZ – M&G se tudi obvežejo, da ne bodo nikjer drugje objavili enakega prispevka.

Specification of the Contributions

Optimal number of pages is 7 to 15; longer articles should be discussed with the Editor-in-Chief prior to submission. All contributions should be written using the ISO 80000.

- Original scientific papers represent unpublished results of original research.
- Review papers summarize previously published scientific, research and/or expertise articles on a new scientific level and can contain other cited sources which are not mainly the result of the author(s).
- Preliminary notes represent preliminary research findings, which should be published rapidly (up to 7 pages).
- Professional papers are the result of technological research achievements, application research results and information on achievements in practice and industry.

Vrste prispevkov

Optimalno število strani je 7–15, za daljše članke je potrebno soglasje glavnega urednika. Vsi prispevki naj bodo napisani v skladu z ISO 80000.

- Izvirni znanstveni članki opisujejo še neobjavljene rezultate lastnih raziskav.
- Pregledni članki povzemajo že objavljene znanstvene, raziskovalne ali strokovne dosežke na novem znanstvenem nivoju in lahko vsebujejo tudi druge (citirane) vire, ki niso večinsko rezultat dela avtorjev.
- Predhodna objava povzema izsledke raziskave, ki je v teku in zahteva hitro objavo obsega do sedem (7) strani.
- Strokovni članki vsebujejo rezultate tehnoloških dosežkov, razvojnih projektov in druge informacije iz prakse in industrije.

— Publication notes contain the author's opinion on newly published books, monographs, textbooks, etc. (up to 2 pages). A figure of the cover page is expected, as well as a short citation of basic data.
— In memoriam (up to 2 pages), a photo is expected.
— Discussion of papers (Comments) where only professional disagreements of the articles published in previous issues of RMZ – M&G can be discussed. Normally the source author(s) reply to the remarks in the same issue.
— Event notes in which descriptions of a scientific or a professional event are given (up to 2 pages).

Review Process

All manuscripts will be supervised shall undergo a review process. The reviewers evaluate the manuscripts and can ask the authors to change particular segments, and propose to the Editor-in-Chief the acceptability of the submitted articles. Authors are requested to identify three reviewers and may also exclude specific individuals from reviewing their manuscript. The Editor-in-Chief has the right to choose other reviewers. The name of the reviewer remains anonymous. The technical corrections will also be done and the authors can be asked to correct the missing items. The final decision on the publication of the manuscript is made by the Editor-in-Chief.

Form of the Manuscript

The contribution should be submitted via e-mail as well as on a USB flash drive or CD.
The original file of the Template is available on RMZ – Materials and Geoenvironment Home page address: **www.rmz-mg.com**.
The contribution should be submitted in Microsoft Word. The electronic version should be simple, without complex formatting, hyphenation, and underlining. For highlighting, only bold and italic types should be used.

Composition of the Manuscript

Title

The title of the article should be precise, informative and not longer that 100 characters. The author should also indicate the short version of the title. The title should be written in English as well as in Slovene.

— Recenzije publikacij zajemajo ocene novih knjig, monografij, učbenikov, razstav … (do dve (2) strani; zaželena slika naslovnice in kratka navedba osnovnih podatkov).
— In memoriam obsega do dve (2) strani, zaželena je slika.
— Strokovne pripombe na objavljene članke ne smejo presegati ene (1) strani in opozarjajo izključno na strokovne nedoslednosti objavljenih člankov v prejšnjih številkah RMZ – M&G. Praviloma že v isti številki avtorji prvotnega članka napišejo odgovor na pripombe.
— Poljudni članki, ki povzemajo znanstvene in strokovne dogodke zavzemajo do dve (2) strani.

Recenzentski postopek

Vsi prispevki bodo predloženi v recenzijo. Recenzent oceni primernost prispevka za objavo in lahko predlaga kot pogoj za objavo dopolnilo k prispevku. Recenzenta izbere uredništvo med strokovnjaki, ki so dejavni na sorodnih področjih, kot jih obravnava prispevek. Avtorji morajo predlagati tri recenzente. Pravico imajo predlagati ime recenzenta, za katerega ne želijo, da bi recenziral njihov prispevek. Uredništvo si pridržuje pravico, da izbere druge recenzente. Recenzent ostane anonimen. Prispevki bodo tudi tehnično ocenjeni in avtorji so dolžni popraviti pomanjkljivosti. Končno odločitev za objavo da glavni urednik.

Oblika prispevka

Prispevek lahko posredujte preko e-pošte ter na USB-mediju ali CD-ju.
Predloga za pisanje članka se nahaja na spletni strani: **www.rmz-mg.com**.
Besedilo naj bo podano v urejevalniku besedil Word. Digitalni zapis naj bo povsem enostaven, brez zapletenega oblikovanja, deljenja besed, podčrtavanja. Avtor naj označi le krepko in kurzivno poudarjanje.

Zgradba prispevka

Naslov

Naslov članka naj bo natančen in informativen in naj ne presega 100 znakov. Avtor naj navede tudi skrajšan naslov članka. Naslov članka je podan v angleškem in slovenskem jeziku.

Information on the Authors
Information on the authors should include the first and last name of the authors, the address of the institution and the e-mail address of the leading author.

Abstract
The abstract presenting the purpose of the article and the main results and conclusions should contain no more than 180 words. It should be written in Slovene and English.

Key words
A list of up to 5 key words (3 to 5) that will be useful for indexing or searching. They should be written in Slovene and English.

Introduction

Materials and methods

Results and discussion

Conclusions

Acknowledgements

References
The sources should be cited in the same order as they appear in the article. They should be numbered with numbers in square brackets. Sources should be cited according to the SIST ISO 690:1996 standards.

Monograph:
[1] Trček, B. (2001): *Solute transport monitoring in the unsaturated zone of the karst aquifer by natural tracers*. Ph. D. Thesis. Ljubljana: University of Ljubljana 2001; 125 p.

Journal article:
[2] Higashitani, K., Iseri, H., Okuhara, K., Hatade, S. (1995): Magnetic Effects on Zeta Potential and Diffusivity of Nonmagnetic Particles. *Journal of Colloid and Interface Science*, 172, pp. 383–388.

Electronic source:
CASREACT – Chemical reactions database [online]. Chemical Abstracts Service, 2000, renewed 2/15/2000 [cited 2/25/2000]. Available on: <http://www.cas.org/casreact.html>.

Podatki o avtorjih
Podatki o avtorjih naj vsebujejo imena in priimke avtorjev, naslov pripadajoče inštitucije ter elektronski naslov vodilnega avtorja.

Izvleček
Izvleček namena članka ter ključnih rezultatov z ugotovitvami naj obsega največ 180 besed. Izvleček je podan v angleškem in slovenskem jeziku.

Ključne besede
Seznam največ 5 ključnih besed (3–5) za pomoč pri indeksiranju ali iskanju. Ključne besede so podane v angleškem in slovenskem jeziku.

Uvod

Materiali in metode

Rezultati in razprava

Sklepi

Zahvala

Viri
Uporabljane literaturne vire navajajte po vrstnem redu, kot se pojavljajo v prispevku. Označite jih s številkami v oglatem oklepaju. Literatura naj se navaja v skladu s standardom SIST ISO 690:1996.

Monografija:
[1] Trček, B. (2001): *Solute transport monitoring in the unsaturated zone of the karst aquifer by natural tracers*. doktorska disertacija. Ljubljana: Univerza v Ljubljani 2001; 125 str.

Članek v reviji:
[2] Higashitani, K., Iseri, H., Okuhara, K., Hatade, S. (1995): Magnetic Effects on Zeta Potential and Diffusivity of Nonmagnetic Particles. *Journal of Colloid and Interface Science*, 172, str. 383–388.

Spletna stran:
CASREACT – Chemical reactions database [online]. Chemical Abstracts Service, 2000, obnovljeno 15. 2. 2000 [citirano 25. 2. 2000]. Dostopno na svetovnem spletu: <http://www.cas.org/casreact.html>.

Scientific articles, review papers, preliminary notes and professional papers are published in English. Only professional papers will exceptionally be published in Slovene.

Annexes

Annexes are images, spreadsheets, tables, and mathematical and chemical formulas.
Annexes should be included in the text at the appropriate place, and they should also be submitted as a separate document, i.e. separated from the text in the article.
Annexes should be originals, made in an electronic form (Microsoft Excel, Adobe Illustrator, Inkscape, AutoCad, etc.) and in .eps, .tif or .jpg format with a resolution of at least 300 dpi.
The width of the annex should be at least 152 mm. They should be named the same as in the article (Figure 1, Table 1).
The text in the annexes should be written in typeface Arial Regular (6 pt).
The title of the image (also schemes, charts and graphs) should be indicated in the description of the image.
When formatting spreadsheets and tables in text editors, tabs, and not spaces, should be used to separate columns. Each formula should have its number written in round brackets on its right side.
References of the annexes in the text should be as follows: "Figure 1…" and not "as shown below:". This is due to the fact that for technical reasons the annex cannot always be placed at the exact specific place in the article.

Manuscript Submission

Contributions should be sent to the following e-mail address: rmz-mg@ntf.uni-lj.si.

In case of submission on CD or USB flash drive, contributions can be sent by registered mail to the address of the editorial board:
RMZ – Materials and Geoenvironment, Aškerčeva 12, 1000 Ljubljana, Slovenia.

The contributions can also be handed in at the reception of the Faculty of Natural Sciences and Engineering (ground floor), Aškerčeva 12, 1000 Ljubljana, Slovenia with the heading "for RMZ – M&G".

Znanstveni, pregledni in strokovni članki ter predhodne objave se objavijo v angleškem jeziku. Izjemoma se strokovni članek objavi v slovenskem jeziku.

Priloge

K prilogam prištevamo slikovno gradivo, preglednice in tabele ter matematične in kemijske formule.
Priloge naj bodo vključene v besedilu, kjer se jim odredi okvirno mesto. Hkrati jih je potrebno priložiti tudi kot samostojno datoteko, ločeno od besedila v članku.
Priloge morajo biti izvirne, narejene v računalniški obliki (Microsoft Excel, Adobe Illustrator, Inkscape, AutoCad ...) in shranjene kot .eps, .tif ali .jpg v ločljivosti vsaj 300 dpi. Širina priloge naj bo najmanj 152 mm. Datoteke je potrebno poimenovati, tako kot so poimenovane v besedilu (Slika 1, Preglednica 1).
Za besedilo v prilogi naj bo uporabljena pisava Arial navadna različica (6 pt).
Naslov slikovnega gradiva, sem prištevamo tudi sheme, grafikone in diagrame, naj bo podan v opisu slike.
Pri urejevanju preglednic/tabel, v urejevalniku besedila, se za ločevanje stolpcev uporabijo tabulatorji in ne presledki.
Vsaka formula naj ima zaporedno številko zapisano v okroglem oklepaju na desni strani.
V besedilu se je potrebno sklicevati na prilogo na način: „Slika 1 ...", in ne „... kot je spodaj prikazano:" saj zaradi tehničnih razlogov priloge ni vedno mogoče postaviti na točno določeno mesto v članku.

Oddaja članka

Prispevke lahko pošljete po elektronski pošti na naslov rmz-mg@ntf.uni-lj.si.

V primeru oddaje prispevka na CD- ali USB-mediju le-te pošljite priporočeno na naslov uredništva:
RMZ – Materials and Geoenvironment, Aškerčeva 12, 1000 Ljubljana, Slovenija

ali jih oddajte na:
recepciji Naravoslovnotehniške fakultete (pritličje), Aškerčeva 12, 1000 Ljubljana, Slovenija s pripisom „za RMZ – M&G".

The electronic medium should clearly be marked with the name of the leading author, the beginning of the title and the date of the submission to the Editorial Office of RMZ – M&G.

Information on RMZ – M&G

— Editor-in-Chief
  Assoc. Prof. Dr. Peter Fajfar
  Telephone: +386 1 200 04 51
  E-mail address: peter.fajfar@omm.ntf.uni-lj.si

— Secretary
  Ines Langerholc, Bachelor in Business Administration
  Telephone: +386 1 470 46 08
  E-mail address: ines.langerholc@omm.ntf.uni-lj.si

These instructions are valid from July 2013.

Elektronski mediji morajo biti jasno označeni z imenom vsaj prvega avtorja, začetkom naslova in datumom izročitve uredništvu RMZ – M&G.

Informacije o RMZ – M&G

— urednik
  izr. prof. dr. Peter Fajfar
  Telefon: +386 1 200 04 51
  E-poštni naslov: peter.fajfar@omm.ntf.uni-lj.si

— tajnica
  Ines Langerholc, dipl. poslov. adm.
  Telefon: +386 1 470 46 08
  E-poštni naslov: ines.langerholc@omm.ntf.uni-lj.si

Navodila veljajo od julija 2013.

ISSN 1408-7073